



THE HONG KONG
POLYTECHNIC UNIVERSITY

香港理工大學

Pao Yue-kong Library

包玉剛圖書館

Copyright Undertaking

This thesis is protected by copyright, with all rights reserved.

By reading and using the thesis, the reader understands and agrees to the following terms:

1. The reader will abide by the rules and legal ordinances governing copyright regarding the use of the thesis.
2. The reader will use the thesis for the purpose of research or private study only and not for distribution or further reproduction or any other purpose.
3. The reader agrees to indemnify and hold the University harmless from and against any loss, damage, cost, liability or expenses arising from copyright infringement or unauthorized usage.

If you have reasons to believe that any materials in this thesis are deemed not suitable to be distributed in this form, or a copyright owner having difficulty with the material being included in our database, please contact lbsys@polyu.edu.hk providing details. The Library will look into your claim and consider taking remedial action upon receipt of the written requests.

The Hong Kong Polytechnic University

Department of Applied Physics

**Sensors based on Organic Thin Film
Transistors**

Mok Sheung Man

A thesis submitted in partial fulfillment of the requirements
for the degree of Master of Philosophy

August 2008



**Pao Yue-kong Library
PolyU · Hong Kong**

CERTIFICATE OF ORIGINALITY

I hereby declare that this thesis is my own work and that, to the best of my knowledge and belief, it reproduces no material previously published or written, nor material that has been accepted for the award of any other degree or diploma, except where due acknowledgement has been made in the text.

Mok Sheung Man



ABSTRACT

Organic thin-film transistor (OTFT) sensors have proven to exhibit very promising properties when used as sensors and detectors. In this thesis, we are going to report on two types of sensors based on OTFTs, i.e. phototransistors and biosensors.

Phototransistors are a type of optical transducers in which light detection and signal amplification are combined in a single device. Organic phototransistors (OPTs) are considered to be one of the feasible applications of OTFT because of their large adsorption properties in ultraviolet (UV) and visible light and the excellent photo current generation efficiency of organic semiconductors. More importantly, OPTs can be fabricated by a solution process, such as printing or spin coating, at room temperature and therefore can be easily integrated in smart clothings, packages, and biological systems as light sensors or biosensors. A light sensitive phototransistor based on the composite of poly(3-hexylthiophene) (P3HT) and titanium dioxide (TiO_2) nanoparticles has been fabricated by a solution process. The device shows a quick change of channel current under light exposure, which can be attributed to a positive shift of the threshold voltage, while no change in the field effect mobility and off current can be observed. The shift of the threshold voltage is induced by the accumulated electrons trapped by the TiO_2 nanoparticles in the channel. The photosensitivity of the device has been found to be dependent on the concentration of TiO_2 nanoparticles, the incident wavelength and the voltage between the source and drain.



OTFT are excellent candidates for the application on disposable sensors due to their potentially low-cost fabrication process. A novel DNA sensor based on OTFTs with semiconducting polymer poly(3-hexylthiophene) has been fabricated by solution process. Both single and double strand DNA molecules are immobilized on the surface of the Au source/drain electrodes of different devices, producing a dramatic change in the performance of the OTFTs, which is attributed to the increase of the contact resistance at the source/drain electrodes. Single strand DNA and double strand DNA are differentiated successfully in the experiments indicating that this is a promising technique for sensing DNA hybridization without labeling.



LIST OF PUBLICATION

1. Sheung Man Mok, Feng Yan, and Helen, L. W. Chan,” Organic phototransistor based on poly (3-hexylthiophene)/TiO₂ nanoparticle composite”, Applied Physics Letter, Vol. 93, pp.023310 (2008)
2. Feng Yan, Sheung Man Mok, Jinjiang Yu, Helen L. W. Chan, Mo Yang,” Label-free DNA sensor based on organic thin film transistors”, Biosensors and Bioelectronics, Vol. 24, Issue 5, pp. 1241-1245, (2009).
3. Feng Yan, Sheung Man Mok, Peng Lin, Helen L. W. Chan, “Sensors Based on Organic Thin Film Transistors” ECS Transactions, in press.



Acknowledgements

I would like to express my deep appreciation to my supervisor Dr. YAN Feng for his scientific insight, guidance, and encouragement throughout the whole period of the research work.

I would also like to express my deepest gratitude to Prof. Helen L.W. Chan for her resourcefulness and advice.

Throughout the course of this research, very valuable contributions and support from Dr WONG Yuen Wah and Dr DAI Ji Yan are gratefully acknowledged.

I am indebted to Miss LAM Ching Yee. Her technical assistance and many illuminating discussions are highly appreciated.

I would also like to give my thanks to colleagues and friends Mr LIN Peng, Mr CHOW Ching Kin, Simon, Mr JIM Kwok Lung, Michael, Mr TANG Yu Ming, and Miss Li Ming Kei, Victoria for their help and assistance.

I gratefully acknowledge the financial support from the Hong Kong Polytechnic University and the technical support provided by the Materials Research Centre of the Hong Kong Polytechnic University.

Finally, I would like to thank my family and friends for their love and support. Most of all I would like express my gratefulness to my father Tung Ming and mother Kwan Fong for their patience, confidence and love.



TABLE OF CONTENTS

	<u>Page</u>
Abstract	I
List of Publication	III
Acknowledgements	IV
Table of Contents	V
List of Figure Captions	VII
List of Table Captions	XIII
Chapter 1: Introduction	
1.1 History of Field Effect Transistor	1-1
1.2 Organic Field Effect Transistor	1-2
1.3 Application of Organic Field Effect Transistor	1-5
1.3.1 Organic Electronics	1-5
1.3.2 OTFT Based Sensor	1-8
1.4 Organic Semiconducting Materials	1-15
1.4.1 Classification of Organic Semiconducting Materials	1-17
1.4.2 <i>p</i> -Type Small Molecules	1-19
1.4.3 <i>p</i> -Type Polymer	1-23
1.4.4 <i>n</i> -Type Semiconductor	1-24
1.4.5 Insulating Dielectric Layer	1-27
Chapter 2: Fabrication of P3HT OTFT	
2.1 P3HT: semiconducting polymer	2-1
2.2 Device structure	2-3
2.3 Working principle	2-7
2.4 Measuring system	2-16
2.5 Preparation of an OTFT with BGBC and TGBC structure	2-19
2.6 Post-annealing effect on P3HT based OTFT device	2-24
2.7 Oxygen doping and moisture interaction	2-30
2.8 Conductivity of P3HT in different environment	2-32



Chapter 3: Organic phototransistor based on TiO₂/P3HT

composite

3.1 Organic phototransistor	3-1
3.2 Motivations	3-5
3.3 Experiments	3-6
3.4 Photo response of TiO ₂ /P3HT OPTs	3-9
3.5 Rutile phase TiO ₂ /P3HT OPTs	3-22
3.6 Conclusion	3-29

Chapter 4: Label-free DNA OTFT sensor

4.1 Introduction of DNA sensor	4-1
4.2 Experiments	4-5
4.2.1 Substrate Preparation	4-5
4.2.2 DNA Immobilization and Hybridization	4-6
4.2.3 Fabrication of Organic Thin Film Transistor	4-8
4.2.4 Signal Acquisition	4-9
4.3. Results and discussions	4-11
4.4. Conclusion	4-20

Reference	5-1
------------------	-----



List of Figure Captions

	<u>Page</u>
Figure 1.2 Number of publications on organic field-effect transistors over the past few years as counted by the Institute for Scientific Information (ISI) Web of Science.	1-3
Figure 1.3.1.1 (a) The 3.5 cm by 3.5 cm organic display has 64×64 pixels. Pixel size is $540 \times 540 \mu\text{m}^2$. (b) Organic e-paper bent to a radius of curvature of ~ 1 cm[10].	1-6
Figure 1.3.1.2 Future applications for new electronics will greatly interest logistics [9].	1-7
Figure 1.3.2.1 Arrangement for the field effect measurements. The gap between the electrodes was 0.2 mm x 4 mm and the quartz plate was of dimensions 25 mm x 25 mm x 30 μm . (Reprint from Laurs[11]).	1-9
Figure 1.3.2.2 Structure of the device suggested by Loi [13].	1-11
Figure 1.3.2.3 Cross-sectional view of the OPTs and the molecular structure of BPTT used by Noh [16].	1-12
Figure 1.4.1 Benzene ring with (a) π -orbitals and (b) effective electron ring.	1-16
Figure 1.4.1.1 Chemical structure of (a) pentacene and (b) polythiophene.	1-17
Figure 1.4.2 Chemical structure of some commonly used small molecules in OTFTs.	1-19
Figure 1.4.3 Chemical structure of some commonly used semiconducting polymers in the field of OTFT.	1-23
Figure 2.1.1 Chemical structure of P3HT with (a) head-to-tail and (b) head-to-head structure.	2-2
Figure 2.1.2 rr-P3HT films with a) edge on and b) flat on orientations of polymer chains.	2-2



Figure 2.2	Schematic diagram of three field-effect transistor configurations, (a) top gate bottom contact (TGBC), (b) bottom gate bottom contact (BGBC) and (c) bottom gate top contact (BGTC).	2-5
Figure 2.3.1	Energy levels of gold and P3HT.	2-7
Figure 2.3.2	Operation mode of FETs a) depletion mode and b) accumulation mode.	2-8
Figure 2.3.3	Transfer characteristics of a P3HT based OTFT.	2-11
Figure 2.3.4	(a-c) Schematic diagram of the basic operating regimes and current-voltage characteristics of a FET.	2-12
Figure 2.3.5	Output characteristics of a P3HT based OTFT.	2-15
Figure 2.4.1	Measurement system: Agilent 4156C analyzer and MBRAUN MB 10 compact glove box.	2-17
Figure 2.4.2	Probe station and LCD display for observing the OTFTs devices.	2-18
Figure 2.5	(a-d) Diagrams showing steps to prepare OTFTs with bottom-gate/bottom-contact structure.	2-19
Figure 2.5.1	(a-e) Diagrams showing steps to prepare OTFTs with top-gate-bottom-contact structure.	2-20
Figure 2.5.2	Transfer characteristics of P3HT based OTFTs.	2-22
Figure 2.5.3a	Transfer characteristics.	2-23
Figure 2.5.2b	Output characteristics.	2-23
Figure 2.6.1	Threshold voltage of samples for different annealing time.	2-24
Figure 2.6.2	Current ON/OFF ratio at different annealing time.	2-26
Figure 2.6.3	Charge-carrier mobility at different annealing time.	2-27
Figure 2.6.4	(a) Mobility against time and temperature; (b) $I_{ON/OFF}$ against time and temperature. (Reprint from G.M. Wang[31])	2-28



Figure 2.6.5	(a) Longer conjugation length, (b) twisted polymer chain with shorter conjugation length.	2-29
Figure 2.6.6	(a) AFM image of 100 °C annealed P3HT sample; (b) AFM image of 200 °C annealed P3HT samples.	2-29
Figure 2.7.1	Schematic diagram of oxygen doping in P3HT device.	2-30
Figure 2.7.2	Schematic diagram of the effect of moisture on P3HT device.	2-31
Figure 2.8.1	Cross-sectional view of a P3HT layer deposited on a glass substrate.	2-32
Figure 2.8.2	Conductance of P3HT sample at different annealing time.	2-33
Figure 2.8.3	Conductance of dedoped P3HT sample under exposure of oxygen.	2-34
Figure 2.8.4a	Conductance of dedoped P3HT sample exposed to air in the absence of light.	2-35
Figure 2.8.4b	Conductance of dedoped P3HT sample exposed to air under light exposure.	2-35
Figure 2.8.5	Conductance of dedoped P3HT sample in vacuum.	2-37
Figure 3.3.1	(a-c) Diagrams showing steps to prepare TiO ₂ /P3HT nanocomposite OPTs.	3-7
Figure 3.3.2	AFM image of (a) Pure P3HT and (b) P3HT:TiO ₂ (1:0.25) sample.	3-8
Figure 3.3.3	Schematic diagram of an OTFT incorporated with TiO ₂ nanoparticle in the device.	3-8
Figure 3.4.1	Transfer characteristics of OTFTs with different TiO ₂ concentrations.	3-9
Figure 3.4.2	Channel current of an OPT (weight ratio of P3HT:TiO ₂ is 1:0.75) measured at different drain voltages V _{DS} and V _{GS} =0V. The rising and falling edges of current correspond to switching on and off a white light illumination of 200μW/cm ² , respectively.	3-10
Figure 3.4.3	Energy band diagram of P3HT and TiO ₂ .	3-11



- Figure 3.4.4 Illustration diagram of electron trapping mechanism, (a) generation of exciton, (b) separation of exciton, and move to different directions and (c) electrons trapped on TiO₂ particles. 3-12
- Figure 3.4.5 Shift of the threshold voltage of the OPT (weight ratio of P3HT:TiO₂ is 1:0.75) calculated from the change of the channel current measured at different V_{DS}. 3-14
- Figure 3.4.6 Shift of the threshold voltage of the OPT (weight ratio of P3HT:TiO₂ is 1:0.75) illuminated with different light intensities and different wavelengths. V_{DS}= -10V. 3-16
- Figure 3.4.7 Absorbance of the P3HT/TiO₂ composite films. Along the arrow, from bottom to top, the weight ratio of P3HT:TiO₂ are 1:0, 1:0.25, 1:0.5, 1:0.75 and 1:1, respectively. 3-17
- Figure 3.4.8 Transfer characteristics of OPTs measured in different incident intensities with constant V_{DS} and V_{GS}. 3-18
- Figure 3.4.9 Illustration diagram of electron trapping mechanism, (a) generation of an exciton in TiO₂, (b) separation of an exciton, and move to different directions and (c) electrons trapped in TiO₂ particles. 3-19
- Figure 3.4.10 Shift of the threshold voltage of the OTFTs with different weight ratios of P3HT:TiO₂ measured under the white light illumination of 200μW/cm² and V_{DS}=-20V . From bottom to top, the weight ratios of P3HT:TiO₂ are 1:0, 1:0.05, 1:0.10, 1:0.25, 1:0.5, 1:0.75 and 1:1, respectively. 3-20
- Figure 3.4.11 AFM image of P3HT/TiO₂ sample with concentration (a) 1: 0.25 (b) 1: 0.50 (c) 1: 0.75 and (d) 1: 1. 3-21



- Figure 3.5.1 Shift of the threshold voltage of the OPT (weight ratio of P3HT:TiO₂ is 1:0.75) illuminated with different light intensities. $V_{DS}=V_{GS}= -10V$. 3-22
- Figure 3.5.2a SEM image of P3HT/TiO₂ (Rutile) sample in 1: 0.75 concentration. 3-24
- Figure 3.5.2b SEM image of P3HT/TiO₂ (Rutile and Anatase) sample in 1: 0.75 concentration. 3-24
- Figure 3.5.3a Shift of the threshold voltage of the OPT (weight ratio of P3HT:TiO₂ is 1:0.25) illuminated with different light intensities and different wavelengths. $V_{GS}=V_{DS}= -10V$. 3-25
- Figure 3.5.3b Shift of the threshold voltage of the OPT (weight ratio of P3HT:TiO₂ is 1:0.50) illuminated with different light intensities and different wavelengths. $V_{GS}=V_{DS}= -10V$. 3-25
- Figure 3.5.3c Shift of the threshold voltage of the OPT (weight ratio of P3HT:TiO₂ is 1:0.75) illuminated with different light intensities and different wavelengths. $V_{GS}=V_{DS}= -10V$. 3-26
- Figure 3.5.3d Shift of the threshold voltage of the OPT (weight ratio of P3HT:TiO₂ are 1:0.25, 1:0.50 and 1:0.75) illuminated with different light intensities at 530nm wavelengths. $V_{GS}=V_{DS}= -10V$. 3-26
- Figure 3.5.11 Time-resolved response of the P3HT/TiO₂ (1:0.75) phototransistor upon irradiation with 1.7 mW/cm² at $V_{GS}=V_{DS}=-10$ V. 3-28
- Figure 3.5.12 Time-resolved response of the phototransistor upon irradiation with 191 mW/cm² at $V_G=V_D=-10$ V. The photo switching of the drain current is reversible with a relaxation time of 10.3 s. Device structure is shown on the right. (Reprinted from Saragi[43]). 3-28



- Figure 4.2.1.1 Diagrams showing steps to prepare OTFTs incorporated with DNA layer in the devices. The thickness of SiO₂ is 500nm. The channel width and length of the OTFTs are 2 mm and 0.2mm, respectively. 4-5
- Figure 4.2.2.1 Florescence images of gold electrodes after the hybridization of DNA. 4-7
- Figure 4.3.1 Performance of the OTFTs with probe immobilized on Au source/drain electrodes for 4 hours. (a) Transfer characteristics of three OTFTS (control, ssDNA and dsDNA). V_{DS} = -40V. (b) Output characteristics of three OTFTs (control, ssDNA and dsDNA). For each device (different colours corresponds to different devices), from top to bottom, the curves are measured at the V_{GS} of -40V, -30V -20V, -10V and 0V, respectively. 4-11
- Figure 4.3.2 Performance of the OTFTs with probe immobilized on Au source/drain electrodes for 48 hours. (a) Transfer characteristics of three OTFTS (control, ssDNA and dsDNA). V_{DS} = -40V. (b) Output characteristics of three OTFTs (control, ssDNA and dsDNA). For each device (different colours correspond to different devices), from top to bottom, the curves are measured at the V_{GS} of -40V, -30V -20V, -10V and 0V, respectively. 4-13
- Figure 4.3.3 Field effect mobilities of the OTFTs with ssDNA and dsDNA layers immobilized on Au source/drain electrodes as a function of immobilization time t (t = 4, 8, 24, 48 hours) of DNA probe and t = 0 corresponds to the control sample. 4-15
- Figure 4.3.4 Diagrams of OTFT and equivalent circuit of (a) control sample, (b) ssDNA sample and (c) dsDNA sample. 4-18



List of Table Captions

	<u>Page</u>
Table 2.6.1 Sulfur and oxygen concentration of P3HT sample at different annealing conditions.(Reprint from Hoshino[30]).	2-25
Table 3.4.1 Device performance of TiO ₂ /P3HT OPTs with different TiO ₂ concentrations.	3-9



Chapter One

Introduction

1.1 History of Field Effect Transistor

The concept of field-effect controlled current was first introduced by J.E. Lilienfeld[1] in 1930 which was used to replace vacuum tubes by solid-state devices in amplifiers. After thirty years, this concept was realized by a silicon-based metal-oxide semiconductor field-effect transistor (MOSFET).[2] Compared to vacuum tube, solid-state MOSFET enjoys the benefits of higher stability and being able to reduce its dimension without altering performance. These unique properties enable the feasibility of combining a number of semiconducting devices into a single chip, thus open up the door for development of integrated circuit (IC). With the aid of rapid development in silicon technology over the past 30 years, semiconductor devices have scaled down to ever smaller dimensions, resulting directly in a constant increase in the number of components per chip and thus scaling down the sizes of electronic equipment. Nowadays, because of the increasing demand of personal electronic device, MOSFET, as a key component of IC, is omnipresence in our environment. Millions of them are located in the



processors that equipped personal computers and other mobile microelectronic devices.

Apart from commercial application, field-effect transistor also serves as an important tool for studying charge transport in solid materials. In particular, it gives direct access to charge mobility. For this issue, low-mobility materials, such as hydrogenated amorphous silicon (a-Si:H)[3], are employed to demonstrate the electric field-induced effect. Address to this purpose, alternative geometry, named thin film transistor (TFT)[4] is used. Conducting channel of conventional MOSFET is constituted by an inversion layer. Contrary to that, conducting channel in TFT is based on an accumulation layer. It is only later that the technological interest of a-Si:H TFTs emerges, when applications where large area is needed appear. Today, a-Si:H TFTs are mainly used in active matrix liquid crystal displays (AM-LCD).

1.2 Organic Thin Film Transistor

The first organic semiconductor was discovered at the late 1940s[5]. However, apart from a very small number of preliminary work on conjugated small molecules and polymers, the first organic semiconductor based transistor was only reported in



1986[6], with a device made on a polythiophene film grown by electrochemical method. Polythiophene belongs to the family of conducting polymers that was discovered in the late 1970s. Ever since the first polymer and small molecule semiconductor thin film transistor was reported, interest in this field has risen steadily for both technological and scientific reasons. The numbers of scientific publications in the field of organic transistors keep increasing, based on the information of the Institute for Scientific Information (ISI) Web of Science, there are 327 publications on organic transistors in 2007, a significant increase compared to 296 in 2006 and 234 in 2005 (Figure 1.2).

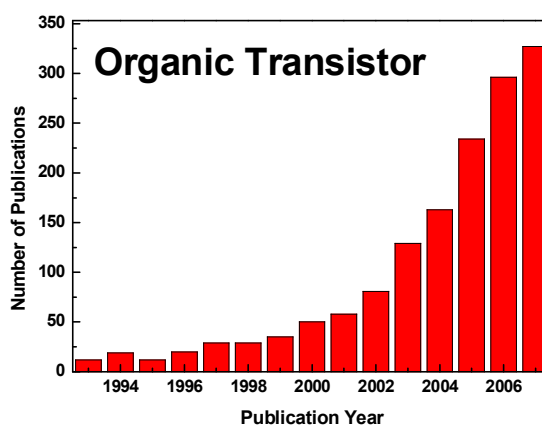


Figure 1.2 Number of publications on organic field-effect transistors over the past few years as counted by the Institute for Scientific Information (ISI) Web of Science.

The reasons for this surge of interest are manifold. The performance of organic thin film transistor (OTFT), which is generally benchmarked against that of a-Si



MOSFET with field-effect mobilities of 0.5-1 cm^2/Vs and ON/OFF current ratios of 10^6 - 10^8 , has improved significantly. Currently, the recorded mobility (μ) values for thin-film OTFTs are 35 cm^2/Vs [7] in the case of vacuum-deposited small molecules and 0.6 cm^2/Vs [8] for solution-processed polymers. Comparing to inorganic thin film transistors, OTFTs have the advantages that the devices can be fabricated at low or even room temperature, whereas several hundred degree Celsius is required for inorganic counterparts. For this reason, inorganic device may not be able to be fabricated on plastic substrate, and additional manufacturing cost is required for high temperature equipment. Besides, one of the most technological attractions is that all the layers of an OTFT including electrode, semiconducting layer and insulating layer are solution processible. By employing low-cost solution processing and direct-write printing method, it is possible to realize large area electronic functions on flexible substrate with low fabrication cost and multi-function devices in one chip can be achieved. As a result, there is now a serious level of industrial interest in using OTFTs for the applications that are currently incompatible with the use of a-Si or other inorganic transistor technologies.



1.3 Application of Organic Field Effect Transistor

1.3.1 Organic Electronics

Along with the increase of human development, more and more natural environments were polluted by lots of industrial and domestic waste. A large number of forests were chopped and rivers were polluted by manufacturing papers for human civilized activities, research on environmental protection becomes much more important. Since most of the materials involved in OTFTs are environmental friendly, and it is possible to fabricate OTFTs on flexible plastic substrates, the first possible application of OTFTs within the next three to five years is flexible, active-matrix electronic-paper displays, for which impressive demonstrations have been developed recently[9, 10] (Figure 1.3.1.1). Although mobility of OTFTs is still insufficient for displaying moving pictures, it can serve the purpose well as handling still text information. Besides the benefit of light weight and flexibility, OTFTs based electronic-paper can be integrated with memory technology that has been rapidly developed for large information storage and thus is a potential candidate for replacing paper prepared by wood chips in the future, which can alleviate the critical pollution problems.

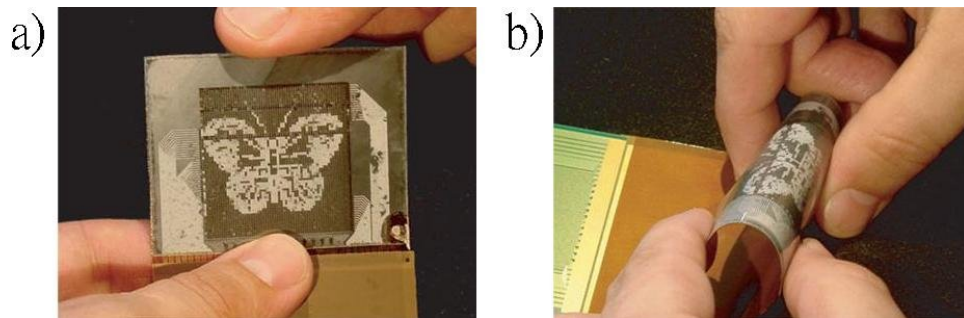


Figure 1.3.1.1 a) The 3.5 cm by 3.5 cm organic display has 64×64 pixels. Pixel size is $540 \times 540 \mu\text{m}^2$. b) Organic e-paper bent to a radius of curvature of ≈ 1 cm [10].

Because of the increasing business trading around the world, raw materials, semi-products and products were shipped around different countries, which involve complicated logistic problems in handling materials storage and arrangement. Conventionally, counting materials relied on manual counting or by scanning the bar code attached on the materials using a bar code scanner, it not only consumed a lot of time, but also was inaccurate when large area required to be covered. To address this problem, radio frequency identification (RFID) tag was invented. A RFID tag is an object that can be applied to or incorporated into a product, animal, or person for the purpose of identification using radio waves. Some tags can be read from several meters away and beyond the line of sight of the reader by emitting radio frequency. Most RFID tags contain at least two parts. One is an integrated circuit for storing and processing information, modulating and demodulating a (RF) signal, and other specialized functions. The second is an antenna for receiving and



transmitting the signal. Once the products are tagged by a RFID tag, all necessary information for numerous products can be reached easily by operator with a RF reader, which simplifies the counting process and improves the efficiency of materials management.

However, one serious drawback is that the fabrication cost for RFID is expensive. If larger number of products needs to be handled, the additional cost for installing RFID tag will increase the management cost a lot which obstructs the use of RFID in logistic field. To deal with the high fabrication cost of RFID, OTFT may be the possible solution. OTFT is solution-processible, low cost and can be fabricated on large area flexible substrates. Therefore, RFID based on OTFT technology is flexible and inexpensive, and large number of them can be installed at low cost on a wide range of objects.

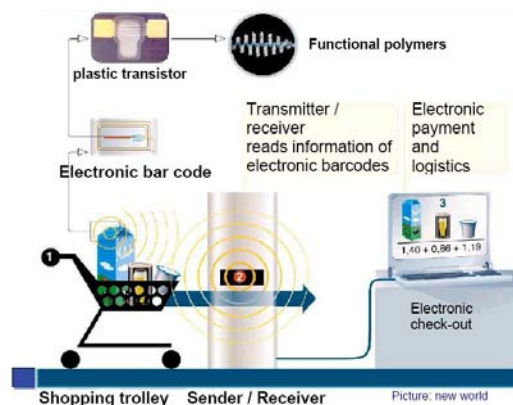


Figure 1.3.1.2 Future applications for new electronics will greatly interest logistics [9].



1.3.2 OTFT Based Sensor

Besides the applications on flexible displays and RFID tags, organic sensors based on OTFTs also draw a lot of research interest. In principle, with respect to the silicon based structures, organic field effect sensors have several advantages, as the low cost of the technology and the possibility to achieve mechanically flexible structures but on the other hand still require high voltages to give measurable currents. Nevertheless, this issue is less relevant, as the mobility of organic semiconductors is continuously increasing towards values comparable with those of amorphous silicon, and high dielectric constant polymers have been extensively studied, making it possible to have, in the near future, flexible organic devices working at low voltages. Therefore shortly after the first working OTFT proposed in 1986[6], researchers start to study OTFT based sensors in the late eighties.

One of the impressive work reported in 1987 by Laurs[11] demonstrated that the performance of organic OTFT varies subjected to oxidizing gases (Figure 1.3.2.1).

Phthalocyanines (Pcs) thin film was deposited on a quartz substrate by vacuum evaporation with gold source and drain electrode. Field effect, photoconductivity and surface electrical conductivity have an order of magnitude change when



exposed to oxygen, iodine or bromine gas, this reversible behavior was caused by charge trapping during gas adsorption. Few years later, a group of Japanese scientists reported a poly(3-hexylthiophene) (P3HT) based OTFT having high sensitivity towards NH_3 [12]. It was observed that mobility and conductivity change by two orders of magnitude. Most of the changes are reversible, and the longer the film stays in the ammonia, the less reversible are the changes. For a short period of time (15–20 min) the effect is 100% reversible after thermal annealing under vacuum condition. Also device performances decrease more rapidly for the sample stored in air than that stored in vacuum, which is due to the gas absorption.

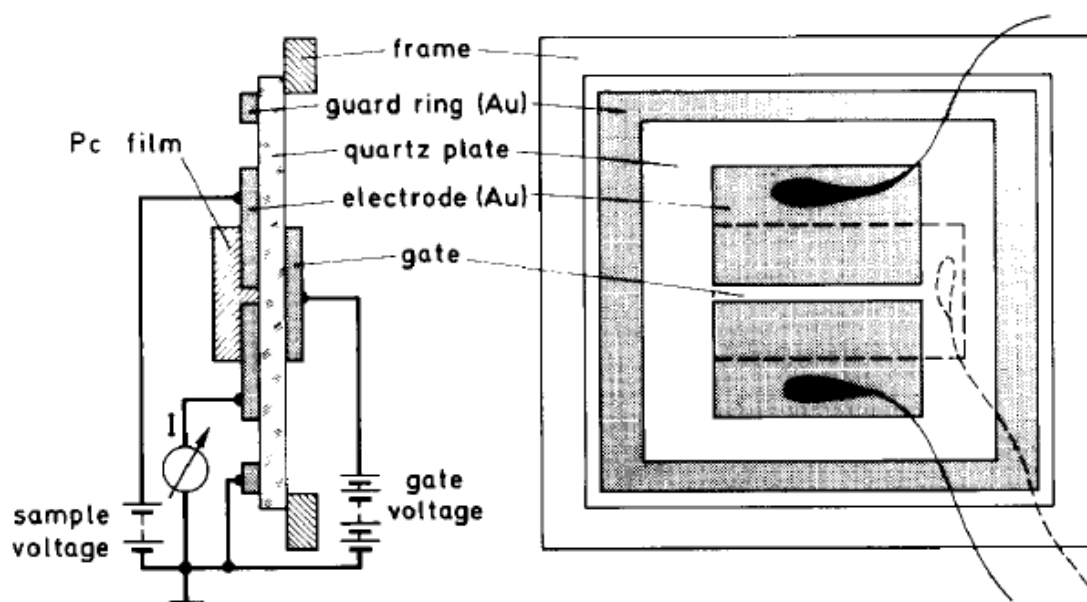


Figure 1.3.2.1 Arrangement for the field effect measurements. The gap between the electrodes was 0.2 mm x 4 mm and the quartz plate was of dimensions 25 mm x 25 mm x 30 μm . (Reprint from Laurs[11]).



Apart from gas sensing properties, Loi[13] fabricated a pentacene based Ion sensitive OTFTs (ISOTFT) with flexible MylarTM as an insulating layer (Figure 1.3.2.2). It shows a decrease of the channel current with basic solutions and an increase with acidic solutions which is due to the accumulation of ions at the interface between the insulating layer and the solution. This work successfully showed that ISOTFT fabricated on plastic substrates could open the way to the fabrication of flexible devices for solution monitoring and other innovative applications, such as smart food packages, which are not possible at present for silicon based devices. Another chemical sensor is reported by Torsi in 2004[14]. Poly -(3,3''-dipentoxy-2,2':5',2''-terthiophene) (poly -DPOT) was dissolved into chloroform and spin-coated on a silicon dioxide wafer with gold source and drain electrodes. Since the adsorption of the analyte will cause an enhancement of the potential barrier at the boundaries between the grains, lower channel current can be observed. This poly-DPOT device shows very fast and reversible responses to 1-hexanol and ethanol molecules, and the best extrapolated sensitivities are as good as 0.7 ng/ppm.

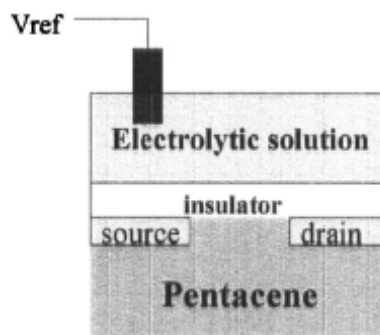


Figure 1.3.2.2 Structure of the device suggested by Loi[13].

Organic semiconducting polymers show large absorption properties for ultraviolet (UV) and visible light, and high efficiency of photo-current generation, thus organic phototransistors (OPTs) are considered to be one of the feasible applications of OTFTs. Without the noise increment associated with avalanche photodiodes, light detection and signal amplification can be carried out in a single phototransistor as an optical transducer. Once the sensitivity and reactivity of OPTs come close to its inorganic counterpart, such devices would be expected to be essential components for a receiver in optical telecommunication systems due to the solution processibility and the potential for large area integrated circuits. A group of Korean scientists showed a UV sensitive OPT in 2005[15]. 2,5-bis-biphenyl-4-yl-thieno[3,2-b]thiophene (BPTT) thin films were vacuum deposited on the SiO₂ surface of a heavily doped silicon wafer followed by the



deposition of gold source and drain electrodes (Figure 1.3.2.3). The device showed photosensitivity and $I_{\text{Ph}} / I_{\text{Dark}}$ of 82 A/W and 2.03×10^5 , respectively. Moreover, the BPTT FETs showed a high UV stability even after 6 h of strong irradiation with an intensity of 50 mW/cm^2 . Shortly after the report of this BPTT based UV sensor, the same group of scientists reported a red light OPT based on pentacene[16]. This pentacene TFTs showed an efficient photo-current response under various intensities of both modulated and continuous red light. Due to the relatively small bandgap of pentacene, it showed a reliable high responsivity of $\sim 1 \text{ A/W}$ and the ratio of photocurrent to dark current ($I_{\text{Ph}}/I_{\text{Dark}}$) was 9000 under visible light at a wavelength of 650 nm.

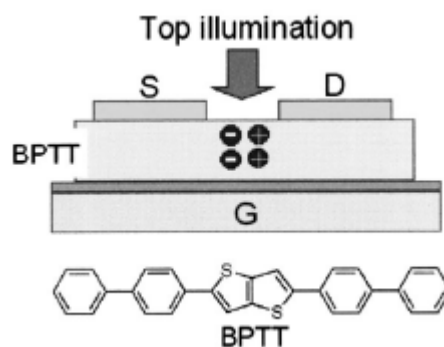


Figure 1.3.2.3 Cross-sectional view of the OPTs and the molecular structure of BPTT used by Noh [16].

Detecting small quantities of bio-molecules is paramount in the diagnosis of disease, drug discovery, and basic researches. Compared with the other techniques, genetic



FET has the advantage of being able to be miniaturized without losing signal to noise ratio since the channel current of a FET is proportional to the width/length ratio of the channel and not related to the area of the device. Therefore FET is ideal for the application in small-sized, high-density and multi-functional micro-array sensors.

Soon after the first OTFT based sensor was discovered in 1986, an immunological FET (immunoFET) was proposed by Schasfoort[17] in 1990. This immunoFET was constituted of an inorganic ion sensitive field effect transistor (ISFET) with a protein membrane covered on the gate electrode. That membrane was fabricated by incubating HSA antigen into a polystyrene-agarose thin film. When the device is placed into a sample solution containing α HSA antibody, HSA and α HSA form an antibody-antigen complexes, resulting in a transient membrane potential, which is measured by the ISFET. By observing the change of ISFET channel current induced by the variation of gate potential, concentration of α HSA can be characterized. After that, a number of biosensors were introduced with similar sensing mechanism. Dzyadevich[18] introduced a glucose-sensitive enzyme field effect transistor (ENFETs) and two ISFETs were employed as the sensing and control devices,



respectively. By comparing the signal difference between these two devices, glucose concentration can be determined. Due to the rapid development of Desoxyribo Nucleic Acid (DNA) technology, fast, low-cost and miniaturized detection methods of DNA molecules are required for both biotechnology and medical diagnostics and scientists start to develop OTFT based DNA sensors. Zhang[19] reported an OTFT based DNA sensor in 2007. A heavy doped silicon wafer with 100nm thick SiO₂ film was employed as a substrate, where doped Si served as a gate electrode while SiO₂ served as a dielectric layer. After the wafer was sonicated by acetone and IPA, two separated 100nm thick gold electrodes were evaporated onto the SiO₂ surface as the source and drain electrodes. Pentacene thin film as the active layer was deposited on the clean SiO₂ wafer by vacuum evaporation. Immobilization of single-stranded DNA (ssDNA) onto the pentacene layer was done by placing the pentacene device into an ssDNA buffer solution. When this ssDNA immobilized OTFT was exposed to double-stranded DNA (dsDNA), hybridization of ssDNA and dsDNA occurred, whereas electron-withdrawing nature of the phosphate groups within the DNA backbone resulted in a positive shift of threshold voltage V_{TH} . By measuring the V_{TH} shift, the dsDNA concentration could be decided.



1.4 Organic Semiconducting Materials

Organic semiconducting molecules are highly conjugated in nature, which means single and double bonds are regularly alternated in the material, accompanied by delocalization of the out-of-plane π electrons in the same molecule. For example, pentacene, which is one of the most widely used material in the field of organic electronics, is formed by five fused hexagonal benzene rings with six alternated single and double bonds inside. Inside the benzene ring, each carbon atom is connected to two other carbon atoms and a hydrogen atom (Figure 1.4.1a), which is similar to the sp^2 -hybridization in an ethylene molecule. The σ bonds of the hexagonal ring are formed by overlapping of two sp^2 orbitals of each carbon atom with the similar orbitals of the adjacent carbon atoms. Whereas C-H σ bond is formed by overlapping of the third sp^2 orbital of each carbon with 1s orbital of a hydrogen. Perpendicular to the plane of these three σ bonds at each carbon is a p orbital which contains the fourth valence electron. The p orbitals on all six carbon atoms can overlap laterally to form a π orbital that creates a ring or cloud of free electrons above and below the plane of the ring (Figure 1.4.1b). Therefore, electrons participating in σ -bonds are considered stationary, whereas along a conjugated path π - electrons are delocalized and regarded as mobile electrons that are free to move.



Semiconducting properties of pentacene are thus constituted by the mobile electrons.

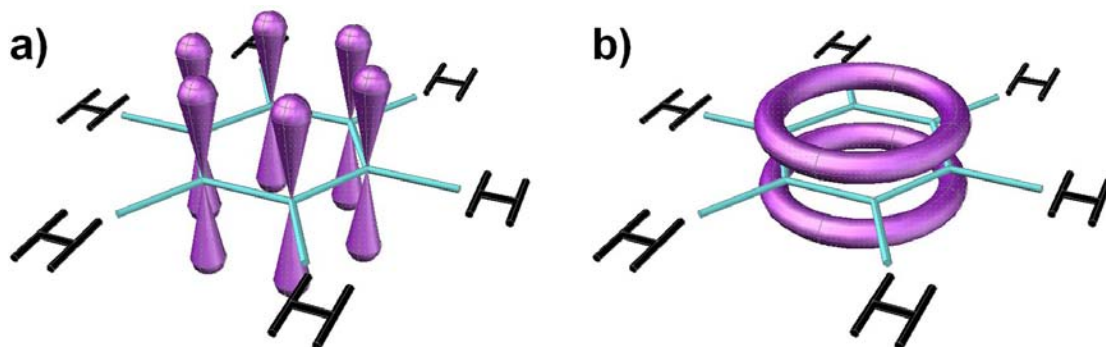


Figure 1.4.1 Benzene ring with a) π -orbitals and b) effective electron ring.

Analogous to the energy band theory used in inorganic semiconductor, a similar system is used to describe the electronic structure for organic semiconductor materials. Due to the much weaker bond strength of π -bonds than σ -bonds, electron transition from a bonding π orbital to an anti-bonding π^* orbital represent the lowest excited state of a conjugated system. This electron transition shares the same concept as inorganic semiconductor which classifies the lowest excited state as the first electron jump from valence band towards conduction band. When compared to inorganic system, the highest occupied molecular orbital (HOMO) in organic system is equivalent to the valence band, whereas the lowest unoccupied molecular orbit (LUMO) the conduction band. The delocalization of electrons across many



π -orbitals results in a split of molecular orbital energy levels to form a spread of energy levels comparable to the energy bands in inorganic materials. As a result, energy required for delocalization of an electron from HOMO level to LUMO level represents the bandgap (E_g) as in inorganic cases.

1.4.1 Classification of Organic Semiconducting Materials

Organic semiconductor can be classified into two main classes, which is low molecular weight materials (small molecules), such as pentacene (Figure 1.4.1.1a), and semiconducting polymer. One of the most widely used semiconducting polymers is polythiophene (Figure 1.4.1.1b). As shown in Figure 1.4.1.1, alternating single and double bonds were clearly show in both pentacene and polythiophene, meaning a conjugated π -electron system was located in both pentacene and polythiophene, giving rise to their semiconductive properties.

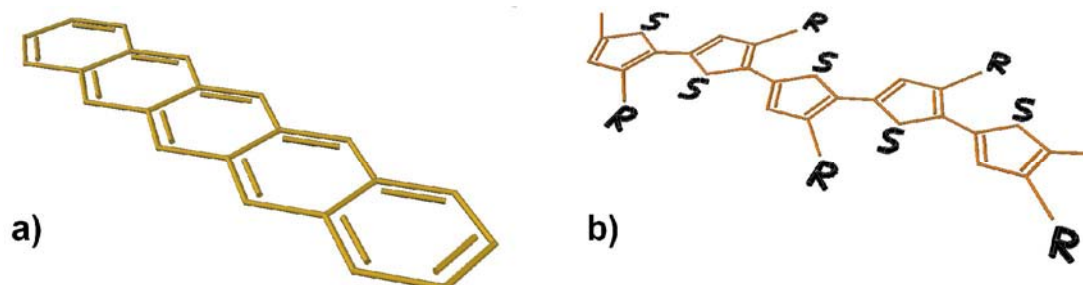


Figure 1.4.1.1 chemical structure of a) pentacene and b) polythiophene.



Besides chemical classification, semiconducting materials can be divided into two groups according to their electrical properties. In the field of inorganic semiconductor, materials are divided into two types, one is *n*-type semiconductor which constituted by doping the solid with certain amount of donor species such that mobilized electrons were provided. On the other hand, when acceptor species were doped, holes were introduced into the material which named as *p*-type. However *n*- and *p*-type organic semiconductors do not cover the same concept, since classification does not depend on the doping species as in inorganic ones. In organic semiconductor, the notion actually covers two different concepts. First, an organic semiconductor is said to be *n*- or *p*-type depend on whether electrons or hole transportation is preferred, that is, one of the electric charge carriers mobility is substantially higher than the other one. These semiconductors are frequently termed electron transport or hole transport materials in the field of organic light-emitting diodes. The second concept refers to charge injection which is now widely accepted than the pervious one. Accordingly, electrons injection is much easier than hole injection in the case of *n*-type materials, while hole injection is preferred for *p*-type. In the scene of energy scheme, an *n*-type semiconductor is characterized by high electron affinity, while the *p*-type semiconductor presents low ionization potential.



Unlike conventional semiconductors, where *n*- or *p*-type semiconducting properties depend on the dopant nature only, organic semiconductor actually depends on the electrode work function. Since the work function of metals is limited in a narrow energy range, many organic compounds will only show electron injection or hole injection, which classified as *n*-type or *p*-type semiconductor. Since the number of *p*-type materials is higher when compared to *n*-type, *p*-type materials will be discussed first.

1.4.2 *p*-Type Small Molecules

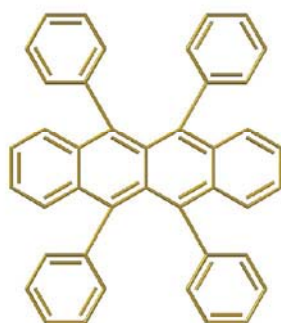
 **α -5T****Tetracene****Rubrene****Pentacene**

Figure 1.4.2 Chemical structure of some commonly used small molecules in OTFTs.



A number of small molecules have been synthesized in the past thirty years, such as BP2T, α -5T, DB-TTF, pentacene, tetracene, 5-chlorotetracene and rubrene (Figure 1.4.2). At present, most of the small molecular devices are fabricated by pentacene or oligothiophenes and their derivatives. Highest mobility now reaches $35 \text{ cm}^2/\text{Vs}$ for pentacene[7] and $1 \text{ cm}^2/\text{Vs}$ for sexithiophene[20]. In the case of pentacene, the five fused benzene rings (Figure 1.4.1a) not only provide a big and continuous π orbital cloud, but also the highly orientated chemical structure resulting in strong crystalline packing in thin films. Strong π overlap between adjacent molecules is found due to the high order crystallization, thus enhances efficient hopping of carriers and results in the highest field effect mobility observed in organic semiconductor thin films. Small molecules shown in Figure 1.4.2 contain clear alternating single and double bonds without side functional groups, which result in high crystallization order of the deposited thin films. Thus higher charge carrier mobility can be achieved compared to the less ordered polymer based devices. Although high mobility can be achieved due to this clear structure, some drawbacks appear. Structure without any side functional groups makes it insoluble in any kinds of organic chemicals. One of the most valuable properties for organic electronic devices is the ability to employ low-cost solution process such as spin



coating, dip coating or printing techniques. However, these small molecules used today are insoluble due to the lack of side functional group, therefore solution process is not possible whereas expensive evaporation and sublimation method are the only options.

Some improvement was done to increase the small molecule device mobility by modifying the insulator-semiconductor interface. Oxide, mainly silicon dioxide, is employed as an insulator for OTFTs. Small molecule vapor is deposited on this oxide layer directly during deposition process. However, due to the dissimilar physical nature of the two media, poor device performance appears because of the highly disorder interface. Conventionally, this problem can be solved by increasing the substrate temperature or depositing the organic film in a slower deposition rate, thus better organization could be achieved. With the aid of chemical engineering, an alternative method is developed. The oxide surface is modified by coating an ultrathin organic monomolecular layer before the vacuum deposition of semiconductor. The self-assembled monolayers (SAM) technique can serve this proposed modification well. Octadecyltrichlorosilane (OTS) and hexamethyldisilazane (HMDS) are the most commonly used SAM to deal with SiO₂,



and positive results have been shown[21, 22].

After a series of efforts that have been done in the field of chemical engineering, small molecule organic semiconductors gain a limited ability to be solution processible by the attachment of flexible side chains onto their main chains. The requirement of side-chain design is rigorous, such that it can impart adequate solubility and film-forming properties without affecting the ability of the molecule to π -stack. Katz[23] reported a solution processed device based on side-chain-substituted small molecule (dihexylanthradithiophene) with a mobility of 0.01–0.02 cm²/Vs, which is still lower than some semiconducting polymers. In addition, aggregation and crystallization of the molecules in the solution may occur if the growth conditions have not been controlled carefully and the non-uniform thin films will show some problems of connectivity and grain orientation.

1.4.3 *p*-Type Polymer

F8T2

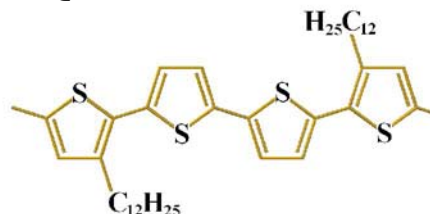
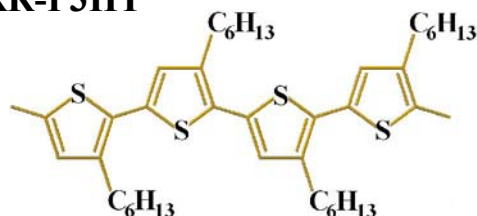
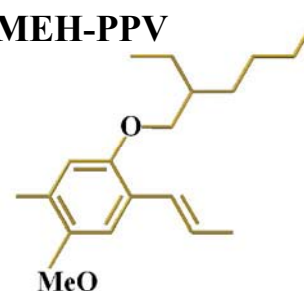
PQT-12

RR-P3HT

MEH-PPV


Figure 1.4.3 Chemical structure of some commonly used semiconducting polymers in the field of OTFT.

Similar to semiconducting small molecules, a number of semiconducting polymers were found for the use of organic electronics. Polymers such as F8T2, PQT-12, RR-P3HT, MEH-PPV and their derivatives are widely employed in the OTFTs field, with the aid of functional side group, all of them show good solubility in organic solvents such as chloroform, toluene and xylene etc, therefore low-cost solution process can be employed instead of expensive evaporation method. P3HT will be taken as an example as it is one of the most widely used materials. A number of researchers have shown that P3HT based OTFT can now achieve a high carrier mobility which is close to a-Si TFTs. For example, Sirringhaus[24] reported a P3HT



based OTFT. P3HT was first dissolve in chloroform and spin coated onto a SiO₂/Si substrate. A high field-effect mobilities of 0.1–0.3 cm²/Vs has been achieved. As shown in Figure 1.4.3, P3HT contains two-dimensional conjugated layers with strong π – π interchain interactions separated by layers of soluble and insulating side chains. With this chemical structure, highly microcrystalline and anisotropic lamellar microstructure can be achieved. This microstructure results in a fast and efficient in-plane charge transport which contributes to the relatively high carrier mobility. However, P3HT can be easily oxidized by air, which is common for all *p*-type semiconducting polymers with low ionization potentials (typically less than 4.9–5.0eV), OTFTs based on P3HT normally show a large positive shift of threshold voltage after being exposed to air. As a result, the response of threshold voltage towards air enables the possibility for such *p*-type materials to constitute a gas sensor.

1.4.4 *n*-Type Semiconductor

n-type organic semiconductors are rare compared to *p*-type organic semiconductors, which mean most of the OTFT devices only show hole accumulation at the semiconductor-dielectric interface instead of electron transport



in the conduction channel. The reason is that most of the source/drain materials employed have high work functions, which close to the HOMO level and hence prefer hole injection rather than electron injection. However, in order to replace the inorganic complementary logic circuits with organic ones, *n*-type OTFT is needed. Also, *n*-type materials are required in the field of organic solar cell to provide depletion region between *p-n* junctions for the conversion of solar energy to electrical energy. Therefore, the study of high electron affinity *n*-type organic materials becomes extremely important. Recently, several OTFTs with electron field-effect conduction have been reported. Both vacuum evaporation and solution-processed method were employed to deposit these organic semiconductors with relatively high electron affinity ($EA > 3.5$ eV) [33].

Recently, fullerene C_{60} and *N,N'*-dialkyl-3,4,9,10-perylene tetracarboxylic diimide derivatives are the most famous *n*-type organic semiconductors. Most of them show high charge carrier mobility up to 0.5 cm^2/Vs which is analogous to *p*-type materials like P3HT and PPV. Several *n*-type OTFTs have also been reported. Babel[25] reported a solution-processed poly(benzobisimidazobenzophenanthroline) (BBL) OTFT with high electron mobility up to 0.03 – 0.1 $\text{cm}^2/\text{V s}$. Due to an



electron affinity of 4.0–4.4 eV, this bottom-gate configured OTFT shows good stability during measurement in air. Another solution-processed *n*-type OTFT was reported by Facchetti[26] in 2004, a diperfluorohexyl-substituted quinque- and quaterthiophene thin film was deposited on a HMDS-treated SiO₂/Si substrate, electron mobility up to $4\text{--}8 \times 10^{-4} \text{ cm}^2/\text{Vs}$ was achieved. However relatively low electron affinity (2.8–2.9 eV) of the fluoroalkyl- substituted thiophene molecules leads to an electron trapping problem, which is directly reflected in the high threshold voltage (>25V) in this device. Waldauf[27] also showed a *n*-type OTFT which was based on methanofullerene phenyl C61-butyric acid methyl ester (PCBM). Bottom-gate structure with organic dielectric and calcium source/drain electrodes was used, and field-effect mobility of $3\text{--}4 \times 10^{-3} \text{ cm}^2/\text{Vs}$ was achieved.



1.4.5 Insulating Dielectric Layer

Apart from semiconducting layer, dielectric layer also plays an important role in a transistor device, because both charge accumulation and transport process in the transistor takes place near the dielectric-semiconductor interface. Therefore, device performance is greatly affected by the properties of interface and the dielectric layer. Device parameters such as mobility and threshold voltage depend not only on the nature of the semiconductor but also on the chemical structure and dielectric properties of the insulator.

There are a number of strict requirements for dielectric materials which can be employed as an insulating layer for FET. First of all, high dielectric breakdown strength is required to avoid dielectric breakdown which limits operation voltage. Second, impurity concentration should be minimized, otherwise charge trapping in these impurities will lead to an unstable threshold voltage. Also, as discussed before, charge accumulation occurs near the dielectric-semiconductor interface, dielectric layer especially for bottom gate configuration should have a very low surface roughness, otherwise transition of charge carrier will be greatly affected. Besides, in order to stabilize the device, and lower its manufacturing cost, the dielectric



material should also be environmentally stable, easily processible, and compatible with preceding and subsequent processing steps. Apart from the above basic requirements, another important requirement for the dielectric layer is high dielectric constant ϵ (also named k), since capacitance of a dielectric layer with thickness d and area A equals to $\epsilon\epsilon_0 A/d$, which represents the amount of charge that can be induced by an applied gate voltage V_{GS} .

Silicon dioxide (SiO_2) with dielectric constant of 3.9 and electric strength in the order of 10^7 V/cm makes it suitable as a dielectric layer in transistor. With the aid of silicon technology, material properties and processing condition of SiO_2 are well known. SiO_2 with well controlled surface roughness and thickness can be achieved by thermal growth on silicon wafer, hence heavy doped silicon wafer with thin SiO_2 is conventionally employed as substrate, gate electrode and dielectric layer for transistor purpose. However, as discussed before, because of the rapid development of IC technology, device size for each component keeps reducing thus capacitance for each transistor decreases as area is reduced. In order to achieve a certain amount of charges in the transistor channel with reasonable operation voltage, two approaches were used. First approach is to reduce the dielectric thickness, thus



more charge can be induced without changing the materials nature. However, reduction of layer thickness not only increases the applied electric field strength which limits the maximum applied voltage to avoid dielectric breakdown, but also raises the leakage problem that makes the device no longer suitable for use. Another approach for this issue is to increase the dielectric constant, capacitance per unit area increases for each device with the use of high-k materials, such that leakage problem can be avoided since thickness no longer needs to be reduced to increase capacitance. Recently, high-k materials such as Al_2O_3 ($\epsilon=10$), Ta_2O_5 ($\epsilon=25$) and TiO_2 ($\epsilon=20-41$) have also been investigated for the application as gate dielectric of transistor. However all of them include SiO_2 and other oxides suffer from high temperature process and poor flexibility, which makes it impossible for the application in flexible electronics.

Another option to solve this problem is to replace inorganic materials with organic insulating polymers. Polymers can be processed from solution and thus do not require high temperature processing. In addition, their chemical structures can be changed to achieve a wide range of properties for different purposes. Therefore, insulating polymers, such as Poly(methyl methacrylate) (PMMA) ($\epsilon= 3.5$, similar to



SiO₂), Polyvinylpyrrolidone (PVP) ($\epsilon= 4.5$), high-k polymer Poly(vinylidene fluoride) (PVDF) ($\epsilon= 8$) and cyanoethylpullulan (CyEP) ($\epsilon= 12$), have drawn a lot of research attention for their easy processing and relatively high dielectric constant to replace inorganic oxide. Besides, high-k oxide nanoparticles can be mixed with those insulating polymers to form 0-3 nanocomposites which further increase their k values whereas solution processability remains.

Chapter Two

Fabrication of P3HT OTFT

2.1 P3HT: semiconducting polymer

Poly (3-hexylthiophene) (P3HT) is employed in our experiment as the semiconducting active layer. P3HT with greater than 98.5% regioregularity is purchased from Sigma-Aldrich without further purification. After the pioneering work of Sirringhus and coworkers[28], it is now well established that the performance of polymer OTFTs crucially depends on the chemical and structural ordering of the polymer. High order first depends on the regioregularity of the polymer; that is, the percentage of regioregular head-to-tail attachment of the alkyl side chains to the beta position of the thiophene rings. Figure 2.1.1 shows both of the head-to-tail (Figure 2.1.1a) and head-to-head (Figure 2.1.1b) structure of P3HT polymer. It is believed that high order of regioregularity in head-to-tail structure contributes to higher charge mobility because of the better polymer chain packaging, which in other words, higher crystallinity.

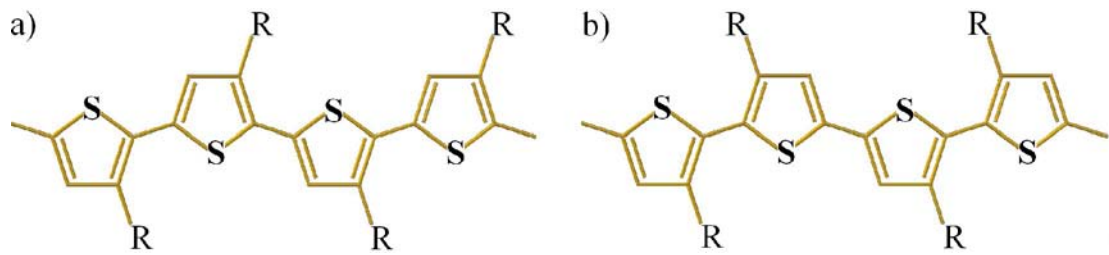


Figure 2.1.1 Chemical structure of P3HT with **a)** head-to-tail and **b)** head-to-head structure.

Comparatively high mobility can be achieved by P3HT because of the high order of crystallinity and strong inter-chain interaction, such that charge carriers are no longer confined to a single chain. However, besides the high degree of crystallinity, orientation of the lamellar structure also plays an important role in the charge transfer. The work by the Cambridge group[29] showed that two orientations could be found in P3HT films, one with the polymer chains edge on the surface (Figure 2.1.2a), and the other one with the chains flat on (Figure 2.1.2b).

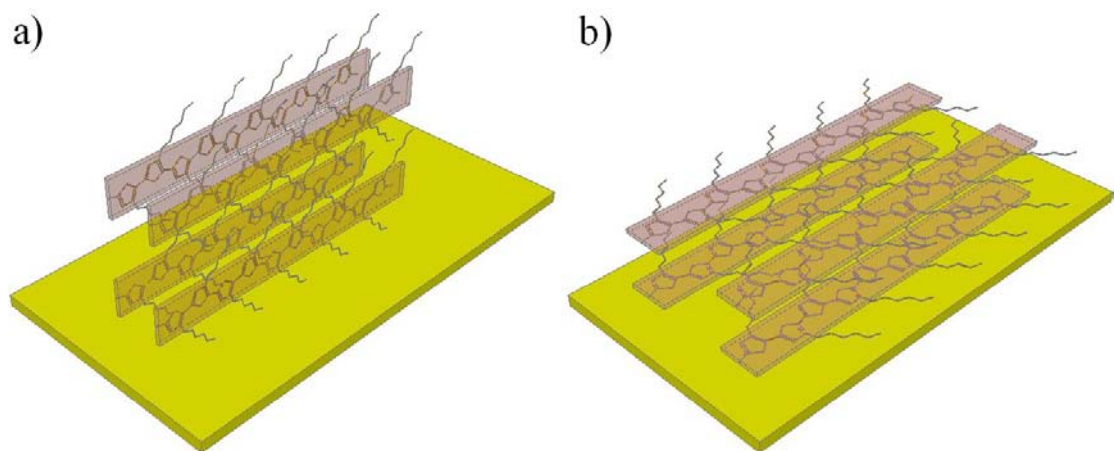


Figure 2.1.2 rr-P3HT films with a) edge on and b) flat on orientations of polymer chains.

The first orientation with polymer chains edge on the substrate is believed to have better performance, since conjugated rings are perpendicular to the transport direction, therefore charge carrier transports across the π - π stacking direction from the source to drain electrode, and hence advance the charge mobility of the device. OTFTs with mobility up to $0.1 \text{ cm}^2/\text{Vs}$ are achieved by using highly regioregular and well crystal orientation controlled P3HT as active materials.

2.2 Device structure

An organic field-effect transistor requires the following components (shown in Figure 2.2): (1) a thin semiconducting layer that is often deposited by spin coating, dip casting or vacuum evaporation; (2) a gate electrode; (3) an insulating gate dielectric layer that separates the semiconducting layer and the metal gate electrode; (4) source and drain electrodes of width W (channel width) and separation distance L (channel length), which are in contact with the semiconducting active layer. In order to achieve more efficient charge injection from source to channel, low work function metals, such as aluminum, are always employed as source or drain electrode for n -type OTFTs whereas high work

function metals (gold, etc.) for *p*-type devices. Gate electrode can be a metal or a conducting polymer which depends on the application purpose, such as indium tin oxide (ITO) for transparent devices, and Poly(3,4-ethylenedioxythiophene) poly(styrenesulfonate) (PEDOT/PSS) for flexible substrates. But very often, in order to simplify and standardize the fabrication process to study charge mobility of semiconducting materials instead of device structure, highly doped silicon wafers with a thermally grown silicon dioxide layer serve as substrate, dielectric layer, and gate electrode at the same time.

As mentioned before, various materials are involved in constructing OTFT with different materials nature, leading to compatible problems and complicating the fabrication processes. For example, in organic-inorganic hybrid devices, the inorganic dielectric layer requires high temperature process to achieve an anticipated capacitance, whereas it will cause decomposition of the organic materials. In order to solve this problem, different device structures were employed in different cases.

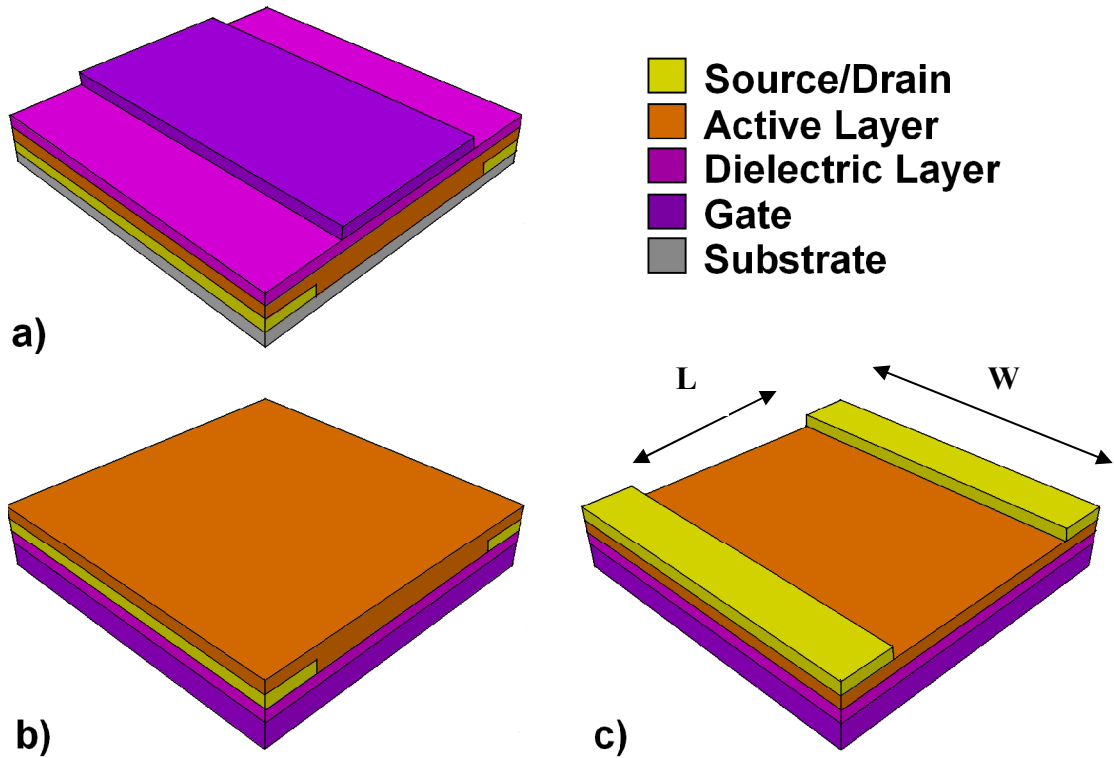


Figure 2.2 Schematic diagram of three field-effect transistor configurations, **a)** top gate bottom contact (TGBC), **b)** bottom gate bottom contact (BGBC) and **c)** bottom gate top contact (BGTC).

The most commonly found structures (in relation to the substrate) are the top gate bottom contact (TGBC, Figure 2.2a), bottom gate bottom contact (BGBC, Figure 2.2b), and bottom gate top contact (BGTC, Figure 2.2c) structures. Transistors with different device configurations show different behaviors even the same materials were employed. The relative positions of injection electrode to the gate and semiconductor-dielectric interface are both important. BGBC structure is different from TGBC and BGTC since the charges are directly injected into the accumulation

channel in BGBC device whereas source/drain electrodes are in contact with the back of the channel in the other two structures. Thus, injected charges have to pass through a thin layer of undoped low-conductivity semiconductor layer before it reaches the accumulation channel. Apart from this, surface roughness of a thin film fabricated by a different deposition process also makes a great impact on the device performance. For example, in top gate structure, dielectric thin film is deposited on the semiconductor layer. If the semiconductor layer has a poor surface roughness due to solution-process procedures, lower charge mobility can be observed due to rough interface for charge accumulation. Besides, once the top contact structure is employed, metal electrodes deposited on the semiconductor layer by evaporation method will introduce trap states and thus device performance will be affected. Finally, some restriction occurs due to the difference in materials nature, which limits the choice of device configuration. As mentioned before, if high-k oxide is chosen as an insulator, only bottom gate configuration is allowed due to high temperature-process requirement.

2.3 Working principle

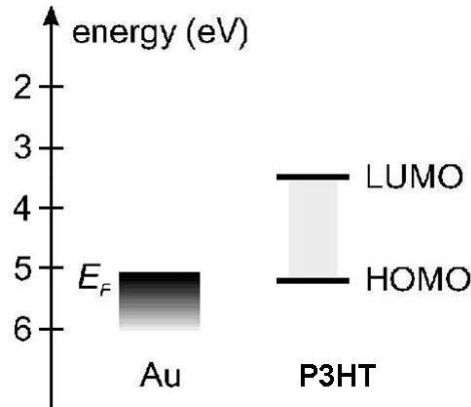


Figure 2.3.1 Energy levels of gold and P3HT.

Since P3HT and gold are commonly used organic semiconductor and source/drain electrode in OTFTs, so they are chosen as an example to explain the working mechanism of OFETs. A BGBC device structure is employed and fabricated on a $\text{SiO}_2/n\text{-type Si}$ substrate, whereas SiO_2 is used as a dielectric layer and $n\text{-type Si}$ as a gate electrode and substrate. Gold source and drain electrodes are deposited by thermal evaporation and P3HT active layer is spun onto the substrate by spin coating. When positive biased voltage is applied on the gate electrode, an electric field sets up across the dielectric layer and hence, negative charges are induced in the channel. As shown in Figure 2.3.1, energy difference between LUMO level of P3HT and Fermi level of gold is larger than 1 eV. This large energy

barrier makes electron injection very unlikely to happen. Because of the suppression of charge injection, almost no current passes through the channel from source to drain electrode. Only small leakage current through the insulating layer can be detected, and this state is regarded as depletion mode (shown in Figure 2.3.2a). On the other hand, if gate biased voltage is reversed to negative, induced hole at source electrode can be injected into P3HT easily because of the good matching between the Fermi level in gold and the HOMO level in P3HT. Injected charge then accumulates at the dielectric-semiconductor interface. When sufficient charges are accumulated at the interface, conducting channel establishes and charges can be driven from source to drain by applying a second voltage across the source and drain electrodes. This conduction states is regarded as accumulation mode (shown in Figure 2.3.2b).

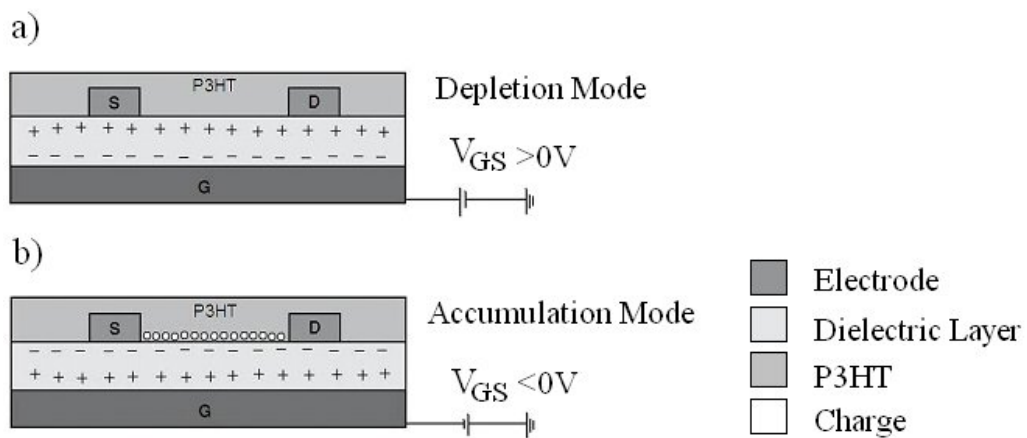


Figure 2.3.2 Operation mode of FETs a) depletion mode and b) accumulation mode.

When the applied gate voltage is higher than a threshold voltage (V_{TH}), the induced mobile charges Q_{mob} per unit area at the source contact are related to the gate voltage (V_{GS}), as given below:

$$Q_{mob} = C_i (V_{GS} - V_{TH}) \quad (2.1)$$

where C_i is the capacitance of gate insulator per unit area.

Since there is potential gradient across the source-drain electrodes, induced charge density also depends on the position along the channel (x), which is calculated in the following equation:

$$Q_{mob} = C_i (V_{GS} - V_{TH} - V(x)) \quad (2.2)$$

Neglecting diffusion, the source-drain current (I_{DS}) induced by the carriers is:

$$I_{DS} = W \mu Q_{mob} E_x \quad (2.3)$$

where W is the conduction channel width. μ equals to charge mobility and E_x represents the electric field strength at position x across the channel.

Since there is a potential gradient across the conduction channel, E_x can be substituted as dV/dx and put eq. 2.2 into eq. 2.3, we find:

$$I_{DS} dx = W \mu C_i (V_{GS} - V_{TH} - V(x)) dV \quad (2.4)$$

The gradual channel expression for the drain current can then be obtained by integration of the current increment from $x = 0$ to L , which is from $V(x) = 0$ to V_{DS} , hence:

$$I_{DS} = \frac{W}{L} \mu C_i \left[(V_{GS} - V_{TH}) V_{DS} - \frac{1}{2} V_{DS}^2 \right] \quad (2.5)$$

In the linear regime with $V_{DS} \ll V_{GS}$, this can be simplified to:

$$I_{DS \text{ lin}} = \frac{W}{L} \mu_{\text{lin}} C_i (V_{GS} - V_{TH}) V_{DS} \quad (2.6)$$

In the saturation regime with $V_{DS} \geq V_{GS} - V_{TH}$, substituting V_{DS} with $V_{GS} - V_{TH}$:

$$I_{DS \text{ sat}} = \frac{W}{2L} \mu_{\text{sat}} C_i (V_{GS} - V_{TH})^2 \quad (2.7)$$

From equations 2.6 and 2.7, linear and saturation mobility can be obtained. By plotting $I_{DS \text{ lin}}$ against V_{GS} , a constant slope at accumulation region will appear.

$$\mu_{\text{lin}} = \frac{L}{WC_i V_{DS}} (\text{Slope}) \quad (2.8)$$

Similarly, plotting square root of $I_{DS\ sat}$ against V_{GS} , a constant slope at accumulation region will appear, such that:

$$\mu_{sat} = \frac{2L}{WC_i} (\text{Slope})^2 \quad (2.9)$$

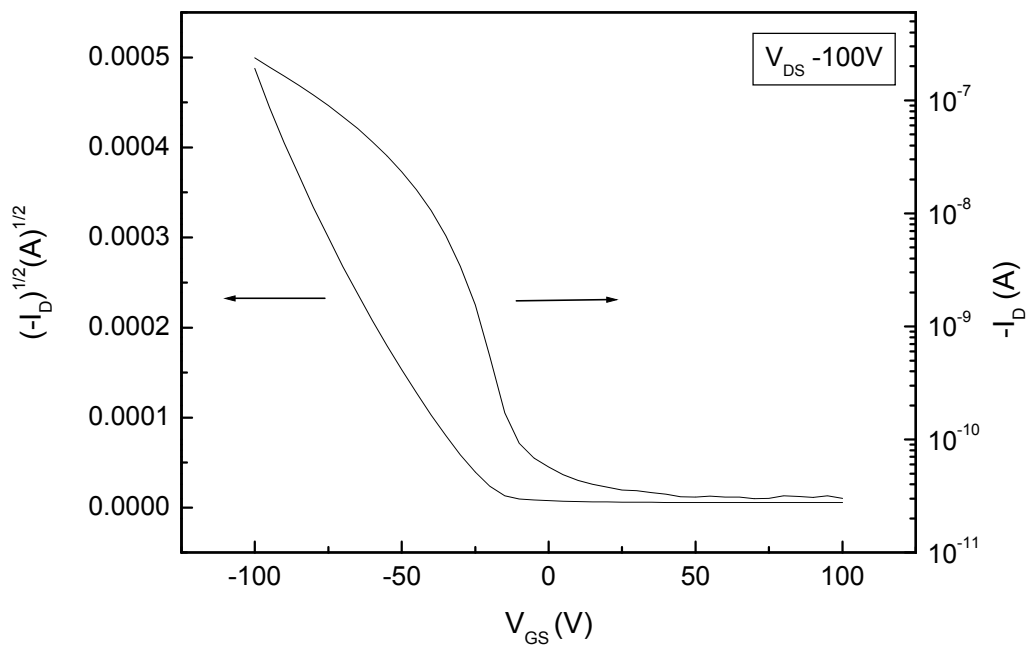


Figure 2.3.3 Transfer characteristics of a P3HT based OTFT.

A typical transfer characteristics curve of the fabricated OTFT device in the saturation regime is shown in Figure 2.3.3. As mentioned before, saturation mobility can be obtained from this transfer characteristics curves. Besides the mobility, several device performance parameters such as threshold voltage (V_{TH}),

onset voltage (V_{ON}) and current ON/OFF ratio ($I_{ON/OFF}$) can also be extracted. As shown in the semilog plot, channel current with obvious change for several orders of magnitude between depletion and accumulation modes can be easily observed. Therefore, the V_{ON} , at which channel current abruptly increases above a defined low off-current level, can be extracted. $I_{ON/OFF}$ ratio can also be observed from the semilog plot easily by comparing the current at ON state to OFF state, which is about 10^4 in this example. Finally, as described by equation 2.7, square root of saturation channel current should be linearly dependent on the effective applied gate voltage, which is applied gate voltage minus the threshold voltage ($V_{GS} - V_{TH}$). Hence the threshold voltage can be extracted by extrapolating the linear fit to zero.

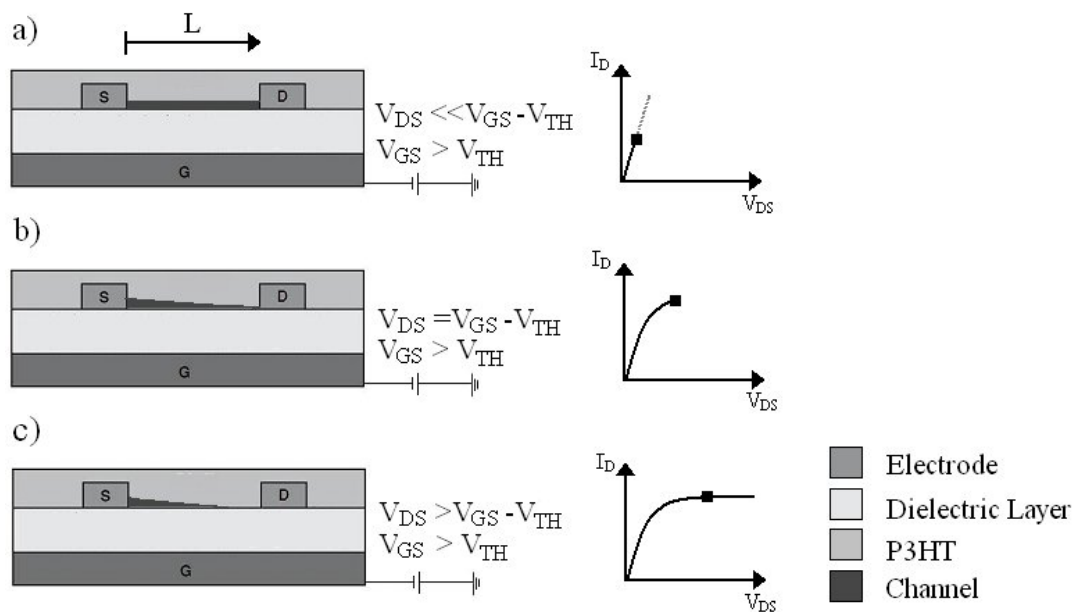


Figure 2.3.4 a-c Schematic diagram of the basic operating regimes and current-voltage characteristics of a FET.

Figure 2.3.4a-c is the illustration curves of the basic operating regimes and associated current-voltage characteristics of a field-effect transistor. As mentioned before, if *p*-type material is used, the electrons induced by positive gate bias are suppressed to inject into the channel. Whereas hole accumulation at insulator/semiconductor interface occurs when negative gate bias is applied, and the total number of accumulated charge is proportional to V_{GS} and capacitance C_i of the insulator. However, because of the presence of trap states, induced charges have to fill all the deep traps before it can be mobile and thus contribute to the conduction current. As a result, gate voltage has to be larger than a threshold voltage to ensure that every trap state is filled, and the additional V_{GS} will then contribute to charge accumulation in the conduction channel, therefore actual effective gate voltage is $V_{GS}-V_{TH}$. On the other hand, an internal potential at the interface may have been set up due to the donor (acceptor) states or interface dipoles, such as an opposite voltage applied to turn off the channel even zero gate voltage is applied.

As shown in Figure 2.3.4a, a uniform conduction channel is formed at the interface if V_{GS} is higher than V_{TH} and no source-drain bias is applied. When source-drain voltage increases (still far smaller than V_{GS}), a linear gradient of charge density sets

up between these two electrodes with a higher density at the injecting source and a lower density at the extracting drain. This state is named as the linear regime, in which channel current increases directly proportional to applied V_{DS} . Also potential $V(x)$ within the channel increases linearly from the source ($x=0$, $V(x)=0$) to V_{DS} at the drain electrode ($x=L$, $V(x)=V_{DS}$).

In the second state, when source-drain voltage keeps on increasing to a point that V_{DS} equals to $V_{GS}-V_{TH}$, a depletion region is formed in the channel just next to the drain electrode because threshold voltage is now larger than the difference of local potential $V(L')$ (where $L' \rightarrow L$) and the gate voltage, at which the channel is said to be “pinched off” (Figure 2.3.4b) and reaches its maximum value.

Since electric field across the depletion region is comparatively high, such that space-charge-limited saturation current $I_{DS, sat}$ can still be swept from the pinch-off point towards drain electrode and makes the pinch-off channel still conducting.

Further increasing the drain voltage however cannot increase the current, but leads to an expansion of the depletion region which further shortens the channel.

However, potential drop between pinch-off point and source remains because

potential at the pinch-off point remains at $V_{GS} - V_{TH}$, therefore channel current becomes saturated and remains at $I_{DS\ Sat}$ (Figure 2.3.4c).

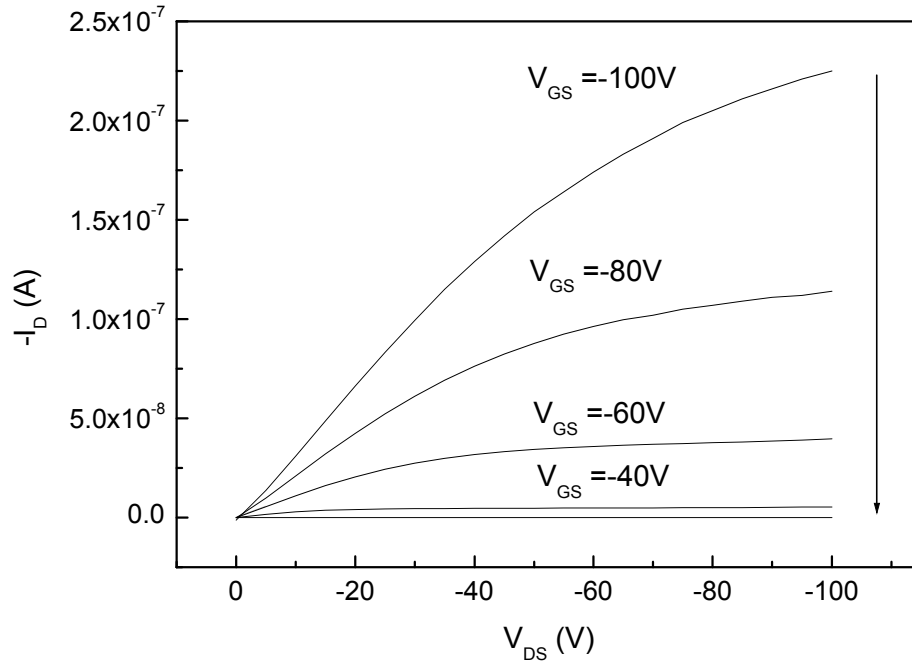


Figure 2.3.5 Output characteristics of a P3HT based OTFT.

Figure 2.3.5 shows a typical output characteristics curves of the fabricated OTFT.

This is the same device as shown in Figure 2.3.3, which is a P3HT based OTFT device prepared by spin coating method on a heavy doped *n*-type silicon wafer with 500nm thick silicon dioxide surface. As shown in the figure, conduction channel cannot be established when the applied gate voltage is zero, therefore channel

current I_D remains at a low value which is close to zero. When the gate voltage is increased, conduction channel is set up between source-drain electrodes that make the channel current increases to a high value. When the source-drain voltage increases to a value that is close to the applied gate voltage, the increase of channel current slows down and becomes saturated at a certain value.

2.4 Measurement system

Electrical measurements are performed in a nitrogen environment at room temperature using an Agilent 4156C precision semiconductor parameter analyzer (Figure 2.4.1), with each device electrically isolated via the patterned P3HT layer. The Agilent 4156C precision semiconductor parameter analyzer is specially designed for measuring transistor performances such as transfer characteristics and output characteristics with the sensitivity in the order of femto ampere. With careful adjustment and wiring, the noise level can now be controlled in the order of several pico- to femto-ampere level. Compared to the signal current which is in the order of several hundred pico-ampere, the noise signal can be neglected.

All devices are prepared and fabricated under atmospheric environment, and then transferred into a glove box for post-annealing process and measurement. This glove box is purchased from MBRAUN, (model number MB 10 compact), which can provide an environment of pure nitrogen gas with both O₂ and humidity concentration under 0.1 ppm.

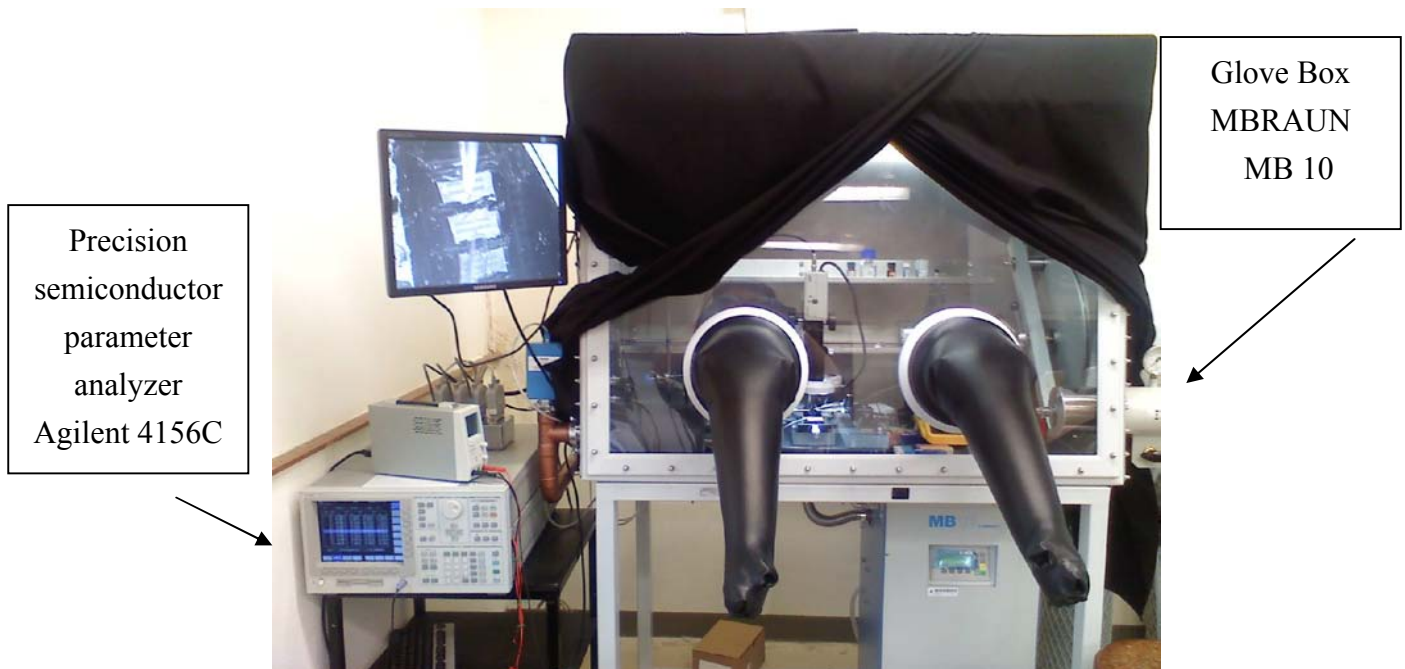


Figure 2.4.1 Measurement system: Agilent 4156C analyzer and MBRAUN MB 10 compact glove box.

In order to reduce the leakage current and make the device compact, probing areas of electrodes are less than 1 mm² which makes it difficult to be observed by naked eye. To address this issue, a probe station system constructed by a CCTV camera with three positioners installed. Figure 2.4.2 shows the probe station system together with the LCD monitor for measuring the OTFTs device. With the aim of

microscopy function of the CCTV camera, OTFTs can be observed clearly through the LCD display.

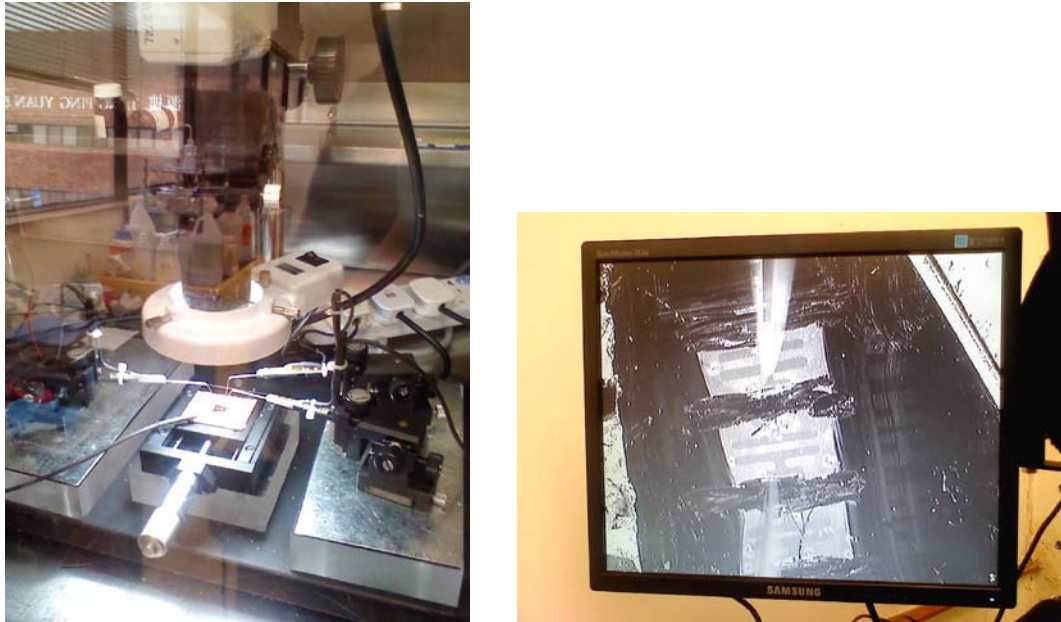


Figure 2.4.2 Probe station and LCD display for observing the OTFTs devices.

2.5 Preparation of OTFTs with BGBC and TGBC structures

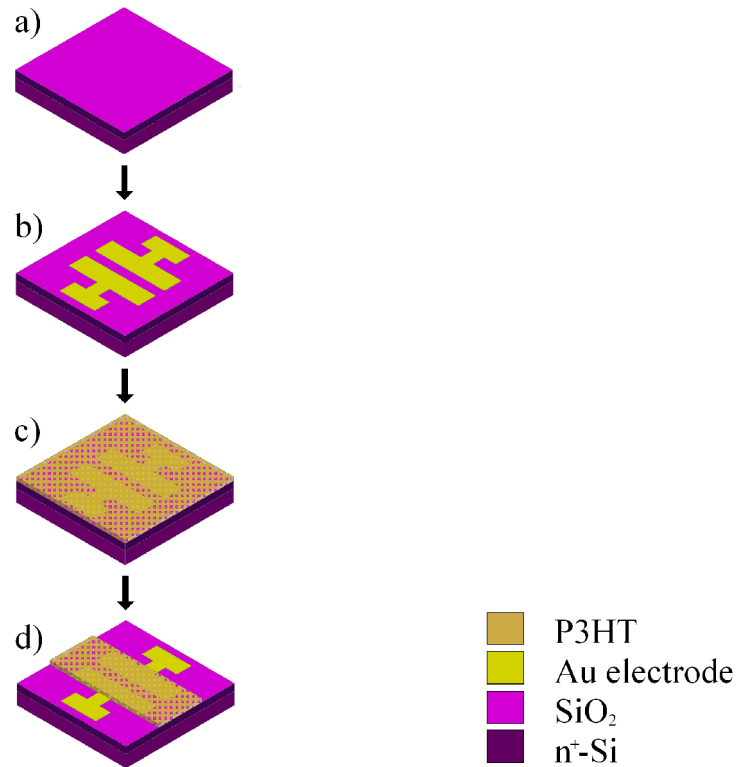


Figure 2.5(a-d) Diagrams showing steps to prepare OTFTs with bottom-gate/bottom-contact structure.

Figure 2.5(a-d) illustrates the fabrication procedures of a solution processed OTFT device with bottom-gate/bottom-contact structure. In order to simplify the fabrication process, a heavy doped n -type silicon wafer with 300nm thick thermally grown silicon dioxide surface substrate is employed as the dielectric layer, gate electrode and substrate at the same time. Since conduction channel is accumulated at the surface of SiO_2 , as a result the device performance greatly depends on both surface roughness and cleanness of SiO_2 . In order to improve the device properties,

SiO₂/n-Si substrate is cleaned by sonicated in acetone, isopropanol and deionized water to remove organic contamination. Following the cleaning process, 40nm thick and 2mm wide gold source-drain electrodes are deposited on the SiO₂ surface by thermal evaporation method with 0.1mm separation to each other through a shadow mask (Figure 2.5b). P3HT polymer is dissolved into chloroform solution with a concentration of 20mg/ml, and then filtered by a 450nm syringe filter. 30nm thick P3HT film is spun on the patterned substrate by spin coating method with a spinning speed of 3500 revolutions-per-minute (Figure 2.5c). Since the conductivity of P3HT thin film is not negligible and because of the common gate structure, a large P3HT area will therefore cause serious current leakage. To minimize the leakage problem, P3HT layer is removed by chloroform except for the channel area (Figure 2.5d). Finally the device is annealed at 120°C for one hour under nitrogen environment to increase its crystallinity and to remove remained organic solvent and oxygen [31].

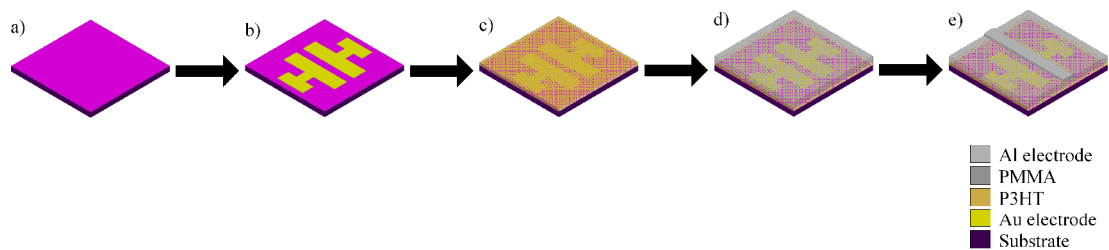


Figure 2.5.1(a-e) Diagrams showing steps to prepare OTFTs with top-gate/bottom-contact structure.

Figure 2.5.1 (a-e) shows the fabrication procedure for a top-gate/bottom contact device. Gold electrodes are evaporated on a cleaned glass substrate through a shadow mask, and a 50nm thick P3HT thin film is spun onto the patterned substrate by spin coating method. After being dried on an 80 °C hotplate for several minutes to remove the remaining solvent, The sample is coated with a thin PMMA film on the P3HT layer by using a PMMA/MEK solution with a concentration of 10mg/ml. Device is annealed on a hotplate at 100°C for one hour to remove the MEK solvent and an aluminum gate electrode aligned between the source-drain electrodes is then deposited on the PMMA layer by evaporating Al through a shadow mask.

OTFTs based on P3HT are known to have unstable device performance under atmosphere. This unstable device performance appears because of oxygen doping and moisture interaction with P3HT surface. Low charge-carrier mobility and current ON/OFF ratio, high leakage current and threshold voltage, together with the un-saturated behavior in the output curve show that P3HT based OTFT might not be suitable to be operated under atmosphere. However this undesirable behaviors caused by oxygen and moisture is reversible and performance can be recovered by post-thermal annealing under vacuum or N₂ environment. Since these samples are

prepared and fabricated under atmosphere, oxygen and moisture doping is unavoidable. In order to solve this problem, devices are annealed at 100 °C for 1 hour under nitrogen environment in the glove box with oxygen and moisture concentration kept under 0.1 ppm after the removal of extra P3HT layer.

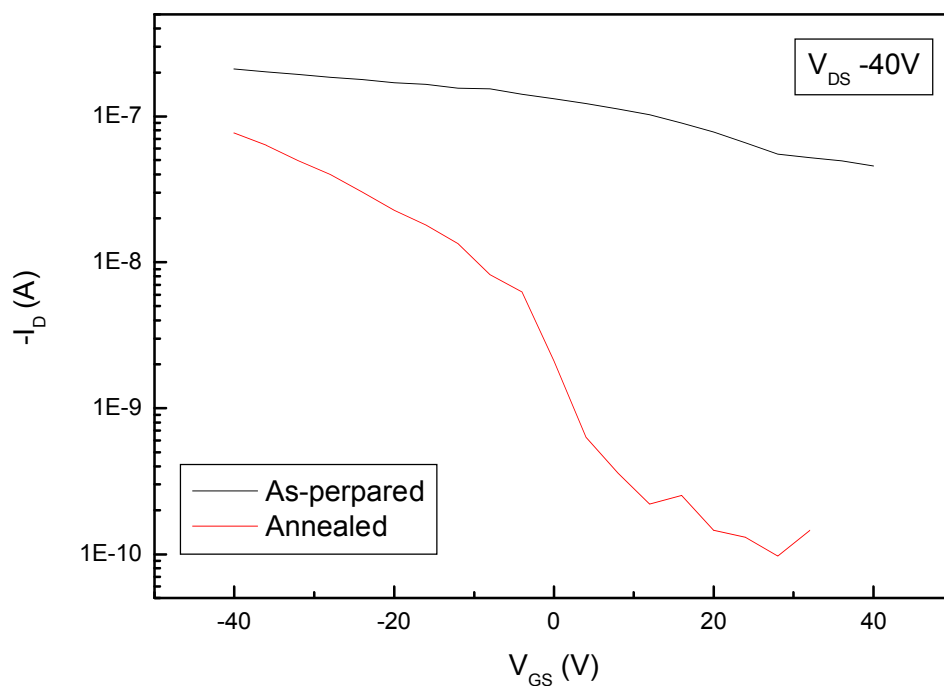


Figure 2.5.2 Transfer characteristics of P3HT based OTFTs.

Figure 2.5.2 shows the transfer characteristics of a as-prepared device having the same device structure as shown in Figure 2.2.3 which is annealed under nitrogen environment at 100°C for 1 hour. By comparing the transfer characteristics between

pre-annealed and annealed sample, it shows an increase in carrier mobility and $I_{ON/OFF}$, reduction of leakage current and threshold voltage change from 40V to 6V, which demonstrates that post-thermal annealing can recover and enhance the performance of P3HT device due to the atmosphere exposure. With the aim of post-annealing process under nitrogen environment, stable and repeatable P3HT based OTFT device can be achieved on silicon wafer. Figure 2.5.3a-b shows some of the device performance.

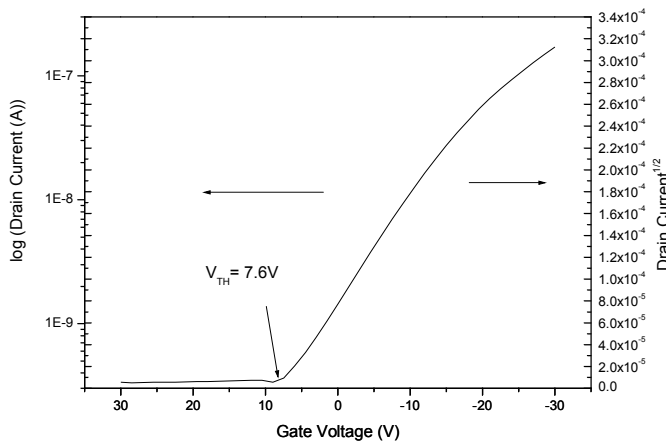


Figure 2.5.3a Transfer characteristics.

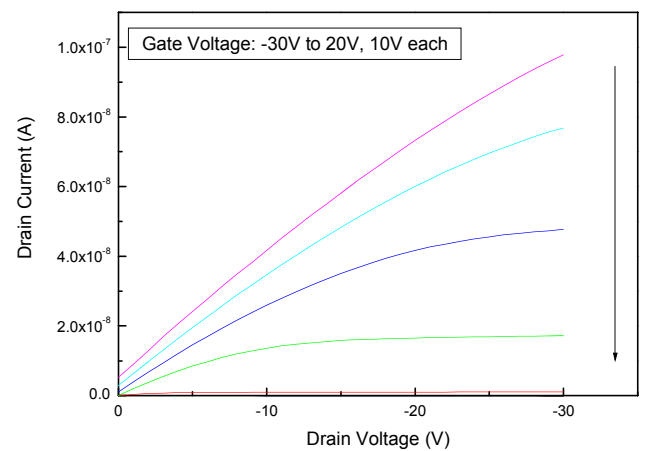


Figure 2.5.3b Output Characteristics.

- BGBC configuration on 300nm thick SiO₂ wafer.
- Spin coating 98.5% rr-P3HT in chloroform solution.
- W/L=13.3 ;sat. Mobility = $1.4 \times 10^{-3} \text{ cm}^2/\text{Vs}$; $I_{ON/OFF}$: $\sim 10^3$; V_{TH} : 7.6 V.

2.6 Post-annealing effect on P3HT based OTFT device

In order to study how the annealing process affects the device performance, an annealing test is conducted. Five P3HT based OTFT samples using BGBC structure with gold as source-drain electrode are annealed for 0, 1, 1.5, 2, and 2.5 hours under nitrogen environment at 100°C after fabrication. Transfer characteristics and output characteristics of these samples are measured before and after the annealing process. Threshold voltage, $I_{ON/OFF}$ ratio and charge-carrier mobility are extracted from these current-voltage characteristic curves.

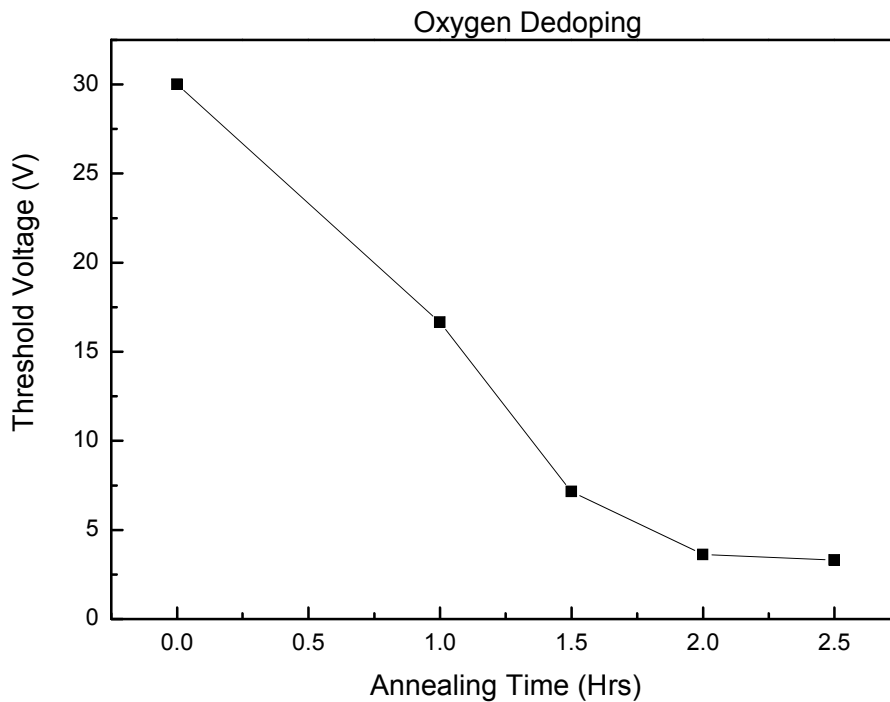


Figure 2.6.1 Threshold voltage of samples for different annealing time.

Figure 2.6.1 shows that when annealing time increases, threshold voltage reduces to

a low value. By increasing the annealing time, threshold voltage shifts from 30V to 16.65V in one hour, to 7.15V in one hour and thirty minutes, to 3.6V in two hours and achieves minimum value of 3.3V after annealed for two hours and thirty minutes. As mentioned before, threshold voltage shifted to a positive value represents impurities trap, which is believed to be due to oxygen doping inside the P3HT layer during preparation and fabrication process. As a result, reduction of threshold voltage can be an indirect proof of dedoping of oxygen, which demonstrates that longer annealing time can remove more oxygen dopant, similar result could be found from Hoshino's work[30] in 2004. From Table 2.6.1, it shows that oxygen concentration keeps decreasing by increasing the annealing temperature which has the similar effect as increasing in annealing time.

Table 2.6.1 Sulfur and oxygen concentration of P3HT sample at different annealing conditions (Reprint from Hoshino[30]).

Sulfur and oxygen concentrations as determined by RBS

Sample	Composition
Control	7.7 at% S; 15 at% O
40°C	7.5 at% S; 12 at% O
60°C	7.5 at% S; 12 at% O (O-rich on the top $2 \times 10^{17}/\text{cm}^2$ layer)
80°C	7.0 at% S; 6 at% O
100°C	7.0 at% S; 5 at% O (slightly more O-rich on the surface)
120°C	6.5 at% S; < 1 at% O
140°C	7.2 at% S; < 1 at% O

Sulfur was used as a marker for the polythiophene layer.

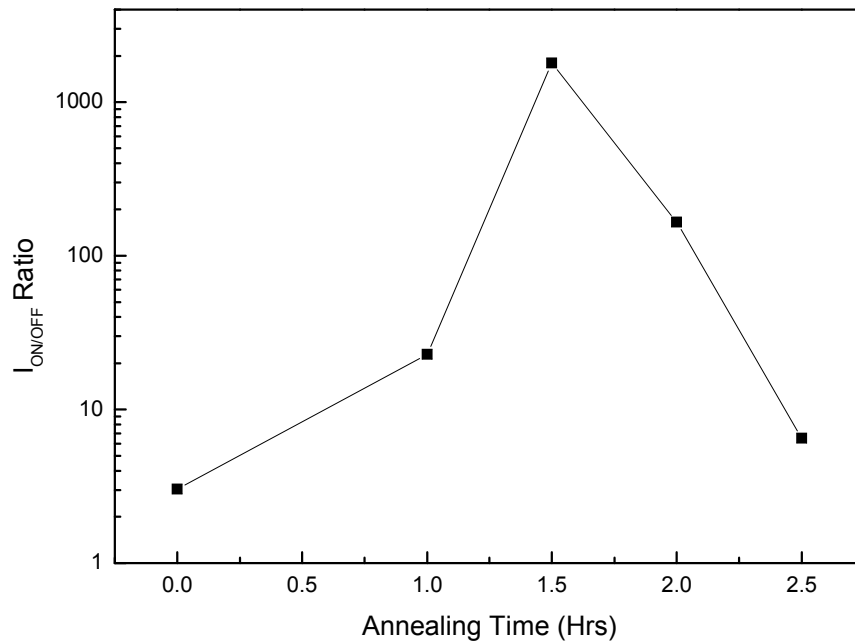


Figure 2.6.2 Current ON/OFF ratio at different annealing time.

Figure 2.6.2 shows the increase of $I_{ON/OFF}$ ratio by thermal annealing, which achieves a maximum value of 1800 at one hour and thirty minutes annealing time. Ratio reduces when annealing time increases. High ON/OFF ratio can be achieved by increasing charge-carrier mobility, thus increasing maximum channel current at device ON state. In the mean time, reduction of leakage current at device OFF state also contributes to maximize the current ON/OFF ratio.

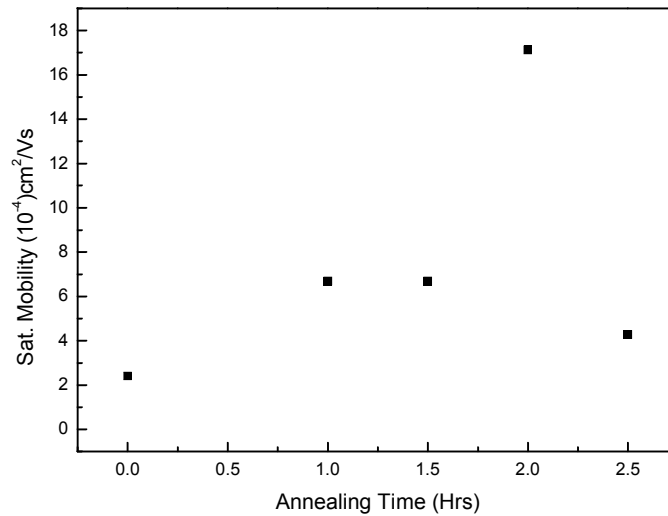


Figure 2.6.3 Charge-carrier mobility at different annealing time.

Figure 2.6.3 shows that saturation mobility of P3HT based OTFT under different annealing times, which achieves maximum value after annealed for two hours under nitrogen environment, and reduces for further annealing. Due to better polymer chain alignment by thermal annealing, crystallinity increases and hence mobility increases. However if further annealing process is conducted, excess energy causes the polymer chain to twist and shorten the conjugation length which leads to the decay of mobility.

B.A. Mattis et al[31] also demonstrated similar behavior as shown in Figure

2.6.4a-b that mobility and $I_{ON/OFF}$ ratio reach maxima at certain annealing time and temperature.

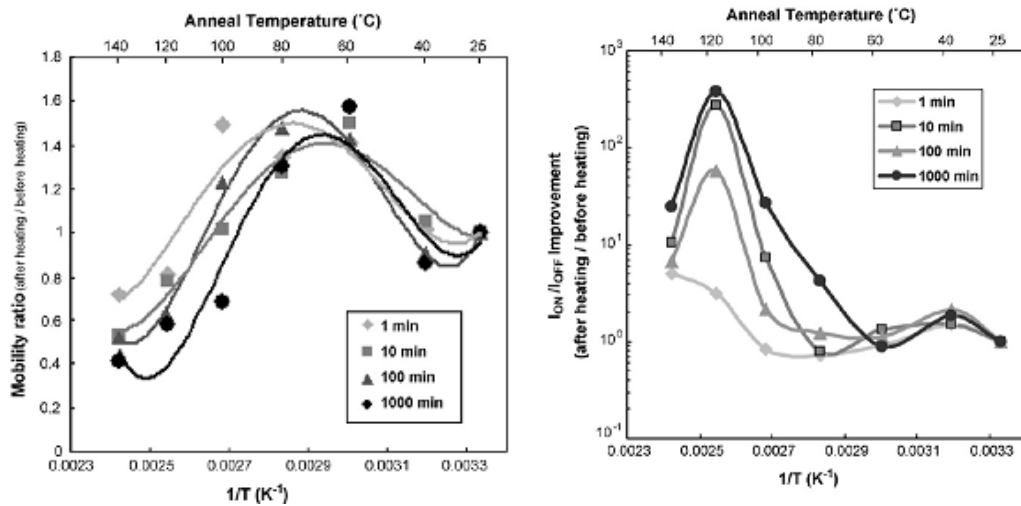


Figure 2.6.4 a) Mobility against time and temperature; b) $I_{ON/OFF}$ against time and temperature. (Reprint from B.A. Mattis [31])

In conclusion, the annealing effect on $I_{ON/OFF}$ ratio and mobility can be contributed to four reasons: 1) Thermal annealing can lower the oxygen concentration and reduce oxygen p -dopant, thus leakage current is suppressed. 2) Thermal process provides energy for polymer chain alignment. Carrier mobility increases for better ordering of P3HT chain, resulting in larger ON current. 3) Reduction of impurities concentration also decreases the scattering probability of conducting hole in the active layer, hence ON current increases. 4) Longer time or higher temperature annealing leads to polymer chain twist and shortening of P3HT conjugation length (Figure 2.6.5), resulting in reduction of mobility, and hence the ON current drops.

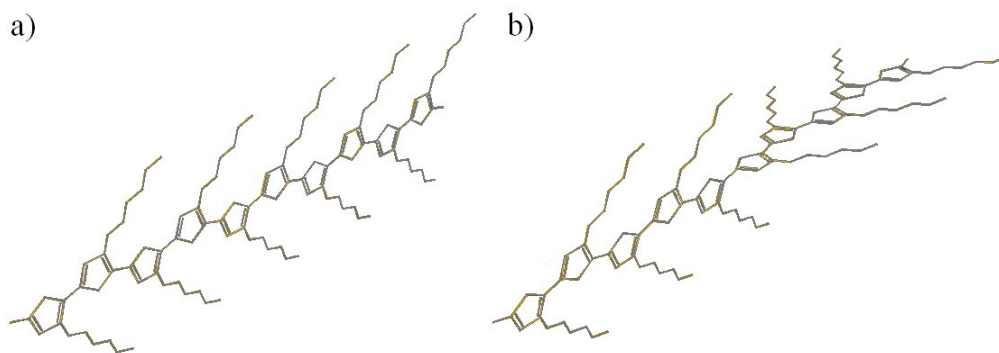


Figure 2.6.5 a) Longer conjugation length, b) twisted polymer chain with shorter conjugation length.

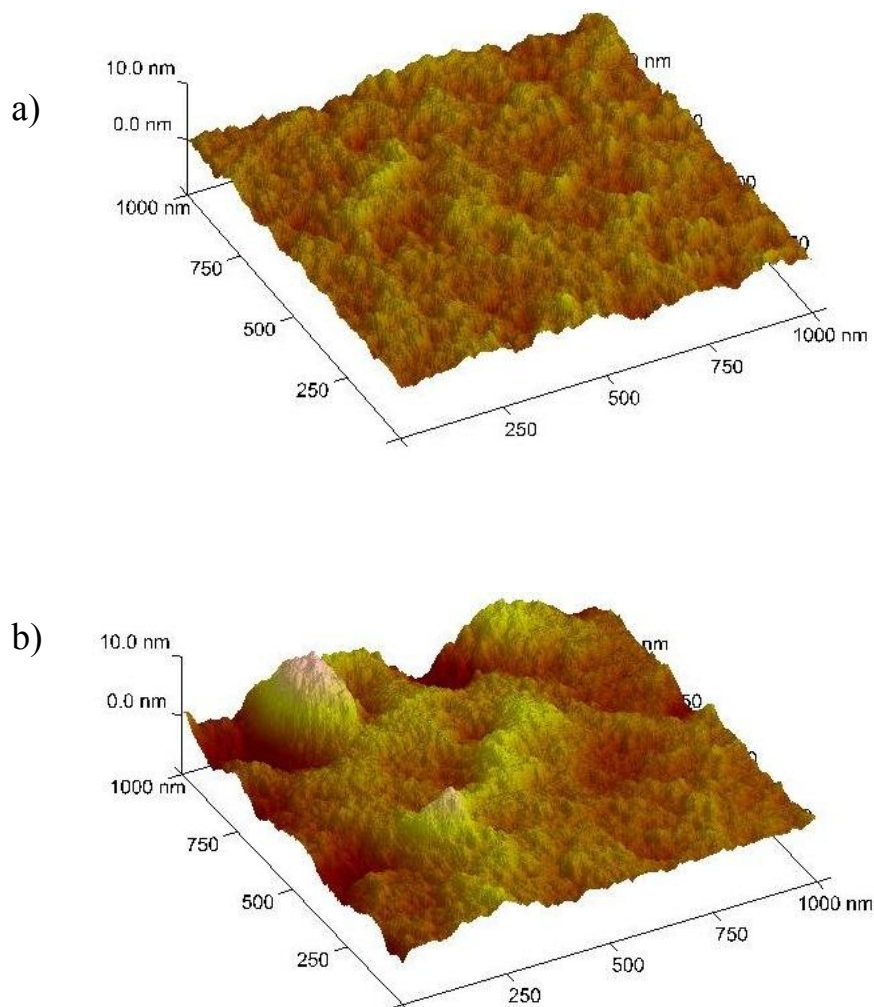


Figure 2.6.6 a) AFM image of 100 °C annealed P3HT sample; b) AFM image of 200 °C annealed P3HT samples.

Figures 2.6.6(a & b) show the surface morphologies of P3HT samples which have been annealed at 100°C and 200°C, respectively. The sample which has been annealed at 100°C has a surface roughness of $R_{\text{max}} = 6.39\text{nm}$ and $R_a = 0.632\text{nm}$, whereas $R_{\text{max}} = 18.2\text{nm}$ and $R_a = 1.35\text{nm}$ are observed for the 200°C annealed one. The increase of surface roughness is believed to be due to the high annealing temperature (melting temperature of P3HT is 178°C), which leads to the twist of polymer chains and hence aggregation occurs. It is also the reason why device performance decays after annealing at high temperature.

2.7 Oxygen doping and moisture interaction

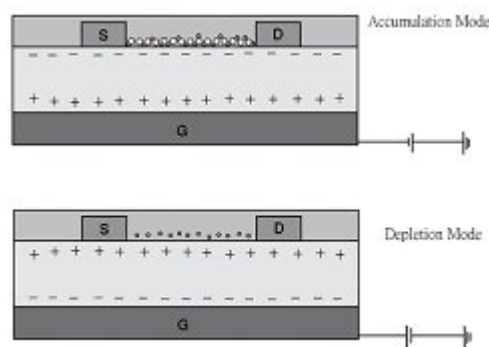


Figure 2.7.1 Schematic diagram of oxygen doping in P3HT device.

As discussed in the previous page, oxygen can affect the P3HT based OTFT

device. Reason for this is that, during solution preparation and device fabrication process, oxygen as *p*-type dopant will dope in the P3HT matrix (shown in Figure 2.7.1), which causes the production of localized states within the π - π^* gap, hence conductivity of the film increases.

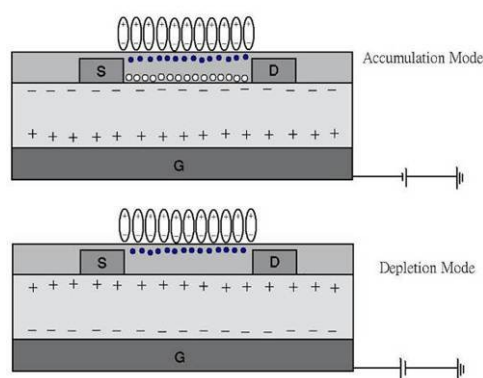


Figure 2.7.2 Schematic diagram of the effect of moisture on P3HT device.

Besides oxygen, moisture also plays an important role for performance decay. Unlike oxygen, moisture reaction is rapid. Since molecular size of water molecule is larger than oxygen, moisture effect is believed to be due to the interaction with P3HT surface instead of diffusion. The larger dipole momentum of water molecules (1.94D) can generate hole in the semiconducting active layer surface (Figure 2.7.2), which provides alternative path for current conduction even in hole-depletion mode, hence leads to the poor saturation and high OFF current behaviors in output characteristics.

2.8 Conductivity of P3HT in different environment

In order to study the conductivity of P3HT in different environment, a series of conductivity test have been done. A glass substrate is separated and cleaned to remove the surface organic pollutants. Two separated electrodes are sputtered on the substrate followed by the deposition of P3HT layer by spin coating (shown in Figure 2.8.1). By measuring the current-voltage characteristics between these two electrodes, conductance of the P3HT can be extracted.

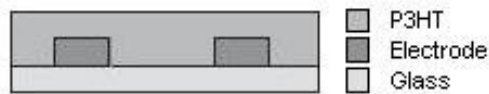


Figure 2.8.1 Cross-sectional view of a P3HT layer deposited on a glass substrate.

Figure 2.8.2 shows the conductance of five samples with different annealing time, which shows a continuous reduction in conductivity when the annealing time increases. This is due to the fact that oxygen and moisture are removed from the P3HT layer by thermal annealing under nitrogen condition, thus density of mobile charge caused by *p*-dopant oxygen and moisture interaction decreases and conductance is reduced.

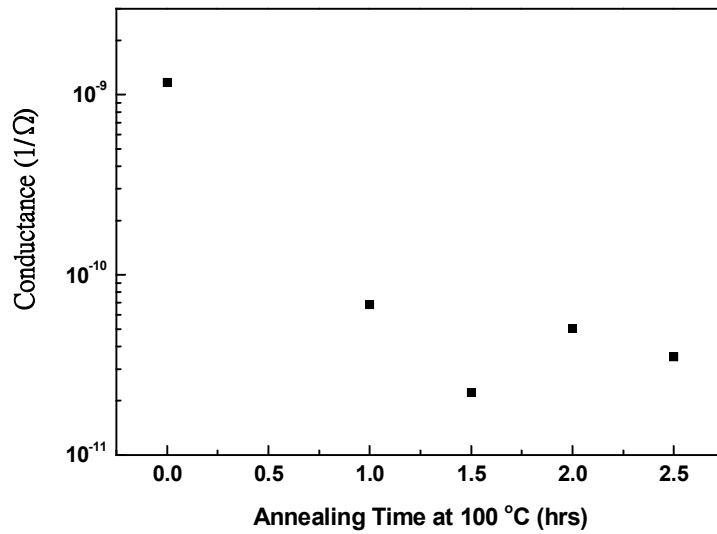


Figure 2.8.2 Conductance of P3HT samples at different annealing time.

As discussed before, oxygen might contribute to the high leakage current of P3HT based OTFT by *p*-type doping. In order to study this effect, a P3HT sample is first annealed in nitrogen environment for one hour to remove doped oxygen. Then the sample is kept in vacuum for another one hour before the measurement. The next step is to fill pure oxygen gas into the vacuum sample container and measure the current-voltage characteristics between two separated electrodes every two minutes.

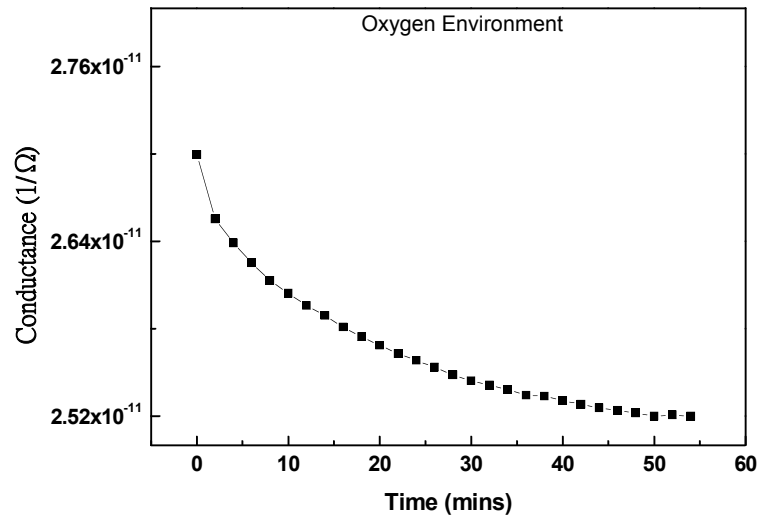


Figure 2.8.3 Conductance of dedoped P3HT sample under exposure of oxygen.

As shown in Figure 2.8.3, conductance of P3HT layer keeps reducing after exposure to oxygen. It is believed that oxygen doping is caused by diffusion which requires high energy supply. Therefore diffusion process is not obvious at room temperature in a short period of time. Besides, Chabinyk[32] suggested that oxygen might not be a strong dopant in the absence of light, therefore conductivity of P3HT only varies slightly when compared to other exposure conditions.

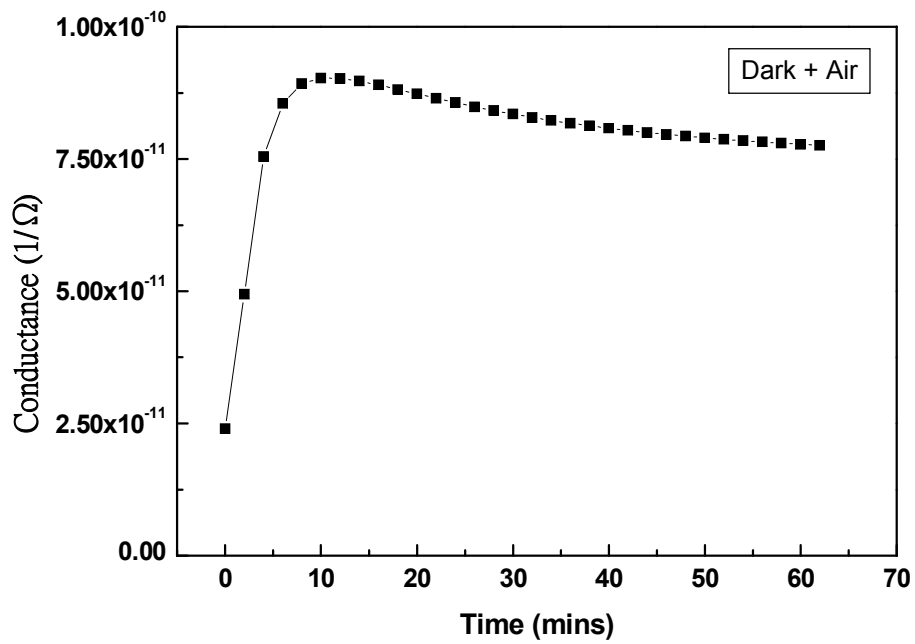


Figure 2.8.4a) Conductance of dedoped P3HT sample exposed to air in the absence of light.

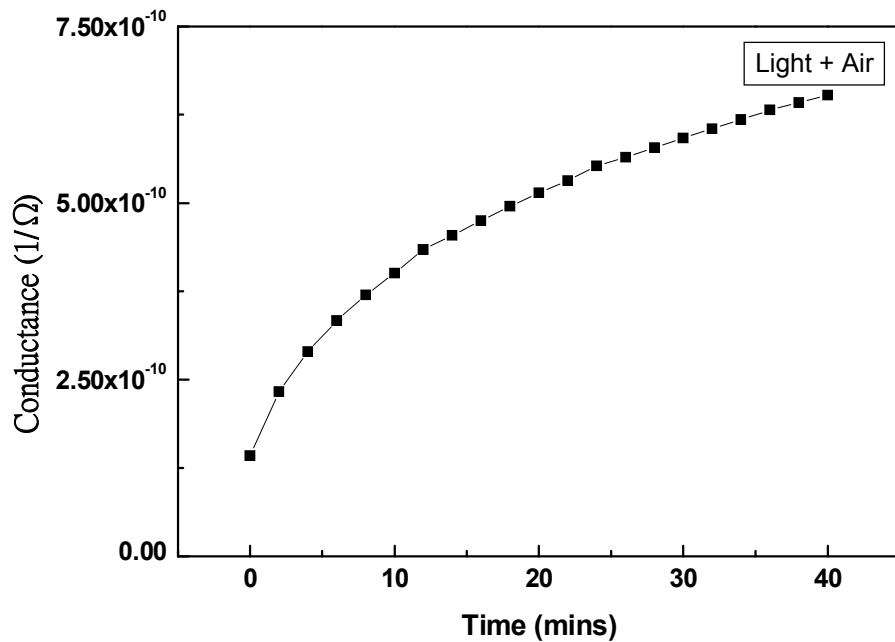


Figure 2.8.4b) Conductance of dedoped P3HT sample exposed to air under light exposure.

Conductance of P3HT layer is being continuously monitored every two minutes after air is introduced into the vacuum sample container in the absence or presence of light source. Figure 2.8.4a shows that after the induction of air into the dark container, conductance of P3HT increases for ~450% in eight minutes, and saturates after sixty minutes with total increment of 400%. The rapid change is due to the high humidity of atmospheric air. Water molecule interacts with P3HT surface instead of slow penetration, therefore mobile charge is introduced quickly, which leads to the rapid change of conductance. Figure 2.8.4b shows that when light source is irradiated on the P3HT sample, conductance raises more than 335% in one hour. Since P3HT is a light sensitive material that can be employed in solar cell and photovoltaic devices, the conductance change can be attributed to the interaction between oxygen molecules and charges generated in P3HT by photon absorption.

Instead of nitrogen post-annealing to dedope the impurities dopant, placing the doped sample into vacuum also gives similar result. A P3HT sample is prepared and placed into atmosphere condition overnight to allow oxygen doping and moisture interaction. After conductance rises to a saturation value, the sample is placed into a vacuum glove box and monitored every two minutes. Figure 2.8.5 shows the

conductance of the P3HT sample kept in vacuum for over 28 hours, reflecting a slow recovery process.

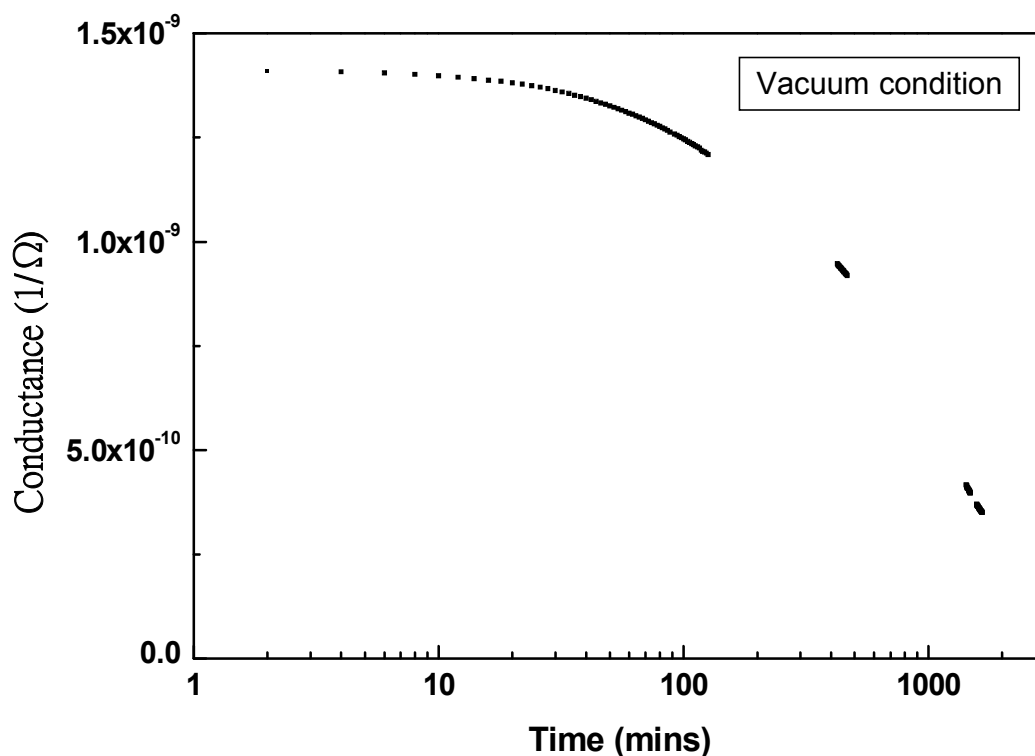


Figure 2.8.5 Conductance of dedoped P3HT sample in vacuum.

Owing to the insufficient energy support for molecule movement at room temperature and tightly bounded water dipole to P3HT functional group, the recovery process is very slow compared to that done at high temperature. It takes 28 hours to reduce 75% of conductance at room temperature process, while just one

hour to reduce more than 94% at 100°C. Although the recovery process at room temperature under vacuum is time consuming, it has an advantage that temperature remains at low value will not alter the crystal structure or contents of organic components in P3HT.

Chapter Three

Organic phototransistor based on TiO₂/P3HT composite

3.1 Organic phototransistor

The study on organic materials including small molecules and polymers for their applications in the electronics and semiconductor industry has been of great scientific and technological interest for several decades. Although electronic materials research has been dominated by the impressive performance of inorganic materials for many years, the attraction of using organic or plastic devices is driven by many virtues of organic materials, including flexibility, low cost, light weight, solution-processibility, bio-compatibility and environmental friendliness[33-35].

Phototransistors are a type of optical transducer in which light detection and signal amplification are combined in a single device without the noise increment associated with avalanche photodiodes[36]. Organic phototransistors (OPTs) are considered to be one of the feasible application of organic thin film transistor (OTFT) because of their large adsorption properties in ultraviolet (UV) and visible

light and the excellent photo current generation efficiency of organic semiconductors[16, 37-45]. More importantly, some OPTs can be fabricated by solution process[43-45], such as printing or spin coating, at room temperature and therefore can be easily integrated in smart clothes, packages, and biological systems as light sensors, biosensors and multifunctional sensors.

OPTs fabricated by thermal evaporation of some oligomers including pentacene[16, 37-39], 2,5-bis-biphenyl-4-yl-thieno[3,2-b]thiophene (BPTT)[15], rubrene[40],

N-[7-(N,N-diphenylamino)-9,9'-spirobifluoren-2-yl]-N'-(2,5-di-tert-butylphenyl)-3,4:9,10-perylenetetracarboxylicdiimide (DPASP)[41], and

2,7-bis-(N,N'-diphenylamino)-2',7-bis(biphenyl-4-yl)-9,9'-spirobifluorene

(Spiro-DPSP)[42], have been found to be very photo sensitive. Normally, a positive shift of the threshold voltage of a OPT can be observed under illumination, which can be attributed to trapping of electrons generated by photons at the insulator/semiconductor interface of the device. However, as explained by M. Debucquoy et al[37], the photosensitivity of pentacene organic TFTs shares the same mechanism of bias stressing effect. Therefore the photo sensitive behaviour of

this type of phototransistor is normally associated with the instability of the device performance, which will be a shortcoming in its real application.

Solution processible OPTs based on conjugated polymers, such as poly(9,9-dioctylfluorene-co-bithiophene) (F8T2)[42], poly(3-octylthiophene-2,5-diyl) (P3OT)[43] and blends of poly(2-methoxy-5-(3,7-dimethyloctyloxy))-1,4-phenylenevinylene (MDMO-PPV) and methanol [6,6]-phenyl C₆₁-butyric acid methyl ester (PCBM) have been reported. Light illumination can induce pronounced changes both in threshold voltage and off current of the devices, which can be attributed to trapping of electrons at the semiconductor/insulator interface and light induced photocurrent, respectively. It is worth noting that all of the OPT devices based on conjugated polymer or oligomers that have been reported show relatively long response time (> 1 s) to light illumination, which may limit their applications. Although most papers are focusing on the magnitude of current change under illumination, we consider stability and fast response under light illumination is also very important for the application of OPTs.

Semiconducting polymer poly(3-hexylthiophene) (P3HT)[33] is solution processible and feasible for roll to roll process. It has a field effect mobility up to $\sim 0.1 \text{ cm}^2 / \text{Vs}$ [24], which is near the value for amorphous silicon, thus it is a promising material for applications in OTFTs and solar cells. However, OPT devices based on P3HT have rarely been reported. We find that OTFTs based on P3HT/TiO₂ nanoparticle composite film are photo sensitive and show promising performance in terms of response time and stability, which will be reported in this thesis.

3.2 Motivations

Recently, attempts to fabricate highly sensitive solution processible photodetectors have attracted much attention in view of many benefits, such as easy fabrication, low cost and flexibility. We consider that OPTs based on the hybrid films of semiconducting polymers (P3HT) and inorganic nanoparticles (TiO₂) are attractive for such applications since the large interface-area-to-volume ratio in the composite film can improve detection sensitivity, and more importantly, OTFTs are good amplifiers that can greatly enhance the detection sensitivity.

OPTs based on P3HT/TiO₂ composites are especially important for the applications in UV detectors since TiO₂ can strongly absorb UV light. In recent years, much research has been focused on high performance solid-state UV detectors since it can be used in various commercial and military applications. In general, UV detectors fall into two categories: photodetectors and thermal detectors. UV photodetectors can be used in space communications, ozone layer monitoring and flame detection. Flame sensors can be used to monitor the status of pilot lights and burner flames in large industrial furnaces and in other applications for the control of high temperature systems. Currently, light detection in the UV spectral range still uses

Si-base optical photodiodes which shows relatively low responsivity since the room temperature bandgap of Si is only 1.2 eV. With the advent of optoelectronic devices fabricated on wide direct bandgap materials, it becomes possible to produce high performance solid-state photodetectors that are sensitive in the UV region. GaN-based UV photodetectors are already commercially available. Photodetectors based on ZnSe, ZnO and AlGaIn etc. have also been demonstrated. The advantages of developing UV sensitive OPTs are obvious for their easy fabrication and low cost.

3.3 Experiments

The OPTs based on the TiO₂/P3HT nanocomposite is fabricated on a SiO₂/n-type Si substrate. Regioregular P3HT with head-to-tail linkages of 98% was purchased from Sigma-Aldrich, and used as received without additional purification. TiO₂ nano-powder with the size of 50nm-100nm and a mixture phase of anatase and rutile was purchased also from Sigma-Aldrich. P3HT and TiO₂ powders are dissolved in chloroform. The mixture solution is heated and stirred with a magnetic stirrer for a few days to dissolve the P3HT entirely. In order to distribute TiO₂ nano-powders into the P3HT thin film uniformly, the mixture solution is sonicated in an ultrasonic bath before spin-coating.

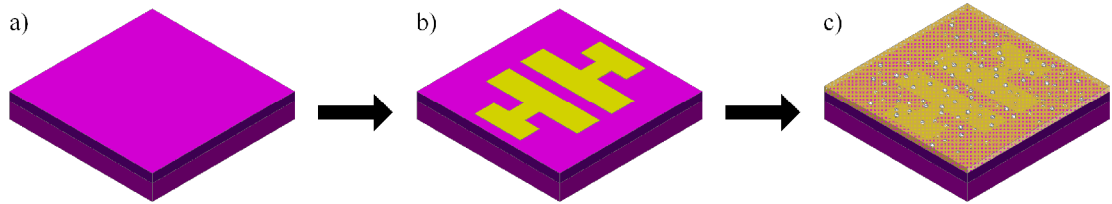


Figure 3.3.1 a-c) Diagrams showing steps to prepare TiO₂/P3HT nanocomposite OPTs.

The resistivity of the heavily doped *n*-type Si is 0.001 ohm·cm. The thickness of the thermally grown SiO₂ is 300nm. As discussed before, surface cleanness of SiO₂ can greatly affect the device performance, therefore the SiO₂/ *n*-type Si is sonicated in acetone, IPA and D.I. water to remove organic contamination on the surface (Figure 3.3.1a). After the cleaning process, Au source/drain electrodes are deposited through a shadow mask on top of the SiO₂ film by thermal evaporation with channel width/length of 2000μm/200μm (Figure 3.3.1b). Here, the *n*-type Si layer acts as the gate electrode and the SiO₂ layer the gate insulator. The mixture solution is spin coated on the substrate in air (Figure 3.3.1c). Then the device is annealed at 120°C for 2 hours in a glove box filled with high purity N₂. All devices are measured in the glove box with a semiconductor parameter analyzer (Agilent 4156 C). Devices with different ratio between P3HT and TiO₂ have been fabricated to find the most photosensitive composition.

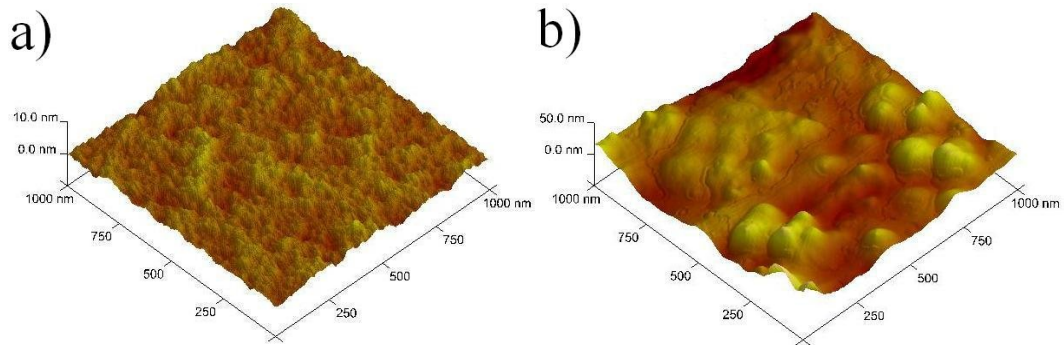


Figure 3.3.2 AFM image of **a)** Pure P3HT and **b)** P3HT:TiO₂ (1:0.25) sample.

Figure 3.3.2a shows the AFM image of a pure P3HT control sample, and Figure 3.3.2b shows the nanocomposite sample. From the AFM image, we can find that TiO₂ nanoparticles are embedded into the P3HT layer. TiO₂ particles are confirmed in the size between 50 to 100nm diameter. Due to ultrasonic treatment, TiO₂ particles distributed uniformly with little aggregation. Figure 3.3.3 show the schematic diagram of an OPT based on the P3HT/TiO₂ nanocomposite.

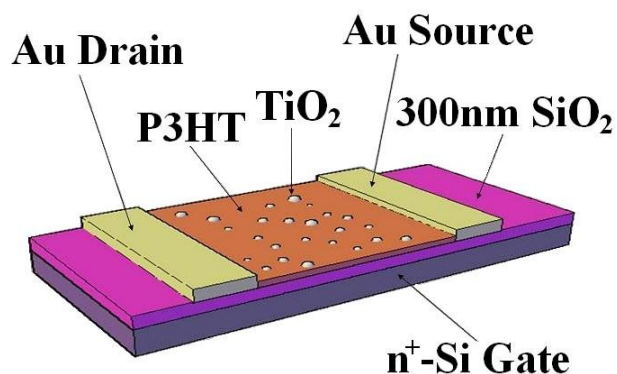


Figure 3.3.3 Schematic diagram of an OTFT incorporated with TiO₂ nanoparticle in the device.

3.4 Photo response of TiO₂/P3HT OPTs

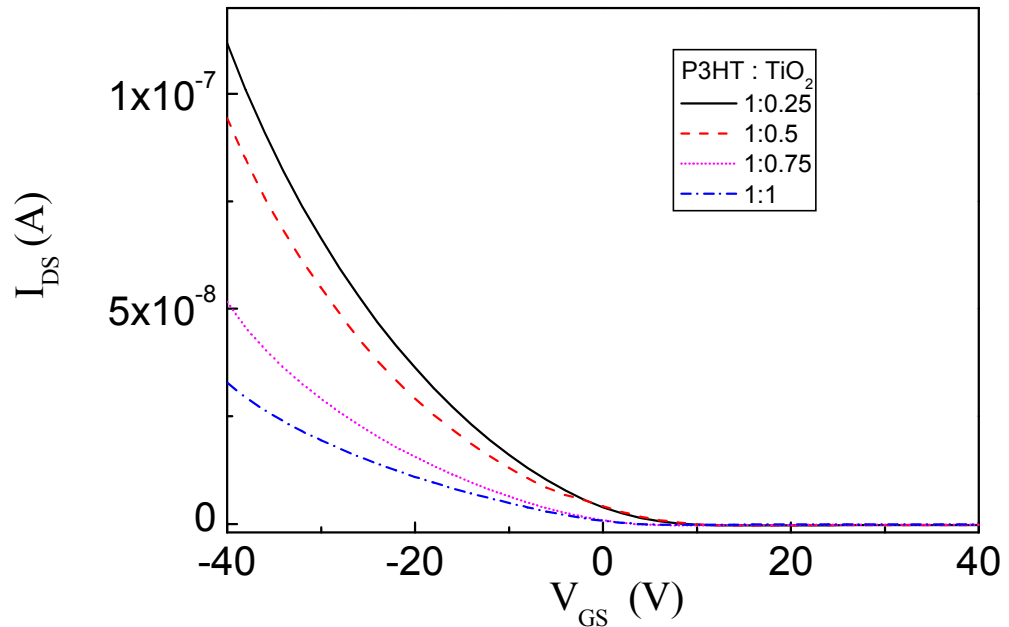


Figure 3.4.1 Transfer characteristics of OTFTs with different TiO₂ concentrations.

Table 3.4.1 Device performance of TiO₂/P3HT OPTs with different TiO₂ concentrations.

P3HT:TiO ₂ (weight ratio)	1:0.25	1:0.50	1:0.75	1:1
Sat. Mobility (x10 ⁻⁴) (cm ² /Vs)	6.68	6.02	3.31	1.86
V _{TH} (V)	5.59	4.42	3.98	7.96
I _{ON/OFF} ratio	2812	1125.96	425.54	467.29

As shown in Figure 3.4.1 and Table 3.4.1, transfer characteristics of OTFTs with different TiO₂ concentrations in P3HT have been measured. The effective field effect mobility decreases with the increase of TiO₂ concentration, which can be

attributed to the TiO₂ nanoparticles that impede the transport of holes in the channel.

Because of the reduction of saturated hole mobility, ON current also decreases with increasing TiO₂ concentration, hence I_{ON/OFF} ratio also drops.

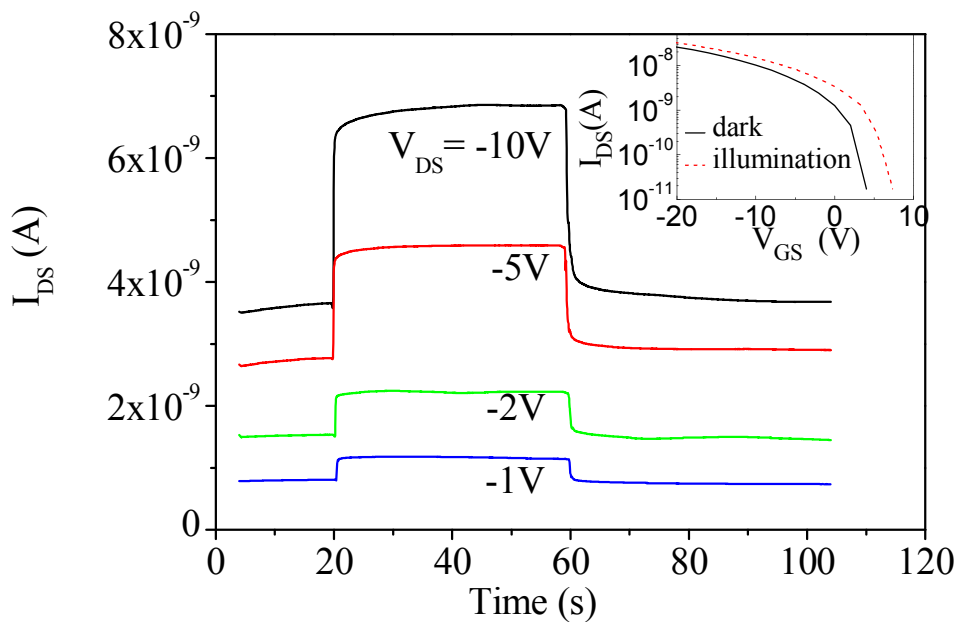


Figure 3.4.2 Channel current of an OPT (weight ratio of P3HT:TiO₂ is 1:0.75) measured at different drain voltages V_{DS} and $V_{GS}=0V$. The rising and falling edges of current correspond to switching on and off a white light illumination of $200\mu W/cm^2$, respectively.

All the OTFTs based on P3HT/TiO₂ composite film are photosensitive. As shown in Figure 3.4.2, the channel current of a device (weight ration of P3HT:TiO₂ = 1:0.75) changes sharply under light illumination. The photo sensitive channel currents have

been measured at different V_{DS} (10V, 5V, 2V, 1V) and under the same V_{GS} (0V). The inset of Figure 3.4.2 shows the transfer characteristics ($V_{DS} = -10V$) of the device measured in dark condition and under white light illumination of $200\mu W/cm^2$, respectively. The transfer curve exhibits a parallel shift to positive gate voltage under light illumination and no evident change can be found in the field effect mobility, OFF current and sub-threshold slope. Therefore light illumination only induces a change in the threshold voltage of the OTFT and this change can be directly calculated from the variation of channel current. It can be found that the channel current changes by two orders of magnitude in the sub-threshold region due to the light exposure.

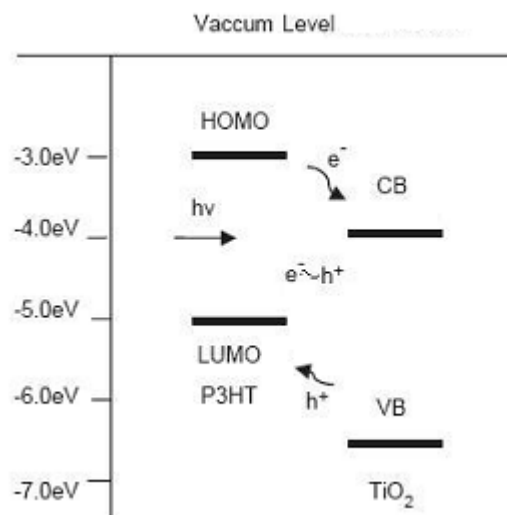


Figure 3.4.3 Energy band diagram of P3HT and TiO₂.

Both P3HT and TiO₂ are widely used components in organic solar cells, and their energy band diagram is shown in Figure 3.4.3. Composite of P3HT and TiO₂ forms a type-II heterojunction (staggered gap) at the interface, which can induce the charge separation of excitons once they move to the interface.

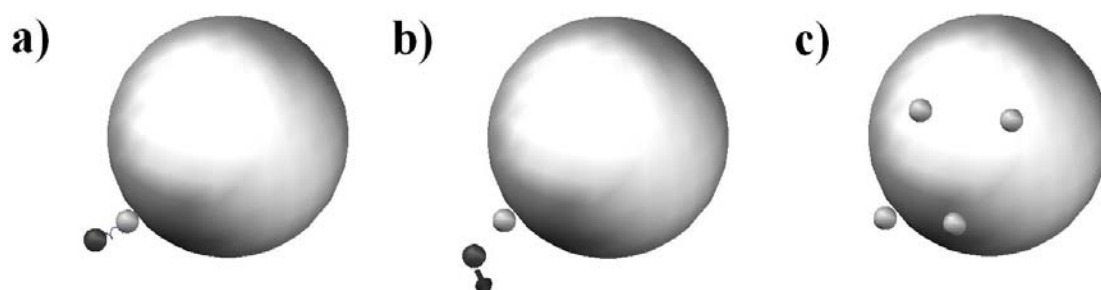


Figure 3.4.4 Illustration diagrams of electron trapping mechanism, **a)** generation of exciton, **b)** separation of exciton, and move to different directions and **c)** electrons trapped on TiO₂ particles.

In the case of OPT, P3HT and TiO₂ play the similar role for generation and separation of excitons into mobile electrons and holes as in solar cell. Figures 3.4.4 (a-c) illustrate the mechanism of electron trapping in TiO₂. As shown in Figure 3.4.4a, photons absorbed by P3HT generate excitons in the film, within the lifetime and before the recombination, charge separation of the excitons may occur at the TiO₂/P3HT interface since the level of the conduction band (4.3eV) of TiO₂ is lower than that of the lowest unoccupied molecular orbit (LUMO) (3.0eV) of P3HT[46].

Separated holes move towards P3HT, whereas electrons move towards TiO₂ (Figure 3.4.4b). However, since TiO₂ particles are all separated from each other instead of forming a continuous conducting path, the separated electrons trapped into the TiO₂ particles become immobilized. Therefore more electrons will be trapped into the TiO₂ nanoparticles since more and more excitons are generated and separated until energy level alters and stops further electron injection (Figure 3.4.4c).

For the application of P3HT/TiO₂ composite in an organic solar cell, high conductivity and continuous paths for electron transport among TiO₂ particles and the anode of the device are critical issues for the device efficiency. We consider that photosensitivity of the OTFT based on P3HT/TiO₂ is also due to the charge separation of excitons at the interface of P3HT and TiO₂. Electrons trapped in TiO₂ nanoparticles will increase the potential of the channel which can be regarded as a floating body effect of the transistor[47]. Therefore as more electrons are trapped in the channel, a bigger shift of the threshold voltage can be induced.

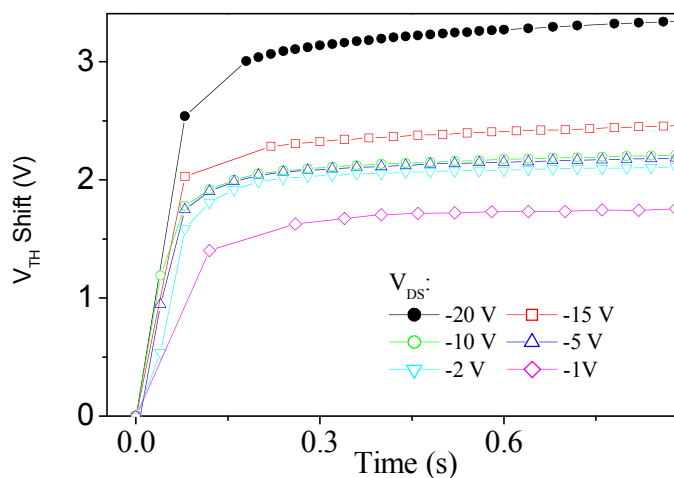


Figure 3.4.5 Shift of the threshold voltage of the OPT (weight ratio of P3HT: TiO₂ is 1: 0.75) calculated from the change of the channel current measured at different V_{DS} .

Figure 3.4.5 shows the shift of threshold voltage under light illumination measured at different source-drain voltage. Charge separation of excitons can be enhanced by applying electric field. We found that higher voltage between source and drain (V_{DS}) can induce higher shift of threshold voltage under the same light illumination, which means higher V_{DS} induces higher density of electrons trapped in the TiO₂ nanoparticles. So this is a clear evidence for field enhanced charge separation of excitons[48] at the interface of P3HT and TiO₂. On the other hand, our experiments show that the influence of gate voltage on charge separation in the channel is negligible. Normally a gate voltage only can induce electric field in the active layer

within several nanometers from the semiconductor/gate insulator interface[49] and thus it has little effect on the charge separation of excitons in the channel.

It is worth noting that the OFF current of the phototransistors measured in dark condition and under light illumination show little difference. Therefore, photocurrent in the channel generated by photon absorption, i.e. by photovoltaic effect[45], is negligible in organic devices, which is different from the device based on the composite of MDMO-PPV /PCBM[45]. In our sample, since TiO₂ nanoparticles do not form a continuous conduction path of electrons in the channel, the contribution of electrons to the channel current is very small. In the case of phototransistors based on MDMO-PPV /PCBM, PCBM may form a network for electron conduction in the channel and thus the transfer curve of this type of devices shows pronounced changes in ON/OFF current and the sub-threshold slope under light illumination.

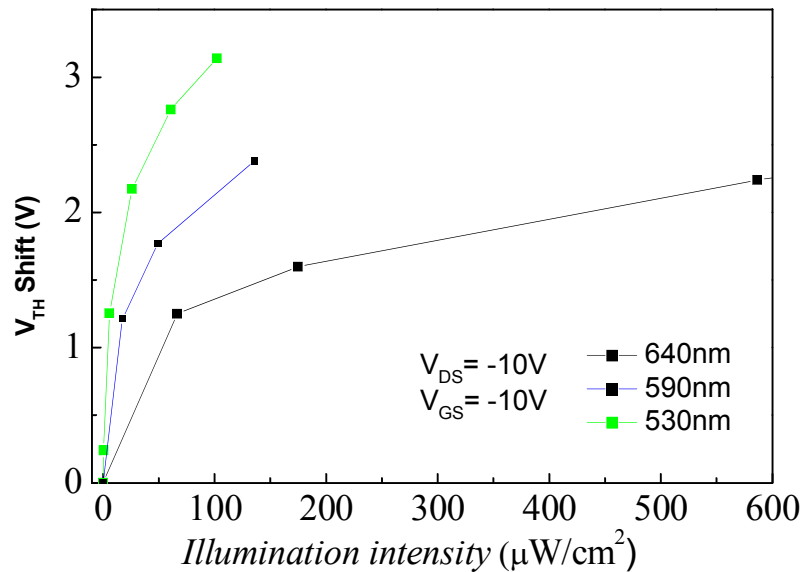


Figure 3.4.6 Shift of the threshold voltage of the OPT (weight ratio of P3HT:TiO₂ is 1:0.75) illuminated with different light intensities and different wavelengths. $V_{DS} = -10\text{V}$.

The photosensitivity of the organic phototransistors is dependent on light intensity and wavelength. A device with P3HT:TiO₂ = 1:0.75 has been measured under three different wavelengths (530nm, 590nm and 640nm). As shown in Figure 3.4.6, the shift of the threshold voltage of the transistor shows a nonlinear relationship with light intensity. This nonlinear behavior can be attributed to the following process. Most of the TiO₂ nanoparticles in the channel are not connected to the source/drain electrodes and the trapped electrons accumulate in the nanoparticles. Therefore the built-in electric field at the interface between TiO₂ and P3HT induced by the

accumulated electrons will retard the charge transfer at the interface and induce a lower photosensitivity at higher light intensity. Another possible reason that may induce lower photosensitivity at higher light intensity is the occurrence of exciton-exciton annihilation within the P3HT layer, resulting effectively in a decrease in the exciton lifetime[46].

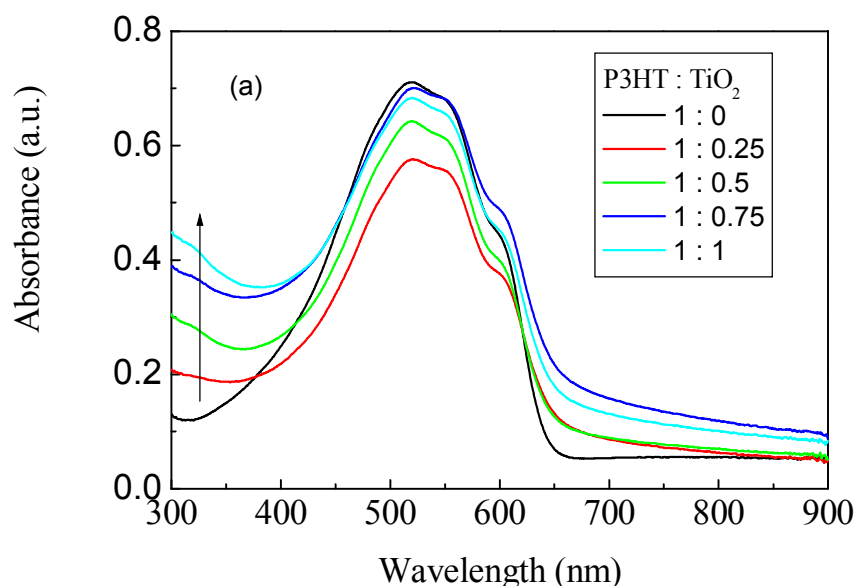


Figure 3.4.7 Absorbance of the P3HT/TiO₂ composite films. Along the arrow, from bottom to top, the weight ratio of P3HT:TiO₂ are 1:0, 1:0.25, 1:0.5, 1:0.75 and 1:1, respectively.

The photosensitivity of the device is obviously related to the light absorbance of the composite film. As shown in Figure 3.4.7, pure P3HT and P3HT/TiO₂ composite thin films both exhibit a maximum light absorbance at 520nm and a decreasing

value with increasing wavelength. Maximum light absorbance appears at 520nm corresponding to the bandgap energy of $\sim 2.2\text{eV}$ for P3HT. In addition, it can be found that TiO₂ nanoparticles increase the light absorbance in the UV region.

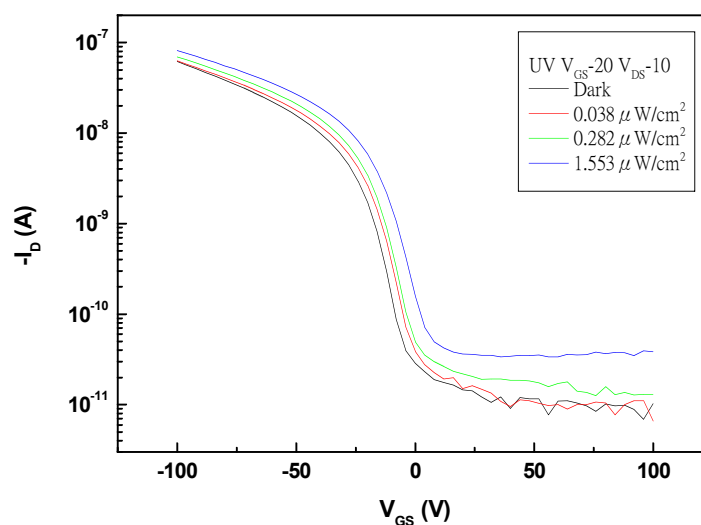


Figure 3.4.8 Transfer characteristics of OPTs measured in different incident intensities with constant V_{DS} and V_{GS} .

Figure 3.4.8 shows the photo-response of the P3HT/TiO₂ OPTs under different UV incident intensity. 10 volts of threshold voltage shift appears under $1.553 \mu\text{W}/\text{cm}^2$ UV incident with no obvious change of transfer characteristics expect for a parallel shift towards positive threshold voltage, whereas there is no photo-response for a pure P3HT device under the same incident intensity. Therefore enhancement of photo-response towards UV region is due to the presence of TiO₂, which is also

confirmed by an increase of absorbance in UV region with the increase of TiO₂ as shown in Figure 3.4.7.

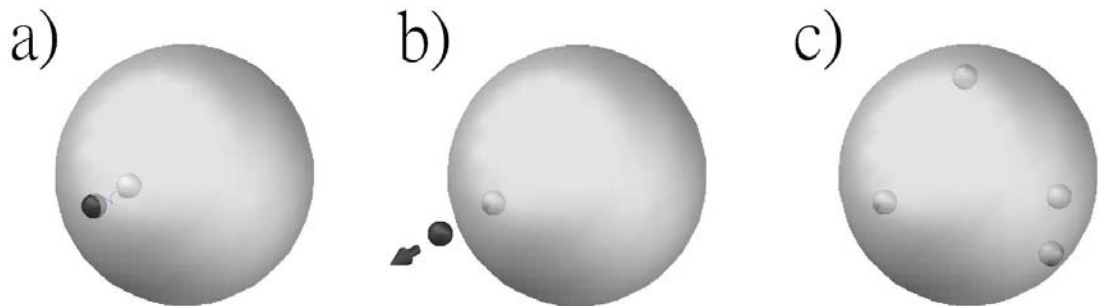


Figure 3.4.9 Illustration diagram of electron trapping mechanism, **a)** generation of an exciton in TiO₂, **b)** separation of an exciton, and move to different directions and **c)** electrons trapped in TiO₂ particles.

The charge trapping mechanism for UV light is different from visible region. When device is exposed to UV light source, excitons will be generated in TiO₂ particles instead of P3HT. Excitons are then separated into electron and hole at the P3HT-TiO₂ interface because of the difference in energy level. Hole is injected into P3HT and escapes from TiO₂ to prevent recombination because of the high hole mobility of P3HT, which also contributes to channel current. On the other hand, isolated TiO₂ particles provide a space for electron trapping to alter threshold voltage as shown in Figure 3.4.9.

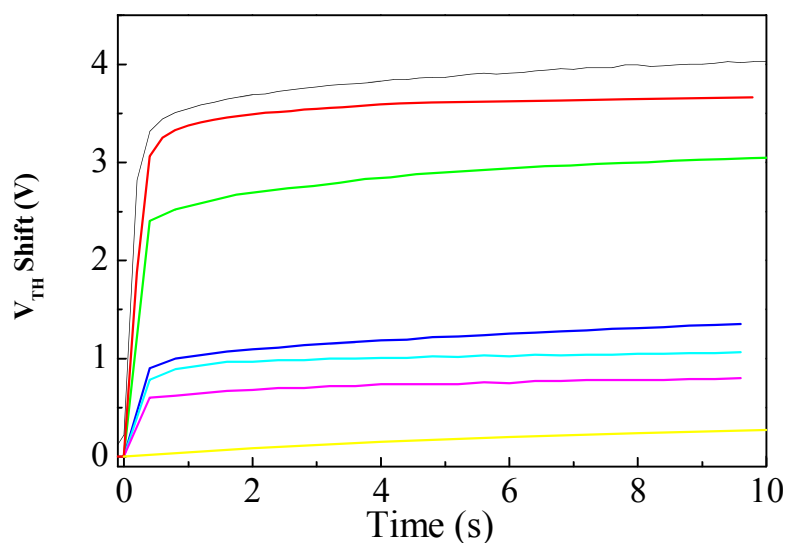


Figure 3.4.10 Shift of the threshold voltage of the OTFTs with different weight ratios of P3HT:TiO₂ measured under the white light illumination of 200 μ W/cm² and V_{DS}=-20V . From bottom to top, the weight ratios of P3HT:TiO₂ are 1:0, 1:0.05, 1:0.10, 1:0.25, 1:0.5, 1:0.75 and 1:1, respectively.

As shown in Figure 3.4.10, the photosensitivity of the OTFT based on P3HT/TiO₂ is dependent on the concentration of TiO₂ nanoparticles in the composite film. The shift of the threshold voltage increases with the increase of TiO₂ weight ratio under the same intensity of light illumination, which can be explained in terms of higher density of electrons trapped in the channel by higher density of TiO₂ nanoparticles.

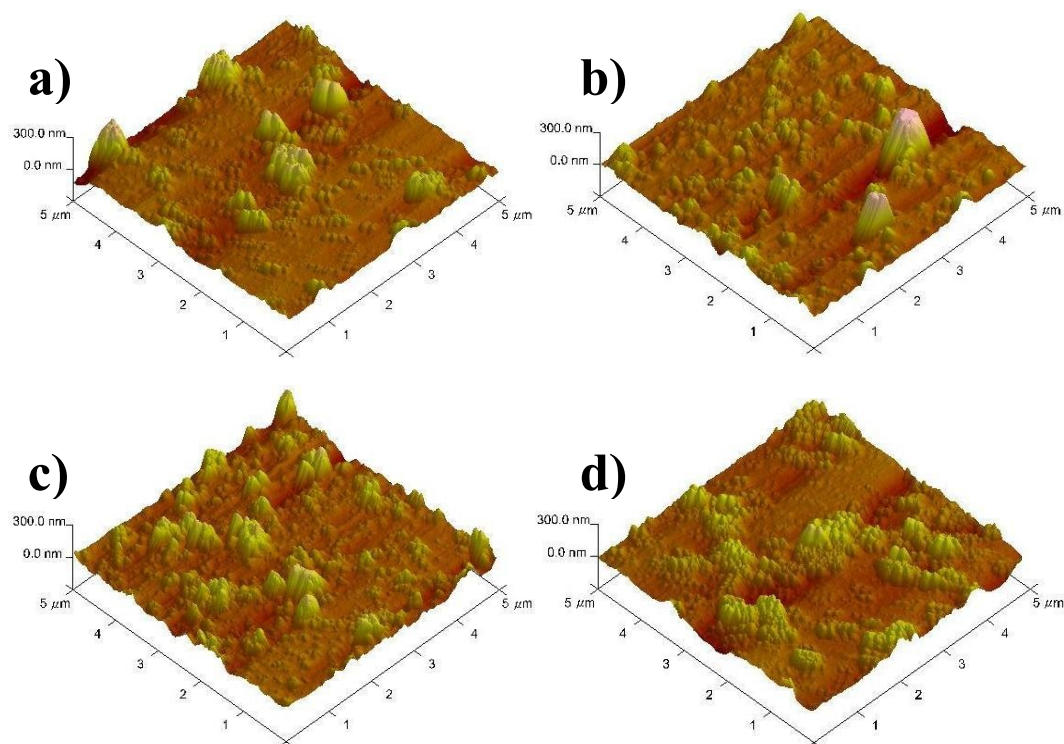


Figure 3.4.11 AFM image of P3HT/TiO₂ sample with concentration **a)** 1: 0.25 **b)** 1: 0.50 **c)** 1: 0.75 and **d)** 1: 1.

As shown in Figures 3.4.11 (a-d), as the concentration of TiO₂ particles increases, nano-particles aggregate into clusters instead of uniformly distributed into the polymer matrix because of the attraction force between them, hence the number of clusters increase with increasing TiO₂ concentration. Since photo-response of this P3HT/TiO₂ nanocomposite based OPT is induced by trapping of electrons into TiO₂ particles, which depend on the interface between P3HT and TiO₂, formation of cluster may reduce the total area of interface and thus the shift of the threshold voltage is no longer linearly dependent on the TiO₂ concentration, as shown in Figure 3.4.10.

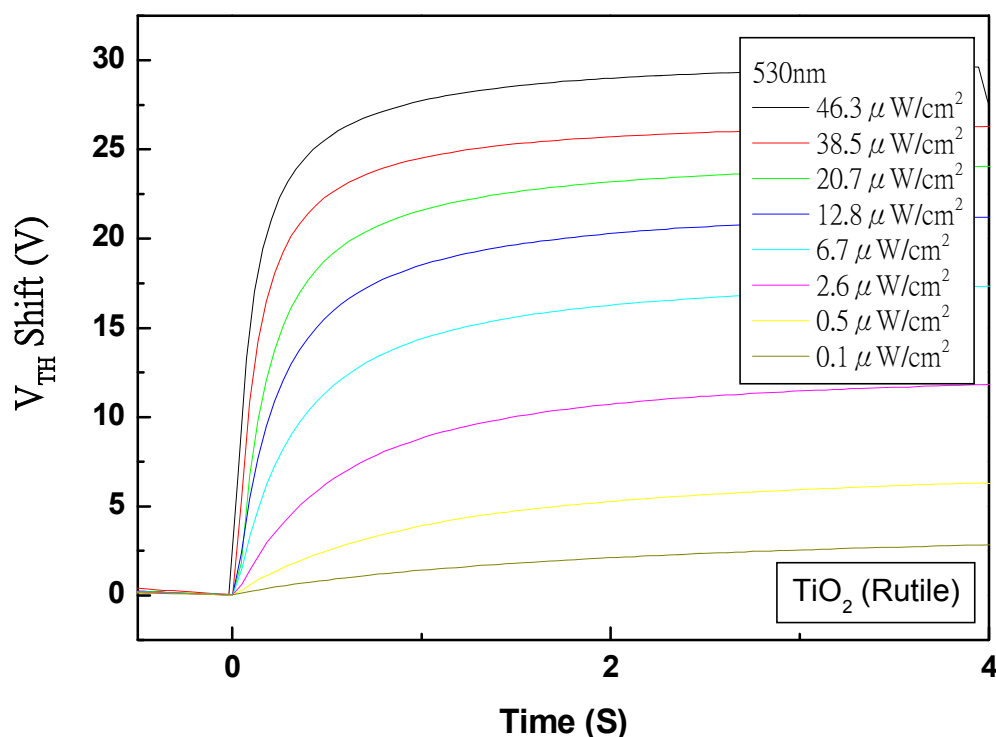
3.5 Rutile phase TiO₂/P3HT OPTs

Figure 3.5.1 Shift of the threshold voltage of the OPT (weight ratio of P3HT:TiO₂ is 1:0.75) illuminated with different light intensities. $V_{DS}=V_{GS}=-10V$.

Apart from using mixture phase of anatase and rutile, single phase TiO₂ is also studied. Rutile phase TiO₂ nano-particles with diameter smaller than 20nm is purchased from Sigma-Aldrich. P3HT and rutile-TiO₂ is dissolved into chloroform and spun on a patterned SiO₂/*n*-Si substrate, followed by post-annealing process at 120°C for one hour under N₂ environment. Figure 3.5.1 shows the shift of threshold voltage of the rutile-TiO₂/P3HT OPT (weight ratio of P3HT:TiO₂ = 1:0.75) under

different incident intensity with 530nm wavelength. It is found that the degree of shift is larger than that in OPTs based on mixture phases and response time towards light incident decreases with the increase of light intensity.

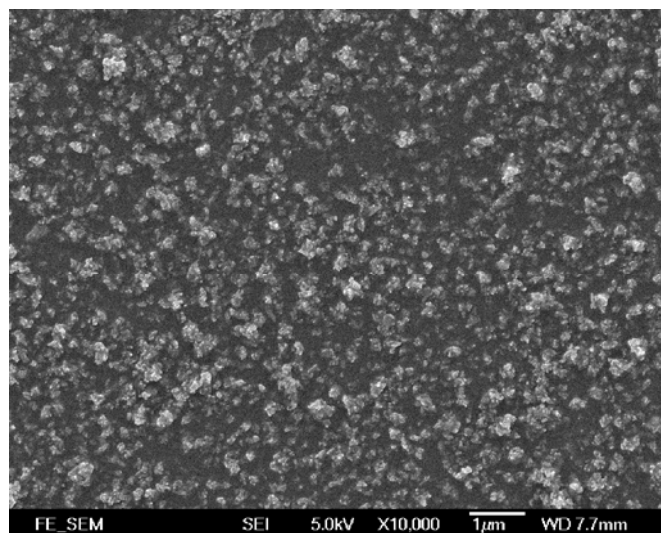


Figure 3.5.2 a) SEM image of P3HT/TiO₂ (Rutile) sample in 1: 0.75 concentration.

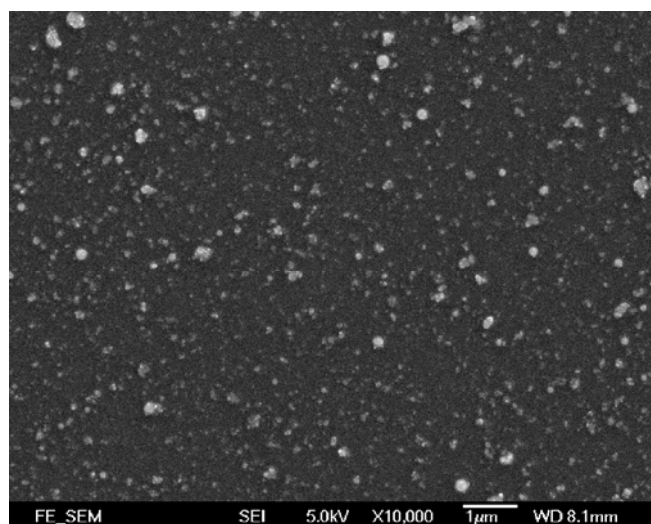


Figure 3.5.2 b) SEM image of P3HT/TiO₂ (Rutile and Anatase) sample in 1: 0.75 concentration.

As shown in Figure 3.5.2, diameter of the rutile TiO₂ is smaller and they can uniformly embed and distribute in the P3HT matrix, whereas cluster is formed in sample with mixture phases. Therefore the reason for larger threshold voltage shift appeared in rutile sample can be contributed to the increase of interface area.

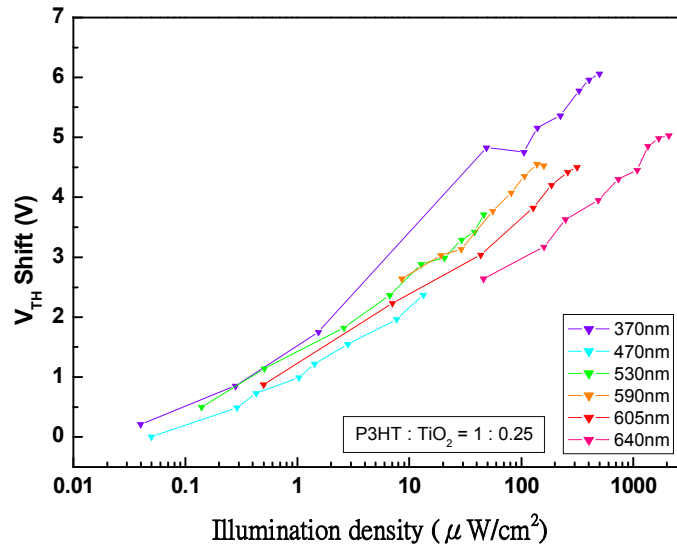


Figure 3.5.3a) Shift of the threshold voltage of the OPT (weight ratio of P3HT:TiO₂ is 1:0.25) illuminated with different light intensities and different wavelengths. $V_{GS}=V_{DS}=-10\text{V}$.

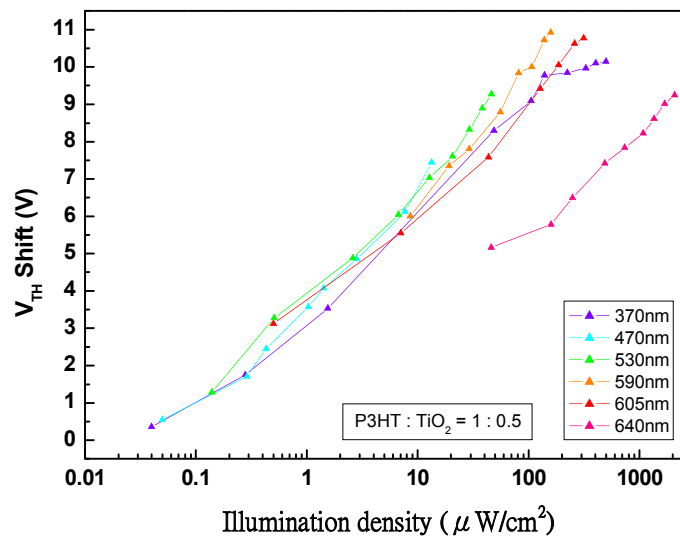


Figure 3.5.3b) Shift of the threshold voltage of the OPT (weight ratio of P3HT:TiO₂ is 1:0.50) illuminated with different light intensities and different wavelengths. $V_{GS}=V_{DS}=-10\text{V}$.

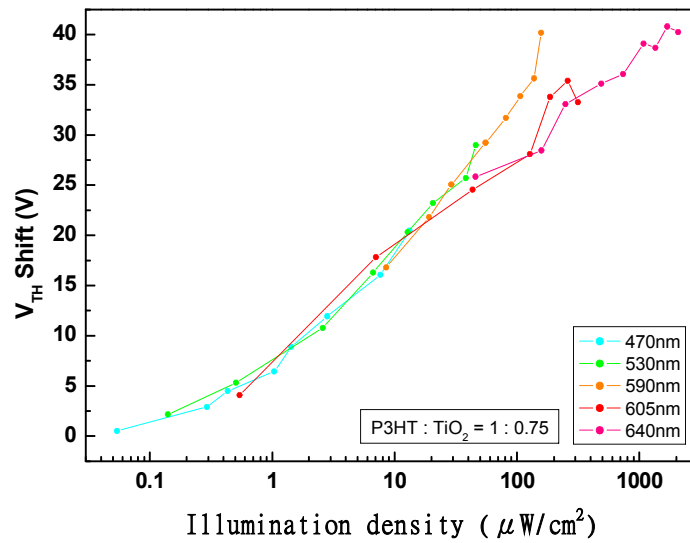


Figure 3.5.3c) Shift of the threshold voltage of the OPT (weight ratio of P3HT:TiO₂ is 1:0.75) illuminated with different light intensities and different wavelengths. $V_{GS}=V_{DS}=-10V$.

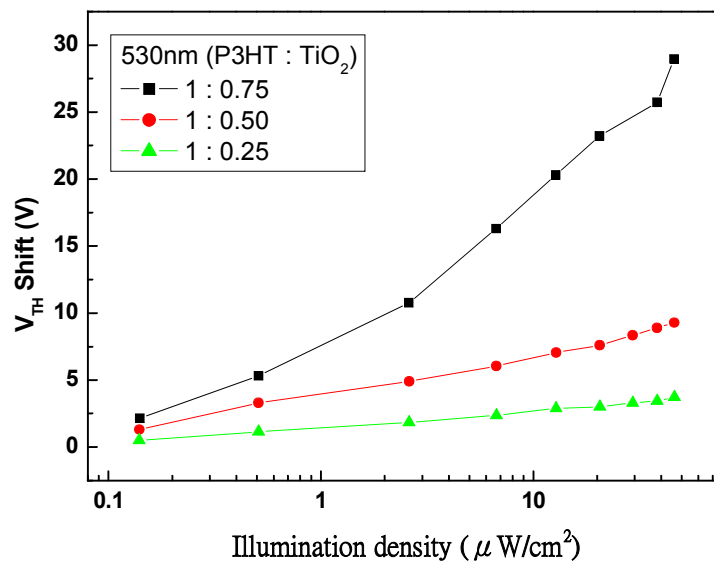


Figure 3.5.3d) Shift of the threshold voltage of the OPT (weight ratio of P3HT:TiO₂ are 1:0.25, 1:0.50 and 1:0.75) illuminated with different light intensities and different wavelengths. $V_{GS}=V_{DS}=-10V$.

As shown in Figures 3.5.3 a-c), all three OPTs with different TiO₂ concentrations show similar response to light irradiation. Positive photo-response occurred not only in visible light region but also in UV region. As shown in Figure 3.5.3d, sensitivity of the device (slope of threshold voltage shift against light intensity) increases with TiO₂ concentration. For example, threshold voltage changes by 3.71V in the sample with small TiO₂ concentration (P3HT: TiO₂ = 1:0.25) while it changes by 28.96V in higher TiO₂ concentration (P3HT: TiO₂ = 1:0.75) under the same irradiation condition.

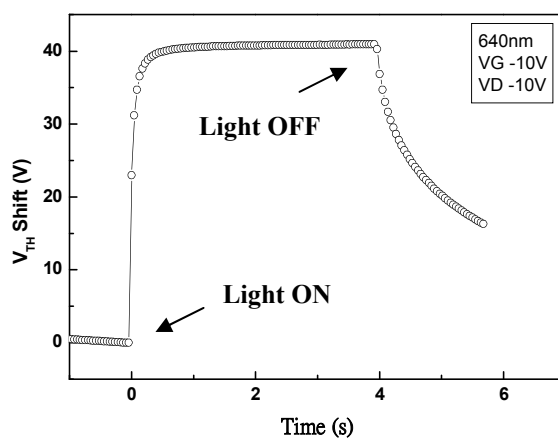


Figure 3.5.11 Time-resolved response of the P3HT/TiO₂ (1:0.75) phototransistor upon irradiation with 1.7 mW/cm² at $V_{GS}=V_{DS}=-10$ V.

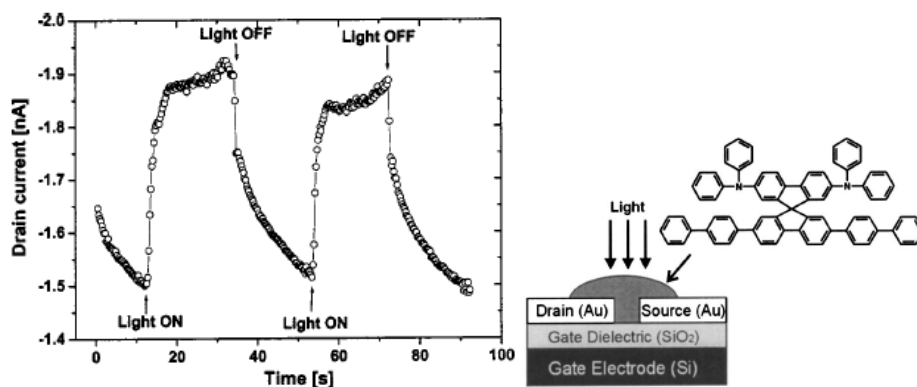


Figure 3.5.12 (Reprinted from Saragi[42]) Time-resolved response of the phototransistor upon irradiation with 191 mW/cm² at $V_{GS}=V_{DS}=-10$ V. The photo switching of the drain current is reversible with a relaxation time of 10.3 s. Device structure is shown on the right.

Comparing Figure 3.5.11 with 3.5.12, we can find that TiO₂/P3HT OPT shows better device performance in terms of response time and stability, which takes less than one second to achieve saturated value, and this saturated value is very stable for several seconds. Obviously, device stability and fast responses are also critical to photosensors.

3.6 Conclusion

In conclusion, photosensitive OTFTs based on the composite film of P3HT and TiO₂ nanoparticles have been fabricated and show a stable performance and relatively fast response time under light illumination. Since the device can be fabricated by solution process, it can be easily integrated into organic circuits and multi-functional sensor chips, which implies a broad potential application in the future.

Chapter Four

Label-free DNA

OTFT sensor

4.1 Introduction of DNA sensor

Detecting small quantities of biomolecules is paramount in the diagnosis of disease, drug discovery, and basic researches. Especially, it is of great scientific and economic importance to develop techniques for nucleic acid detection, which have broad potential applications including gene expression monitoring, pharmacogenomic research and drug discovery, clinical diagnostics, viral and bacterial identification, detection of biowarfare and bioterrorism agents, and forensic and genetic identification, etc. To exploit these opportunities, DNA sensors are required to provide a combination of high sensitivity, selectivity, speed, portability, and low cost. Therefore, DNA micro-array (DNA chip) technology has been developed to offer an unprecedented simultaneous and multiplexed analysis in a high-throughput screening format.

Label-free techniques are of special interest since incorporation of a labelling step into a nucleic acid assay makes it more complex, cumbersome and expensive.

Recently, there has been interest in various technologies such as electrochemical detection[50], surface vibration spectroscopy[51], atomic force microscopy (AFM)[52], scanning Kelvin probe microscopy (SKM)[53], genetic field effect transistor (FET)[54-56] and micro-cantilever[57, 58] to realize high sensitivity, label-free DNA micro-arrays. Compared with the other techniques, genetic FET has the advantage of being able to be miniaturized without losing signal to noise ratio since the channel current of a FET is proportional to the width/length ratio of the channel and not related to the area of the device[49]. Therefore FET is ideal for the application in small-sized, high-density and multi-functional micro-array sensors[59]. On the other hand, biosensors based on FETs can be easily integrated with circuitry to form self-supported DNA detection platform since FET is the key component of an integrated circuit.

DNA sensors based on various FETs have been reported. An integrated array of silicon FET for electronic detection of label-free DNA have been developed[55], which shows a shift in gate voltage for about 80meV corresponding to the adsorption of DNA to the gate insulator - SiO₂. Sakata et al[56] have studied a genetic FET based on *n*-type silicon FET with Si₃N₄ gate insulator. Single strand

DNA probes are immobilized on the surface of the Si_3N_4 gate insulator. Hybridization with target DNA on the sensor has induced a shift of threshold voltage of 11meV. Estrela et al[54] have developed DNA sensors based on extended gate polycrystalline silicon thin film transistors (TFT). A parallel shift of transfer characteristics (drain current versus gate voltage) of 355meV has been observed after the hybridization of single strand DNA probes immobilized on an extended Au gate electrode with its complementary strand. All of the aforementioned genetic FETs are based on electronic detection of intrinsic charge of DNA molecules (negative charge) in an electrolyte. DNA molecules in the electrolyte are screened by mobile counter ions and thus induce a surface potential drop that modulates gate voltage applied on the transistor. The potential drop is influenced by various factors including the concentration of ions in the electrolyte, DNA concentration in the surface and the length of DNA strand[55]. So variations of the threshold voltage of the TFT due to DNA hybridization are diverse in different reports.

Organic thin film transistors (OTFT) are excellent candidates for use in disposable sensors for their easy and low cost fabrication as compared with their inorganic counterparts[33, 35]. Organic materials can be dissolved in various solvents, so that

transistors can be coated or printed at low temperature. In addition, organic semiconductors are biocompatible and flexible thus they can be integrated with biological systems[60-61]. There are several types of OTFT based chemical sensors or biosensors that have been reported. Loi *et al* (2005) have developed organic ion sensitive field effect transistor (ISFET) on flexible plastic film that acts both as substrate and gate dielectric. Tanese[62] *et al* (2005) reported gas sensor based on OTFTs with a gas sensitive organic semiconductor layer.

Zhang[19] *et al* (2007) reported a DNA sensor based on pentacene TFT, in which DNA molecules are immobilized on the surface of semiconductor layer and an unambiguous doping-induced threshold voltage shift up to 20V has been observed. However, the DNA molecules need to be immobilized on the surface of pentacene, which may decrease the stability and repeatability of the device since pentacene film is sensitive to moisture and some ions. To our best knowledge, this is the only paper that reports DNA sensing performance based on OTFTs. In this thesis, we report another type of DNA sensor based on OTFTs, which shows good device performance when DNA molecules are immobilized and hybridized on the surface of source-drain electrodes.

4.2 Experiments

4.2.1 Substrate Preparation

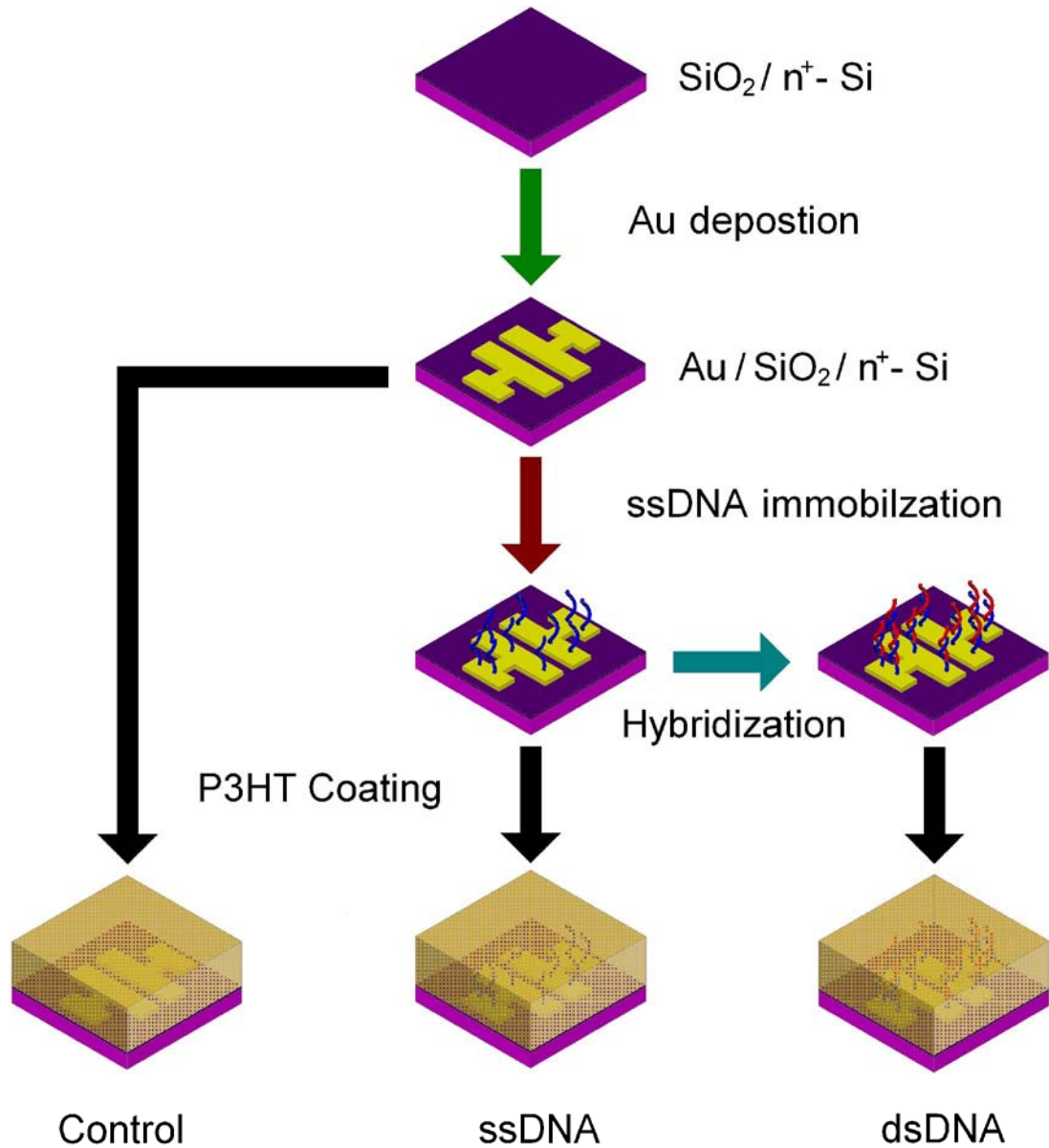


Figure 4.2.1.1 Diagrams showing steps to prepare OTFTs incorporated with DNA layer in the devices. The thickness of SiO_2 is 500nm. The channel width and length of the OTFTs are 2 mm and 0.2mm, respectively.

As shown in Figure 4.2.1.1, OTFTs have been fabricated on a silicon substrate. Highly doped *n*-type silicon wafer with 500nm thick SiO₂ was used as the starting substrate, in which the SiO₂ film and *n*-type silicon acted as the gate insulator and gate electrode, respectively. Then Au source/drain electrodes were deposited on top of the SiO₂ film through a shadow mask with thermal evaporation. The channel length and width for the device were 0.2mm and 2mm, respectively.

4.2.2 DNA Immobilization and Hybridization

To detect the effect of DNA immobilization and hybridization, three identical chips were used as one set of samples in the experiment. The gold electrodes were first washed with acetone, then followed by deionized (DI) water and phosphate buffer solution (PBS) (PH=7.4). The probe single strand DNA (ssDNA) (21 bases, 3'-/3ThioMC3-D/TTT TGT CCT TTG TCG ATA CTG-5' (HPLC Purification)) dissolved in phosphate buffer solution (PBS) (2.0 μM DNA in 75μL PBS) was dropped on the two chips and left for a certain period of time (*t*) to immobilize ssDNA on the Au source/drain electrodes. After the immobilization, the substrate was washed again with PBS. Target DNA (5'-/56-FAM/CAG GAA ACA GCT ATG

AC -3', 17 bases, HPLC Purification) dissolved in PBS (2.0 μ M DNA in 75 μ L PBS) was dropped on one of the two chips and left for around 2 hours for hybridization. After the interaction, the substrate was again washed with PBS.

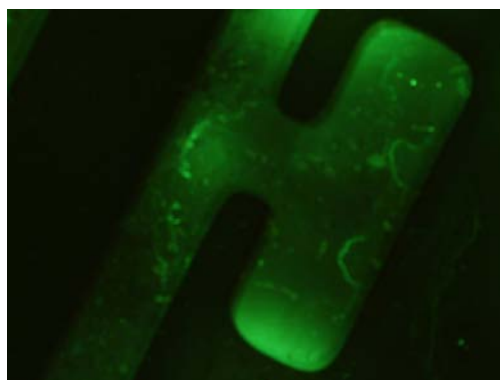


Figure 4.2.2.1 Fluorescence image of gold electrodes after the hybridization of DNA.

Fluorescence images of labelled DNA were obtained using a fluorescence microscope (Nikon ECLIPSE 80i, Japan). Since the target DNA was labelled with 56-FAM group, the immobilization of probe ssDNA and hybridization of the target DNA could be confirmed under the fluorescence microscopy, as shown in Figure 4.2.2.1.

4.2.3 Fabrication of Organic Thin Film Transistor

Then organic semiconductor thin film was spin-coated on top of the three chips after being washed with DI water. Here, the three chips include one control sample without DNA on Au electrodes, one sample with ssDNA and one sample with dsDNA immobilized on Au electrodes. We chose regioregular poly(3-hexiothiophene) (rr-P3HT) (regioregularity is ~98.5%, from Aldrich) as the semiconductor material since rr-P3HT has a relatively high field effect mobility[24], which is close to the value for amorphous Si. Thus, rr-P3HT is a promising material for the applications in OTFT sensors. In the experiment, rr-P3HT was dissolved in chloroform with the concentration of 10mg/ml and spin-coated on the samples with a film thickness of ~20nm. Here, the thickness of the polymer film is not important for the sensor since OTFT is an interfacial device and the channel current normal passes through a very thin layer (less than several nanometers) near the insulator[49]. Then all of the samples were annealed at 60°C for 1 hour to remove the solvent and to improve crystallinity of the P3HT layer.

4.2.4 Signal Acquisition

The DNA sensors based on OTFTs have been characterized using a precision semiconductor parameter analyzer (Agilent 4156C) in a glove box filled with high purity N₂. Device performance of OTFTs, including transfer characteristics and output characteristics of each device, have been measured. For transfer characteristics, the channel current I_{DS} between source and drain was measured as a function of gate voltage V_{GS} under a constant drain voltage V_{DS} . For output characteristics, the channel current I_{DS} was measured as a function of drain voltage V_{DS} under a constant gate voltage V_{GS} and different V_{GS} results in a different curve of I_{DS} versus V_{DS} . To obtain a stable result, channel current was measured for 2 seconds for each value of applied voltage.

One important parameter of OTFT is the field effect mobility of carriers in the channel. In our experiment, the field effect mobility of holes μ in the device can be calculated from the saturation channel current of the device I_{DS} ($|V_{DS}| > |V_{GS}|$) as a function of applied gate voltage V_{GS} :

$$\mu = \frac{2L}{WC_i} \left(\frac{q\sqrt{I_{DS}}}{\alpha V_{GS}} \right)^2 \quad (1)$$

where C_i is the capacitance of gate dielectric per unit area; ϵ_i is the relative dielectric constant of gate insulator; ϵ_0 is the dielectric constant in vacuum; t_i is the thickness of the gate insulator; W and L are channel width and length of the OTFT, respectively.

4.3. Results and discussions

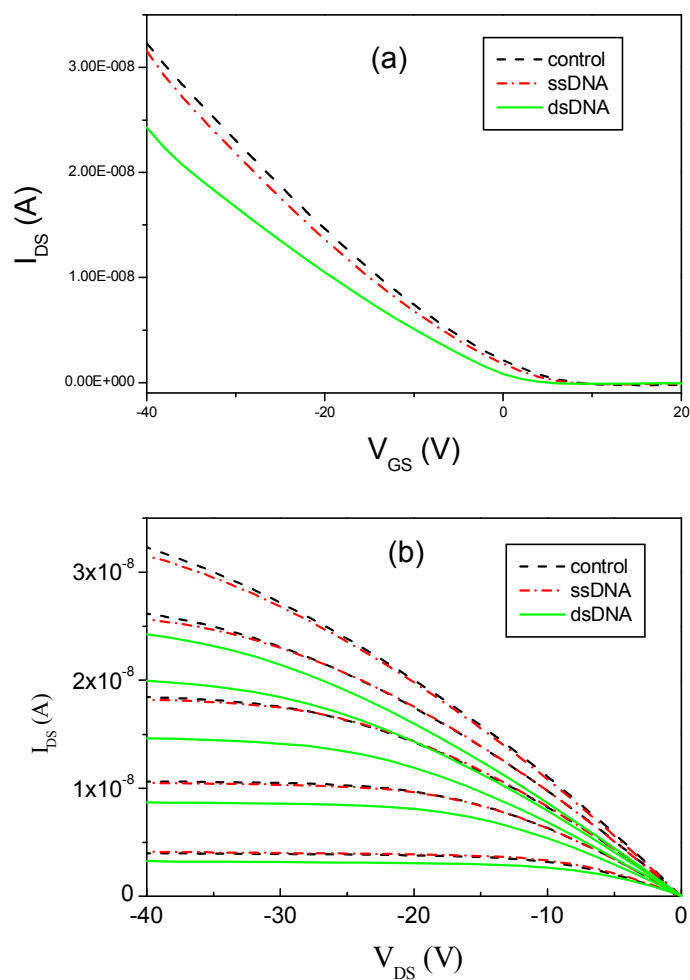


Figure 4.3.1 Performance of the OTFTs with probe immobilized on Au source/drain electrodes for 4 hours. **a)** Transfer characteristics of three OTFTs (control, ssDNA and dsDNA). $V_{DS} = -40V$. **b)** Output characteristics of three OTFTs (control, ssDNA and dsDNA). For each device (different colours correspond to different devices), from top to bottom, the curves are measured at the V_{GS} of -40V, -30V -20V, -10V and 0V, respectively.

To find the influence of the density of DNA molecules immobilized on the Au electrode, several sets of samples with different immobilization time ($t = 4,$

8, 24, 48 hours) of probe ssDNA have been fabricated. For the set of samples with lower density of DNA ($t = 4$ hours), the performance of OTFTs already exhibits big difference to the control sample. Figure 4.3.1a shows channel current as a function of gate voltage measured at a constant drain voltage (transfer characteristics of the three samples: control, ssDNA and dsDNA). Figure 4.3.1b shows the channel current as a function of drain voltage V_{DS} under several different gate voltages (output characteristics, $V_{GS} = -40, -30, -20, -10, 0V$) of the three samples. Under the same applied voltage, the control sample shows the maximum channel current and the sample with dsDNA layer shows the minimum. Therefore a DNA layer between the metal electrode and semiconductor layer decreases the channel current and dsDNA shows bigger effect than ssDNA.

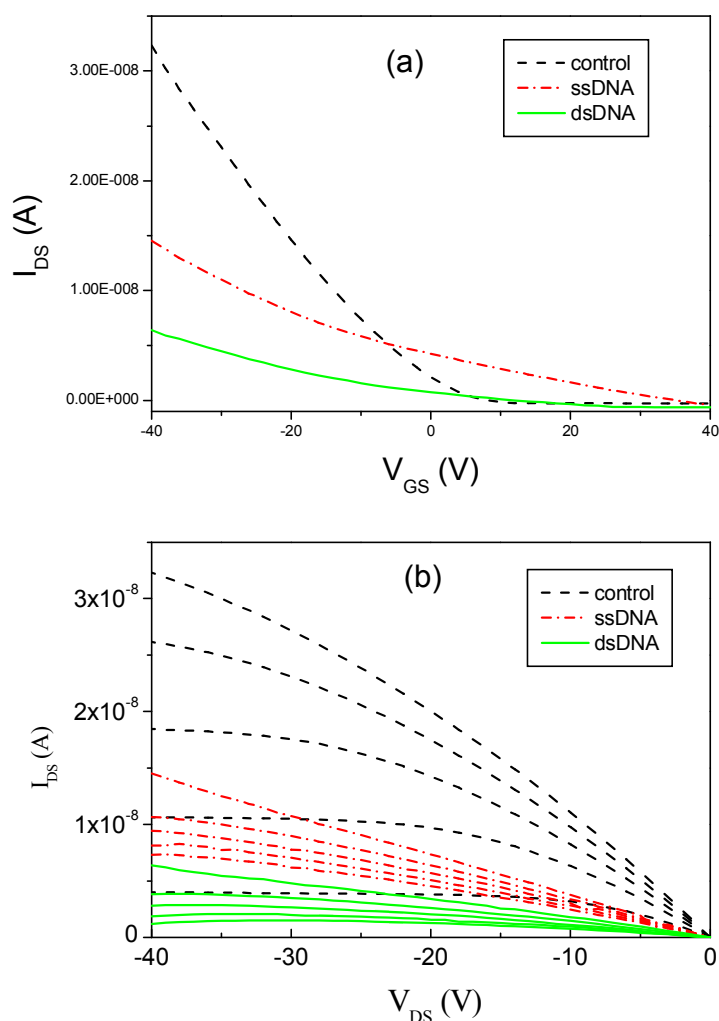


Figure 4.3.2 Performance of the OTFTs with probe immobilized on Au source/drain electrodes for 48 hours. **a)** Transfer characteristics of three OTFTs (control, ssDNA and dsDNA). $V_{DS} = -40V$. **b)** Output characteristics of three OTFTs (control, ssDNA and dsDNA). For each device (different colours correspond to different devices), from top to bottom, the curves are measured at the V_{GS} of -40V, -30V -20V, -10V and 0V, respectively.

For the samples with the highest density of DNA ($t = 48$ hours) immobilized on the electrodes, the transfer and output characteristics have been measured at the

same condition, as shown in Figure 4.3.2a and 4.3.2b, respectively. The device performance exhibits dramatic change compared with the control sample. The ON current of the device with ssDNA is much lower than that of the control sample and higher than that with dsDNA. The threshold voltage of the sample with ssDNA is very different from the other two samples. It is probably due to some ssDNA molecules have been immobilized on the channel region beside the Au electrodes since the immobilization time is relatively long (48 hours). Threshold voltage of an OTFT can shift to positive value if there is some negative charge immobilized in the channel region. In this sample, the positive shift can be attributed to the intrinsic negative charge of DNA molecules in the channel region. This result also suggests that it is not necessary to immobilize DNA for too long time.

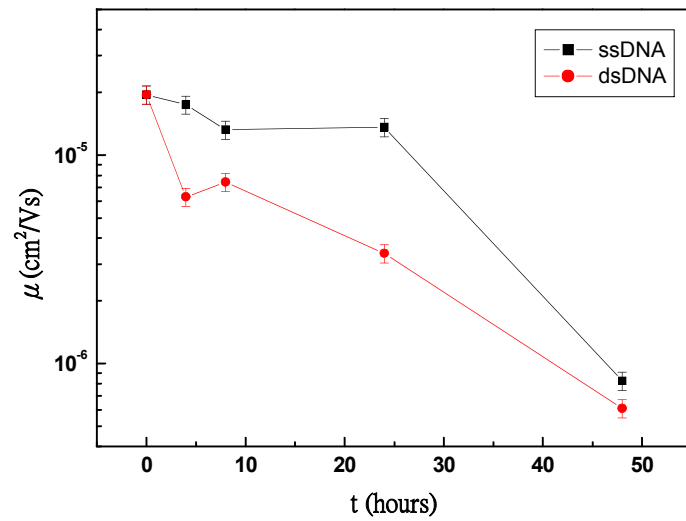


Figure 4.3.3 Field effect mobilities of the OTFTs with ssDNA and dsDNA layers immobilized on Au source/drain electrodes as a function of immobilization time t ($t = 4, 8, 24, 48$ hours) of DNA probe and $t = 0$ corresponds to the control sample.

Field effect mobility of carriers in the OTFTs as given by equation (1) is influenced by the DNA density. For each sample, we have fabricated three identical devices showing very similar performance. As shown in Figure 4.3.3, the field effect mobility for different immobilization time of DNA is the average value of the mobilities calculated from the saturation current of the three identical OTFTs. For each device, the variation of mobility is within $\pm 10\%$ of the average value. Therefore the error bar we set is 10% of the results shown in Figure 4.3.3. It can be found that field effect mobility decreases with the increase of immobilization time of probe DNA on the Au electrodes. Since DNA is immobilized only on the

source/drain electrodes, we consider that a DNA layer increases the contact resistance of the OTFT and thus decreases the channel current.

The effect of DNA layer on the contact resistance can be attributed to two possible reasons. One is due to the high resistance of DNA layer connected in series with the channel resistance. Since a single strand oligonucleotide has 0.34 nm distance between base pairs[53], the maximum length of a DNA with 21 bases is about 7 nm, which also can be regarded as the maximum thickness of the DNA layer. So the thickness of DNA layer is five orders of magnitude smaller than the channel length (0.2mm). In addition, previous studies on single DNA ropes indicate that DNA behaves as a good semiconductor [65,66]. Therefore the influence of the resistance of DNA layer on the channel current is negligible.

Another possible reason can be due to the decrease of injection current from source electrode to the channel, which has been regarded as the main reason for the contact effect in OTFTs[34, 63]. The contact effect at source/drain is very important for the performance of a TFT, which is normally induced by a higher (lower) Fermi level of the metal source/drain electrode relative to the HOMO (LUMO) level of the

semiconductor layer for *p*-channel (*n*-channel) devices. In other words, it is due to a potential barrier at the source or drain contact. The contact resistance is limited by a tunnelling or hopping process of carriers across the barrier. Therefore, a small change of the work function of source/drain electrodes can dramatically influence the contact resistance and the channel current. For a *p*-channel device, the lower the work function of the electrodes is the higher the contact resistance will be. The highest occupied molecular orbital (HOMO) level of P3HT (-5.2eV)[64] is lower than the Fermi level of Au (-5.1eV). Therefore any decrease of the surface potential of Au electrode can induce increase of contact resistance.

It has been reported that immobilization of probe ssDNA molecules on Au electrode and thereafter hybridization with complimentary strands may decrease the work function of the Au surface, as confirmed by SKM measurement[53] and other experiments[54]. This effect is normally induced by surface dipole formed by intrinsic charge of DNA. So detecting a work function change induced by a biological interaction can be a technique employed in nucleic acid micro-array technology.

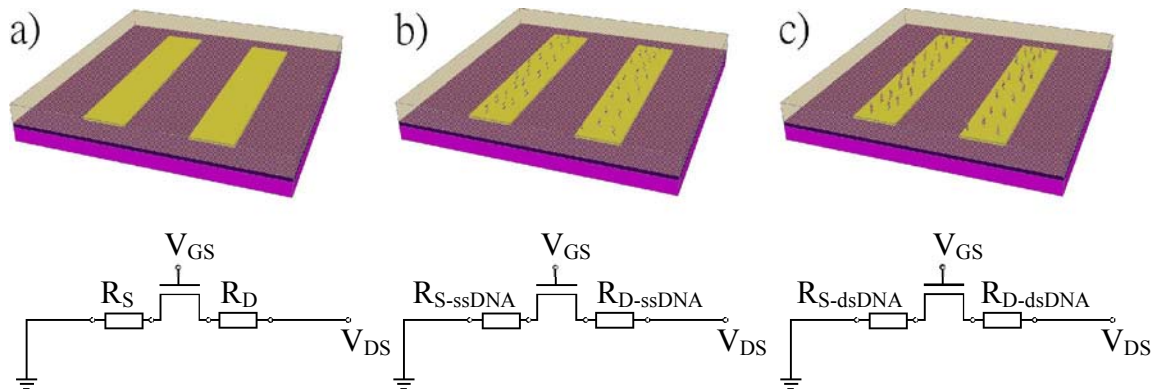


Figure 4.3.4 Diagrams of OTFT and equivalent circuit of **a)** control sample, **b)** ssDNA sample and **c)** dsDNA sample.

In our experiment, since the immobilized DNA layer decreases the work function of the Au source/drain electrodes, increase of contact resistance at source/drain electrodes can be expected. Therefore the decrease of the channel current and the field effect mobility of the devices with DNA immobilized on Au source/drain electrode can be attributed to the increase of the contact resistance and this effect is bigger for higher density of DNA. We can find the decrease of the channel current due to the immobilization of dsDNA is bigger than that of ssDNA, thus dsDNA can change the work function of the electrode more dramatically. As shown in Figure 4.3.4, for control sample, contact resistance R_S and R_D can be attributed to energy difference between Au source/drain electrode and the semiconductor layer. Whereas contact resistance increases to $R_{S-ssDNA}$ and $R_{D-ssDNA}$ after the immobilization of

ssDNA due to the change of metal work function and channel current drops. Contact resistance further increases to $R_{S-dsDNA}$ and $R_{D-dsDNA}$ after the hybridization of dsDNA and channel current decreases to a lower value. Therefore ssDNA and dsDNA are differentiated successfully in the experiments indicating that this is a promising technique for sensing DNA hybridization without labeling. Since it is a mature technique to immobilize DNA molecules on Au electrodes, high density of TFTs functionalized with different DNA probes can be fabricated on a single chip[53]. Compared with the OTFT based DNA sensor developed by Zhang[19] *et al* (2007), our device can be immobilized with DNA more conveniently. In addition, the organic semiconducting layer in our device is coated after the DNA immobilization, therefore unwanted doping effect to organic layer will not occur and a more stable performance can be expected in the device. We consider that this type of OTFTs can be developed as low cost, label-free and disposable DNA sensing micro-arrays. Further work will be carried out to study the effect of DNA sequence, length and mismatch of hybridization on the device performance and the effect of using different types of organic semiconductors as the active layer in an OTFT.

4.4. Conclusion

In conclusion, DNA immobilized on the surface of source/drain Au electrodes of OTFT can dramatically change the channel current and the field effect mobility of the device, which is attributed to the increase of contact resistance at the source/drain electrodes. The increase of contact resistance can be explained in terms of the decrease of work function of the source/drain Au electrode after DNA immobilization and hybridization. Based on this technique the OTFT can be developed to be a low-cost, label-free and disposable DNA sensor since the effect of dsDNA is much bigger than that of ssDNA.

References

- [1] J. E. Lilienfeld, "Method and apparatus for controlling electric current," *US Patent 1745175*, 1930.
- [2] D. Kahng and M.M. Atalla, *IRE Solid-State Devices Research Conference*, 1960.
- [3] G. W. Neudeck and A. K. Malhotra, "An amorphous silicon thin film transistor: Theory and experiment," *Solid-State Electronics*, vol. 19, pp. 721-729, 8. 1976.
- [4] P.K. Weimer, "The TFT - A new thin film transistor," *Proc. IRE*, vol. 50, pp. 1462, 1962.
- [5] M.Pope and C.E. Swenberg, "Electronic processes in organic crystals and polymers," *Oxford University Press, New York*, 1999.
- [6] A. Tsumura, H. Koezuka and T. Ando, "Macromolecular electronic device: Field-Effect Transistor with a polythiophene thin film," *Appl. Phys. Lett.*, vol. 49, pp. 1210, 11/03. 1986.
- [7] O. D. Jurchescu, J. Baas and T. T. M. Palstra, "Effect of impurities on the mobility of single crystal pentacene," *Appl. Phys. Lett.*, vol. 84, pp. 3061-3063, April 19, 2004. 2004.
- [8] I. McCulloch, M. Heeney, C. Bailey, K. Genevicius and I. MacDonald, "Liquid-crystalline semiconducting polymers with high charge-carrier mobility," *Nature Materials*, vol. 5, pp. 328 - 333, 2006.
- [9] W. Clemens, W. Fix, J. Ficker, A. Knobloch and A. Ullmann, "From polymer transistors toward printed electronics," *Journal of Materials Research*, vol. 7, pp. 1963, 2004.
- [10] G. H. Gelinck, H. E. A. Huitema, E. van Veenendaal, E. Cantatore, L. Schrijnemakers, van der Putten, Jan B. P. H., T. C. T. Geuns, M. Beenhakkers, J. B. Giesbers, B. Huisman, E. J. Meijer, E. M. Benito, F. J. Touwslager, A. W. Marsman, van Rens, Bas J. E. and de Leeuw, Dago M., "Flexible active-matrix displays and

shift registers based on solution-processed organic transistors," *Nature Materials*, vol. 3, pp. 106-110, /02print. 2004.

[11] H. Laurs and G. Heiland, "Electrical and optical properties of phthalocyanine films," *Thin Solid Films*, vol. 149, pp. 129-142, 5/25. 1987.

[12] A. Assadi, G. Gustafsson, M. Willander, C. Svensson and O. Inganas, "Determination of field-effect mobility of poly(3-hexylthiophene) upon exposure to NH₃ gas," *Synthetic Metals*, vol. 37, pp. 123-130, 8/1. 1990.

[13] A. Loi, I. Manunza and A. Bonfiglio, "Flexible, organic, ion-sensitive Field-Effect Transistor," *Appl. Phys. Lett.*, vol.86, pp. 103512, 2005.

[14] L. Torsi, M. C. Tanese, N. Cioffi, M. C. Gallazzi, L. Sabbatini and P. G. Zambonin, "Alkoxy-substituted polyterthiophene Thin-Film-Transistors as alcohol sensors," *Sensors and Actuators B: Chemical*, vol. 98, pp. 204-207, 3/15. 2004.

[15] Y. Noh, D. Kim, Y. Yoshida, K. Yase, B. Jung, E. Lim and H. Shim, "High-photosensitivity *p*-channel organic phototransistors based on a biphenyl end-capped fused bithiophene oligomer," *Appl. Phys. Lett.*, vol. 86, pp. 043501, 2005.

[16] Y. Noh and D. Kim, "Organic phototransistor based on pentacene as an efficient red light sensor," *Solid-State Electronics*, vol. 51, pp. 1052-1055, 7. 2007.

[17] R. B. M. Schasfoort, R. P. H. Kooyman, P. Bergveld and J. Greve, "A new approach to immunoFET operation," *Biosensors and Bioelectronics*, vol. 5, pp. 103-124, 1990.

[18] S. V. Dzyadevich, Y. I. Korpan, V. N. Arkhipova, M. Y. Alesina, C. Martelet, A. V. ElSkaya and A. P. Soldatkin, "Application of enzyme Field-Effect Transistors for determination of glucose concentrations in blood serum," *Biosensors and Bioelectronics*, vol. 14, pp. 283-287, 3/15. 1999.

[19] Q. Zhang and V. Subramanian, "DNA hybridization detection with organic thin film transistors: Toward fast and disposable DNA microarray chips," *Biosensors and Bioelectronics*, vol. 12, pp. 3182-3187, 2007.

- [20] M. Halik, H. Klauk, U. Zschieschang, G. Schmid, S. Ponomarenko, S. Kirchmeyer and W. Weber, "Relationship between molecular structure and electrical performance of oligothiophene organic Thin-Film-Transistors," *Adv Mater*, vol. 15, pp. 917, 2003.
- [21] D. Kumakia, T. Umedab, T. Suzukic and S. Tokito, "High-mobility bottom-contact thin-film transistor based on anthracene oligomer," *Organic Electronics*, vol. 8, pp. 921-924, 2008.
- [22] G. Scaviaa, W. Porziob, S. Destrib, L. Barbac, G. Arrighettic, S. Militad, L. Fumagallie, D. Natalie and M. Sampietroe, "Effect of the silanization and annealing on the morphology of thin poly(3-hexylthiophene) (P3HT) layer on silicon oxide," *Surface Science*, In Press.
- [23] H. E. Katz, "Recent advances in semiconductor performance and printing processes for organic transistor-based electronics," *Chem. Mater.*, vol. 16, pp. 4748-4756, 2004.
- [24] H. Sirringhaus, N. Tessler and R. H. Friend, "Integrated optoelectronic devices based on conjugated polymers," *Science*, vol. 280, pp. 1741, 06/12. 1998.
- [25] A. Babel and S. A. Jenekhe, "High electron mobility in ladder polymer Field-Effect Transistors," *J. Am. Chem. Soc.*, vol. 125, pp. 13656-13657, 2003.
- [26] A. Facchetti, M. Mushrush, M. -. Yoon, G. R. Hutchison, M. A. Ratner and T. J. Marks, "Building blocks for *n*-type molecular and polymeric electronics. perfluoroalkyl- versus alkyl-functionalized oligothiophenes (*n*T; *n* = 2-6). systematics of thin film microstructure, semiconductor performance, and modeling of majority charge injection in Field-Effect Transistors," *J. Am. Chem. Soc.*, vol. 126, pp. 13859-13874, 2004.
- [27] C. Waldauf, P. Schilinsky, M. Perisutti, J. Hauch and C.J. Brabec, "Solution-processed organic *n*-type Thin-Film Transistors," *Adv Mater*, vol. 15, pp. 2084, 2003.
- [28] H. Sirringhaus, P. J. Brown, R. H. Friend, M. M. Nielsen, K. Bechgaard, B. M. W. Langeveld-Voss, A. J. H. Spiering, R. A. J. Janssen, E. W. Meijer, P. Herwig and D. M. de Leeuw, "Two-dimensional charge transport in self-organized,

- high-mobility conjugated polymers," *Nature*, vol. 401, pp. 685-688, 1999.
- [29] H. G. O. Sandberg, G. L. Frey, M. N. Shkunov, H. Sirringhaus and R. H. Friend, "Ultrathin regioregular poly(3-hexyl thiophene) Field-Effect Transistors," *Langmuir*, vol. 18, pp. 10176-10182, 2002.
- [30] S. Hoshino, M. Yoshida, S. Uemura, T. Kodzasa, N. Takada, T. Kamata and K. Yase, "Influence of moisture on device characteristics of polythiophene-based Field-Effect Transistors," *J. Appl. Phys.*, vol. 95, pp. 5088-5093, 2004.
- [31] Brian A. Mattis, Paul C. Chang, Vivek Subramanian, "Performance recovery and optimization of poly(3-hexylthiophene) transistors by thermal cycling," *Synthetic Metals* 156 (2006) 1241–1248
- [32] M. L. Chabinyc, R. A. Street and J. E. Northrup, "Effects of molecular oxygen and ozone on polythiophene-based Thin-Film Transistors," *Appl. Phys. Lett.*, vol. 90, pp. 123508, 2007.
- [33] H. Sirringhaus, "Device physics of solution-processed organic Field-Effect Transistors," *Adv Mater*, vol. 17, pp. 2411-2425, 2005.
- [34] Y. Hong, F. Yan, P. Migliorato, S. H. Han and J. Jang, "Injection-limited contact in bottom-contact pentacene organic Thin-Film Transistors," *Thin Solid Films*, vol. 515, pp. 4032-4035, 2/26. 2007.
- [35] F. Yan, Y. Hong and P. Migliorato, "Temperature dependent characteristics of all polymer Thin-Film Transistors based on poly(9,9-dioctylfluorene-co-bithiophene)," *J. Appl. Phys.*, vol. 101, pp. 064501, 2007.
- [36] M. A. Romero, M. A. G. Martinez and P. R. Herczfeld, "An analytical model for the photodetection mechanisms in high-electron mobility transistors," *IEEE Transactions on Microwave Theory and Techniques*, vol. 44, pp. 2279-2287, 1996.
- [37] M. Debucquoy, S. Verlaak, S. Steudel, K. Myny, J. Genoe and P. Heremans, "Correlation between bias stress instability and phototransistor operation of pentacene Thin-Film Transistors," *Appl. Phys. Lett.*, vol. 91, pp. 103508, 2007.

- [38] B. Park, P. Paoprasert, I. In, J. Zwickey, P. E. Colavita, R. J. Hamers, P. Gopalan, P. G. Evans, "Functional self-assembled monolayers for optimized photoinduced charge transfer in organic Field Effect Transistors," *Adv Mater*, vol. 19, pp. 4353-4357, 2007.
- [39] Y. Hu, G. Dong, C. Liu, L. Wang and Y. Qiu, "Dependency of organic phototransistor properties on the dielectric layers," *Appl. Phys. Lett.*, vol. 89, pp. 072108, 2006.
- [40] V. Podzorov and M. E. Gershenson, "Photoinduced charge transfer across the interface between organic molecular crystals and polymers," *Phys. Rev. Lett.*, vol. 95, pp. 016602, 2005.
- [41] T. P. I. Saragi, K. Onken, I. Suske, T. Fuhrmann-Lieker and J. Salbeck, "Ambipolar organic phototransistor," *Optical Materials*, vol. 29, pp. 1332-1337, 7. 2007.
- [42] T. P. I. Saragi, R. Pudzich, T. Fuhrmann and J. Salbeck, "Organic phototransistor based on intramolecular charge transfer in a bifunctional spiro compound," *Appl. Phys. Lett.*, vol. 84, pp. 2334-2336, 2004.
- [43] M. C. Hamilton, S. Martin and J. Kanicki, "Thin-film organic polymer phototransistors," *IEEE Transactions on Electron Devices*, vol. 51, pp. 877-885, 2004.
- [44] K. S. Narayan and N. Kumar, "Light responsive polymer field-effect transistor," *Appl. Phys. Lett.*, vol. 79, pp. 1891-1893, 2001.
- [45] N. Marjanovic, T. B. Singh, G. Dennler, S. Gunes, H. Neugebauer, N. S. Sariciftci, R. Schwodiauer and S. Bauer, "Photoresponse of organic Field-Effect Transistors based on conjugated polymer/fullerene blends," *Organic Electronics*, vol. 7, pp. 188-194, 8. 2006.
- [46] J. E. Kroeze, T. J. Savenije, M. J. W. Vermeulen and J. M. Warman, "Contactless determination of the photoconductivity action spectrum, exciton diffusion length, and charge separation efficiency in polythiophene-sensitized TiO₂ bilayers," *J. Phys. Chem. B*, vol. 107, pp. 7696-7705, 2003.
- [47] H. C. Shin, I. S. Lim, M. Racanelli, W. L. M. Huang, J. Foerstner and B. Y.

- Hwang, "Analysis of floating body induced transient behaviors in partially depleted thin film SOI devices," *IEEE Transactions on Electron Devices*, vol. 43, pp. 318-325, 1996.
- [48] P. Peumans and S. R. Forrest, "Separation of geminate charge-pairs at donor-acceptor interfaces in disordered solids," *Chemical Physics Letters*, vol. 398, pp. 27-31, 11/1. 2004.
- [49] S.M. Sze, "Physics of semiconductor devices, 2nd ed." *Wiley, New York*, 1981.
- [50] E. M. Boon, J. E. Salas and J. K. Barton, "An electrical probe of protein-DNA interactions on DNA-modified surfaces," *Nat Biotech*, vol. 20, pp. 282-286, /03print. 2002.
- [51] K. Miyamoto, K. Ishibashi, K. Hiroi, Y. Kimura, H. Ishii and M. Niwano, "Label-free detection and classification of DNA by surface vibration spectroscopy in conjugation with electrophoresis," vol. 86, pp. 053902, 2005.
- [52] J. Wang and A. J. Bard, "Monitoring DNA immobilization and hybridization on surfaces by atomic force microscopy force measurements," *Analytical Chemistry* vol. 73, pp. 2207-2212, 2001.
- [53] M. Thompson, L. Cheran, M. Zhang, M. Chacko, H. Huo and S. Sadeghi, "Label-free detection of nucleic acid and protein microarrays by scanning Kelvin nanoprobe," *Biosensors and Bioelectronics*, vol. 20, pp. 1471-1481, 2/15. 2005.
- [54] P. Estrela, A. G. Stewart, F. Yan and P. Migliorato, "Field effect detection of biomolecular interactions," *Electrochimica Acta*, vol. 50, pp. 4995-5000, 9/5. 2005.
- [55] F. Pouthas, C. Gentil, D. Cote and U. Bockelmann, "DNA detection on transistor arrays following mutation-specific enzymatic amplification," *Appl. Phys. Lett.*, vol. 84, pp. 1594-1596, 2004.
- [56] T. Sakata, M. Kamahori and Y. Miyahara, "Immobilization of oligonucleotide probes on Si₃N₄ surface and its application to genetic field effect transistor," *Materials Science and Engineering: C*, vol. 24, pp. 827-832, 12/1. 2004.

- [57] G. Shekhawat, S. Tark and V. P. Dravid, "MOSFET-embedded microcantilevers for measuring deflection in biomolecular sensors," *Science*, vol. 311, pp. 1592-1595, 2006.
- [58] G. Wu, R. H. Datar, K. M. Hansen, T. Thundat, R. J. Cote and A. Majumdar, "Bioassay of prostate-specific antigen (PSA) using microcantilevers," *Nat Biotech*, vol. 19, pp. 856-860, /09print. 2001.
- [59] F. Yan, P. Estrela, Y. Mo, P. Migliorato, H. Maeda, S. Inoue and T. Shimoda, "Polycrystalline silicon ion sensitive Field Effect Transistors," *Appl. Phys. Lett.*, vol. 86, pp. 053901, 2005.
- [60] D. T. McQuade, A. E. Pullen and T. M. Swager, "Conjugated polymer-based chemical sensors," *Chem. Rev.*, vol. 100, pp. 2537-2574, 2000.
- [61] C. Bartic and G. Borghs, "Organic thin-film transistors as transducers for (bio) analytical applications," vol. 384, *Anonymous Springer Science & Business Media B.V.*, 2006, pp. 354-365.
- [62] M. C. Tanese, D. Fine, A. Dodabalapur and L. Torsi, "Interface and gate bias dependence responses of sensing organic Thin-Film Transistors," *Biosensors and Bioelectronics*, vol. 21, pp. 782-788, 11/15. 2005.
- [63] L. Burgi, H. Sirringhaus and R. H. Friend, "Noncontact potentiometry of polymer Field-Effect Transistors," *Appl. Phys. Lett.*, vol. 80, pp. 2913-2915, 2002.
- [64] J. Zaumseil and H. Sirringhaus, "Electron and ambipolar transport in organic Field-Effect Transistors," *Chem. Rev.*, vol. 107, pp. 1296-1323, 2007.
- [65] H. W. Fink and C. Schonenberger, "Electrical conduction through DNA molecules," *Nature* 398(6726), 407-410, 1999.
- [66] D. Porath et al., "Direct measurement of electrical transport through DNA molecules," *Nature* 403(6770), 635-638, 2000.